ISABELA BARRETO TOLENTINO

DEVELOPMENT OF A DYNAMIC SIMULATOR FOR CONSEQUENCE ANALYSIS IN PROCESSING PLANTS

DESENVOLVIMENTO DE UM SIMULADOR DINÂMICO DE ANÁLISE DE CONSEQUÊNCIA PARA INDÚSTRIAS DE PROCESSOS

CAMPINAS

2015

UNIVERSIDADE ESTADUAL DE CAMPINAS
FACULDADE DE ENGENHARIA QUÍMICA

ISABELA BARRETO TOLENTINO

DEVELOPMENT OF A DYNAMIC SIMULATOR FOR CONSEQUENCE ANALYSIS IN PROCESSING PLANTS

DESENVOLVIMENTO DE UM SIMULADOR DINÂMICO DE ANÁLISE DE CONSEQUÊNCIA PARA INDÚSTRIAS DE PROCESSOS

Dissertation presented to the Faculty of Chemical Engineering of the University of Campinas in partial fulfillment of the requirements for the degree of Master in Chemical Engineering.

Dissertação apresentada à Faculdade de Engenharia Química da Universidade Estadual de Campinas como parte dos requisitos para a obtenção do título de Mestra em Engenharia Química.

Supervisor: Prof. Dr. Sávio Souza Venâncio Vianna

ESTE EXEMPLAR CORRESPONDE À VERSÃO FINAL DA DISSERTAÇÃO DEFENDIDA PELA ALUNA ISABELA BARRETO TOLENTINO, E ORIENTADA PELO PROF. DR. SÁVIO SOUZA VENÂNCIO VIANNA.

Prof. Dr. Sávio Souza Venâncio Vianna

CAMPINAS
2015

Ficha catalográfica
Universidade Estadual de Campinas
Biblioteca da Área de Engenharia e Arquitetura
Rose Meire da Silva - CRB 8/5974

T575d

Tolentino, Isabela Barreto, 1989-
Development of a dynamic simulator for consequence analysis in processing plants / Isabela Barreto Tolentino. – Campinas, SP : [s.n.], 2015.

Orientador: Sávio Souza Venâncio Vianna.
Dissertação (mestrado) – Universidade Estadual de Campinas, Faculdade de Engenharia Química.

1. Avaliação de riscos. 2. Simulação (Computadores digitais). I. Vianna, Sávio Souza Venâncio,1975-. II. Universidade Estadual de Campinas. Faculdade de Engenharia Química. III. Título.

Informações para Biblioteca Digital

Título em outro idioma: Desenvolvimento de um simulador dinâmico de análise de consequência para indústrias de processos
Palavras-chave em inglês:
Risk evaluation
Simulation
Área de concentração: Engenharia Química
Titulação: Mestra em Engenharia Química
Banca examinadora:
Sávio Souza Venâncio Vianna [Orientador]
Edson Tomaz
Vanderley de Vasconcelos
Data de defesa: 14-07-2015
Programa de Pós-Graduação: Engenharia Química

Folha de aprovação

Dissertação de Mestrado defendida por ISABELA BARRETO TOLENTINO e aprovada em 14 de Julho de 2015 pela banca examinadora constituída pelos doutores:

Prof. Dr. Sávio Souza Venâncio Vianna - Orientador

Prof. Dr. Edson Tomaz (titular)

Dr. Vanderley de Vasconcelos (titular)

ABSTRACT

The current work proposes the development of a dynamic simulator that could be used in processing plants for consequence analysis. All stages of an accident have been studied and implemented in the software based on known empirical and semi-empirical models from the literature, regarding the state of matter of the substance (gas, liquid or two-phase). Based on results of the release rate, dispersion of clouds, pool formation, evaporation and flash processes, the incident outcomes have been determined for different accident scenarios. Thermal radiation and overpressure effects have been analysed for outcomes as jet fire, pool fire, fireball (for radiation) and vapour cloud explosions (for overpressures). Results show good agreement with expected behaviour of the parameters of accidents and also with the literature. A Monte Carlo simulation has been performed to determine the probability and frequency of overpressure based on stochastic parameters such as: discharge distribution, wind direction, wind speed and leak direction. The methodology has been executed with response surfaces based on CFD studies for flammable volume of gases and overpressure. Results demonstrated that such methodology can provide interesting data for risk analysis.

RESUMO

Este trabalho tem como objetivo desenvolver um simulador dinâmico para análise de consequência em plantas químicas industriais. Nele, todas as etapas de um possível acidente foram estudadas e implementadas, baseadas em modelos empíricos e semi-empíricos da literatura para acidentes de gás, líquido e de duas fases (líquido e gás). Através dos resultados obtidos com o estudo do vazamento, da dispersão do material, da possível formação de poça, e dos processos de evaporação e flash, os efeitos dos acidentes foram estimados. Os efeitos de radiação térmica e sobrepressão foram analisados para acidentes que resultam em jato de fogo, poça de fogo e bola de fogo (no caso de radiação) e explosão de nuvem de vapor (no caso de sobrepressão). Os resultados obtidos possuem boa concordância em relação ao comportamento esperado dos parâmetros e daquele esperado pela literatura. Simulação de Monte Carlo também foi realizada para a determinação da probabilidade e frequência de sobrepressões baseada em variáveis probabilísticas, como: descarga, direção e velocidade do vento, e direção do vazamento. A metodologia foi executada utilizando superfícies de respostas obtidas a partir de estudos de CFD para o cálculo do volume de nuvem inflamável e sobrepressão de uma explosão. Os resultados obtidos demonstraram que a metodologia desenvolvida fornece dados interessantes para análise de risco.

CONTENTS

This work is dedicated to my parents and my sister.

Acknowledgment

First of all, I would like to thank God for guiding me throughout life.

I would like to thank my supervisor Prof. Dr. Sávio S. V. Vianna. Thanks for the support, knowledge, trust and help during this work.

I would like to thank my beloved ones: my mom, my dad and my sister. Thanks for always being there for me, for supporting my decisions, for helping me and for being patient with me. Mostly, thanks for the love that surrounds our family.

I am also grateful to all my family, for the love and support.

My deepest gratitude to my friends from University, Manu (Manuella Lech) and Chat (Thalles Andrade), who have joined me through this process and have made this period much easier and lighter for me. Thank you for listening to me when I needed the most, for the friendship, for the many good moments that we have been through and the love.

I am thankful to the Faculty of Chemical Engineering of UNICAMP for the opportunity given to me.

I want to thank CNPq for the financial support.

List of Figures

List of Tables

Nomenclature

ac_c: acceleration parameter [m/s²]
A_h: area of the hole [m²]
A_L: cross sectional area of the liquid inside the vessel [m²]
A_p: area of the pipeline [m²]
A_{pool}: total area of the pool [m²]
A_s: superficial area of the vessel [m²]
A_{tank}: cross sectional area of the vessel [m²]
A_{view}: non-dimensional parameter for the view factor calculation [dimensionless]
B_{view}: non-dimensional parameter for the view factor calculation [dimensionless]
C: concentration of the substance in the cloud [kg/m³]
C_1: discharge coefficient [dimensionless]
C_{cc}: concentration in the centre of the cloud [kg/m³]
C_d: discharge coefficient [dimensionless]
$C_{isopleth}$: concentration at the isopleths [kg/m³]
C_{LFL}: lower flammability limit concentration [kg/m³]
C_p: heat capacity of the liquid [J/kg.K]
C_s: stoichiometric concentration [%vol]
C_T: fuel mole fraction concentration in a stoichiometric fuel-air mixture [dimensionless]
C_{UFL}: upper flammability limit concentration [kg/m³]
C_V: heat capacity at constant volume [J/kg.K]
C_{view}: non-dimensional parameter for the view factor calculation [dimensionless]
D_c, D_i: characteristic source dimensions [m]
D_{centre}: distance from the centre [m]
D_{cc}: distance of the cloud centre [m]
D_{elong}: elongated diameter of the pool [m]
d_{hole}: diameter of the hole [m]
d_p: pipe diameter [m]
D_{pool}: diameter of the pool [m]
d_{tank}: diameter of the tank [m]
D_{view}: non-dimensional parameter for the view factor calculation [dimensionless]
E: total heat of combustion [J]
E_{av}: emissive power [W/m²]
E_c: heat of combustion of the fuel [J/kg]
$E_{c,TNT}$: heat of combustion of TNT [J/kg]
E_r: radiation heat flux [W/m²]
E_{view}: non-dimensional parameter for the view factor calculation [dimensionless]
f, D: meteorological parameters of Marshall's equation for the Pasquill stability classes [dimensionless]
F: frictional loss term [m²/s²]
F_{21}: view factor for the solid plume model [dimensionless]
f_D: Darcy friction factor [dimensionless]
F_p: view factor [dimensionless]

f_{PLG}: fraction of the volume of the pressured tank filled with LPG [dimensionless]
Fr_{10}: Froude number [dimensionless]
F_s: fraction of heat radiated by a fireball [dimensionless]
f_v: fraction of liquid vaporised [dimensionless]
F_{view}: non-dimensional parameter for the view factor calculation [dimensionless]
g: acceleration of gravity [m/s²]
g_0: initial buoyancy factor [m/s²]
g_c: gravitational constant force [kg.m/N.s²]
G_{ERM}: equilibrium mass flux [kg/m².s]
G_{sub}: subcooled mass flux [kg/m².s]
G_{view}: non-dimensional parameter for the view factor calculation [dimensionless]
H: release height above ground [m]
H_{bleve}: lift height of the fireball [m]
h_{fg}: enthalpy change in vaporisation [J/kg]
H_{flame}: flame height [m]
H_{flux}: total heat flux [J/s]
h_L: liquid head above the hole [m]
ΔH^*: modified heat of vaporization [J/kg]
ΔH: net available heat [J/kg]
ΔH_c: heat of combustion [J/kg]
ΔH_v: vaporization heat of the material [J/kg]
k_g: mass transfer coefficient [m/s]
k_g^0: reference mass transfer coefficient [m/s]
k_s: thermal conductivity of the soil [J/m.s.K]
K_x, K_y, K_z: diffusion coefficients in x, y, z directions [m²/s]
L_c: critical pipe length [m]
L_{flame}: length of the flame [m]
l_p: pipe length [m]
L_{vap}: heat of vaporization of the liquid [J/kg]
L_{vessel}: length of the vessel [m]
M: mass inside a vessel [kg]
M_0: initial total gas mass in the pipeline [kg]
$\dot{m}$: evaporation rate [kg/s]
m_b: mass burning rate [kg/m².s]
MW: molecular weight [g/mol]
MW_0: molecular weight of the reference [g/mol]
MW_a: molecular weight of air [g/mol]
MW_f: molecular weight of the fuel [g/mol]
N: non-equilibrium parameter for two-phase discharge [dimensionless]
P: pressure [Pa]
P_0: initial pressure [Pa]
P_a: ambient pressure [Pa]
P_{sat}: saturation vapour pressure at ambient temperature [Pa]

P_{SV}: vapour pressure inside the vessel [Pa]
P_w: water partial pressure [Pa]
Q: total mass released in a puff [kg]
q_0: material volume flux [m³/s]
Q_{flam}: flammable mass [mg]
q_g: heat flux from the ground [J/m².s]
$Q_{m,0}$: initial mass flow rate [kg/s]
Q_m: mass flow rate [kg/s]
R: Sachs-Scaled distance [dimensionless]
Re: Reynolds number [dimensionless]
R_d: release duration [s]
r_{fb}: radius of the fireball [m]
R_g: ideal gas constant [Pa.m³/mol.k]
RH: relative humidity of the ambient [dimensionless]
r_{pool}: radius of the pool [m]
SEP: surface emissive power [J/(m².s)]
SEP_{soot}: surface emissive power of soot [J/(m².s)]
T: temperature [K]
t: time [s]
T_0: initial temperature of the substance [K]
T_a: ambient temperature [K]
T_B: atmospheric boiling temperature of the liquid [K]
t_B: time constant [s]
T_{BP}: boiling point temperature of the liquid [K]
t_c: time taken for total discharge [s]
T_f: adiabatic flame temperature [K]
t_{fb}: duration of the fireball [s]
T_g: temperature of the ground [K]
T_j: jet temperature [K]
T_L: temperature of the liquid [K]
t_{max}: maximum time of the pool fire [s]
t_{pool}: duration of the pool fire [s]
u, v, w: mean wind speeds in the x, y, z directions [m/s]
u': non-dimensional wind velocity [dimensionless]
U: internal energy [J/kg]
u_c: characteristic wind velocity [m/s]
$\overline{u}_f$: fluid velocity [m/s]
u_s: sonic velocity of the gas [m/s]
V: volume of the vessel [m³]
V_0: initial volume of released gas material [m³]
v_0: initial outflow velocity [m/s]
v_{fg}: specific volume change between liquid and vapour [m³/kg]

V_{flam}: flammable volume of the cloud [m³]
V_L: volume of liquid inside the vessel [m³]
V_s: liquid spill rate [m³/s]
W: equivalent in mass of TNT [kg]
W_s: shaft work [J/s]
X: distance from the receiver to the centre of the flame [m]
x: downwind direction [m]
x_{blast}: distance from the blast [m]
x_{bleve}: distance from the receiver to the axis of the fireball [m]
x_{path}: actual path length of the radiation [m]
x_{pool}: distance from the receiver to the pool [m]
y: crosswind direction [m]
$\dot{y}_{max}$: vertical rate of liquid level decrease [m/s]
z: distance above ground [m]
Z: scaled distance [m/kg³]
z_g: compressibility factor [dimensionless]
Δz: difference in vertical height [m]

Greek symbols
Θ_{tilt}: flame tilt angle [radians]
Φ_{max}:: non-dimensional form of the pool spread differential equation [dimensionless]
α_T: mols of reactant per mole of product for a stoichiometric fuel-air mixture [dimensionless]
α_s: thermal diffusivity of the ground [m²/s]
δ_{pool}: pool thickness [m]
η_{TNT}: empirical explosion efficiency [dimensionless]
η_{rad}: fraction of heat of combustion radiated [dimensionless]
ρ_0: density of the released material [kg/m³]
ρ_a: density of the ambient air [kg/m³]
σ_x, σ_y, σ_z: dispersion coefficients in the x, y and z directions [m]
τ_a: atmospheric transmissivity [dimensionless]
τ_{max} and β: parameter for the pool fire calculation [dimensionless]
$\emptyset$: filling degree of the vessel [dimensionless]
$\mathcal{E}$: internal roughness of the pipeline [m]
α: unitless velocity profile correction factor [dimensionless]
γ: heat capacity ratio [dimensionless]
ρ: density [kg/m³]
ς : fraction of the surface of the flame covered by soot [dimensionless]
ψ: equation for the flow type (sonic or sobsonic)

Acronyms

BLEVE: Boiling Liquid Expanding Vapour Explosion
CASE: Consequence Analysis Simulation Environment
CFD: Computational Fluid Dynamics
CPQRA: Chemical Process Quantitative Risk Analysis
DDT: Deflagration to Detonation Transition
FMEA: Failure-Mode Effect Analysis
HAZOP: Hazard and Operability Study
LFL: Lower Flammability Limit
LPG: Liquid Petroleum Gas
TNO: *Toegepast Natuurwetenschappelijk Onderzoek* (Netherlands Organisation for Applied Scientific Research)
TNT: Trinitrotoluene
UFL: Upper Flammability Limit
VCE: Vapour Cloud Explosion

Chapter 1

Introduction

Accidents in chemical and petrochemical industries are always a social problem, and therefore they are objects of study worldwide. Many accidents of huge magnitude were recorded in industrial areas and they impact negatively not only on the industry's image, but they can also cause fatalities and environmental damages.

An example of industrial accident is the one that occurred in 2005 in Texas (EUA), in a BP's refinery (British Petroleum). This accident caused the death of 15 people and left 170 injured. Besides, the damages caused by this accident summed up to one billion dollars. Such accident is considered a domino accident type, as one accident leads to another accident, and so on (ABDOLHAMIDZADEH *et al.*, 2011).

Another reported disaster, which is one of the most documented accident in the history and served as a lesson learned by the chemical engineering field is the accident at Flixborough, in England, 1974 (CROWL and LOUVAR, 2011). The Flixborough Works of Nypro Limited produced caprolactam, a raw material for the production of nylon. Cyclohexane, which volatilizes easily when depressurized, is a raw material of this process. The process consisted of 6 reactors in series and months before the accident, the fifth reactor presented a leakage. The operation continued with the fourth reactor connected directly to the sixth reactor, which means that the fifth reactor was not in use. However, as it was not available in the stock a pipe of the same diameter of the pipes that connected the reactors, it was used a pipe with the diameter 8 inches less than the diameter of the

connecting ones. In order to connect both pipes, it was used flexible bellow-type piping. The accident probably occurred because of overflexing of the pipeline due to internal reactor pressures, which ruptured the bypass. The consequences resulted in 28 deaths (CROWL and LOUVAR, 2011).

The Flixborough event was an important accident in the England chemical industry because it could probably be prevented by proper use of the safety procedures. Since this accident, the safety procedures have been improved in this country.

The vapour cloud explosion (VCE) that occurred in 2009 in the Indian Oil Corporation Ltd., in Jaipur (India) is another example of accident that happened due to an apparently insignificant incident. In most cases the accident is caused by the loss of containment in pipelines or process' equipments, e.g. by mechanical failures usually attributed to human error, like improper maintenance, operation or inspection (CROWL and LOUVAR, 2011). In this case, the incident was the loss of tightness in the hammer blind valve on the delivery line of a tank connected to the suction line of the gasoline pump (SHARMA *et al.*, 2012). What happened due to this incident was a release of gasoline, and the physical effects (explosion and fireball) occurred about 80 minutes later. The investigation of this accident showed that during the 80 minutes when the release of the gasoline was not controlled, about 81 tons of gasoline escaped, which can generate an explosion equivalent to an explosion of 38 tons of TNT (SHARMA *et al.*, 2012). The result of the accident: the entire installation destroyed, as well as great damage of surrounding buildings, and an economic loss of 2,800 million Indian rupees.

Besides these accidents, there are many others that can be described, that occurred in many types of processing plants, just like in the case of oil and gas industry. The European Major Accident Reporting System (MARS), developed and operated since 1984, has a database of industry's accidents in Europe. According to MARS, in the period of 1985 to 2002, 17% of the accidents reported occurred in the petrochemical industry. It is the second major accident industry, which has only fewer accidents than the general chemical industry, which represents 32% of all reported accidents in that period (NIVOLIANITOU *et al.*, 2006).

The main characteristic that makes the petrochemical field such a hazardous industry is that it works generally with huge amount of flammable substances. Therefore, small incident can lead to major accidents. Considering offshore facilities, another important characteristic is the degree of confinement of the structure, which enlarges the potential of an accident, and can also difficult the rescue of workers.

However, even if an accident of great magnitude does not occur in a process plant, it is important to register all accidents with little or almost none consequence, because they could be accidents of great magnitude that did not occur because of random circumstances that permitted them to be controlled immediately (CAROL *et al.*, 2000). The study and registration of all kinds of accidents is crucial as they help determine some patterns and therefore can be useful on preventing future accidents. In chemical plants, for example, the most common type of accident is fire, followed by explosion and toxic release. However, the type of accident that causes larger losses is the vapour cloud explosion (VCE), followed by fires and explosions (CROWL and LOUVAR, 2011). On the other hand, just analysing past events cannot predict the magnitude of another accident's effects, as other factors that are specific for each industry and plant must be taken into consideration in the analysis.

In this context, there are several simulators and methods to calculate the physical effects caused by accidents. Such simulators are very useful on predicting the consequences of an accident and they are used also in the process design, to help decrease the effects of accidents by improving the project of the plant. As accidents begin with an incident, an important phase of the risk analysis is the definition of the incident (for example, the size of the hole in a vessel that causes a leakage). However, the incident definition is one of the most difficult information to obtain, as it can be considered a probabilistic variable.

After the definition of the incident, the physical effects can be estimated using models already used worldwide in the consequence analysis, as well as simulators. One of the most known methods is the CFD (*Computational Fluid Dynamics*). It can be used to obtain numerical solutions for physical effects such as explosion and dispersion from offshore as well as onshore plants. The CFD simulations solve the conservation equations (mass, momentum and enthalpy) and turbulence model (International Association of Oil and Gas Producers, 2010a). Despite using a detailed amount of equations, numeric methods

and providing good estimates, the CFD has also disadvantages in its use. First, the need of so many details of the process in order to use CFD can be inappropriate in some cases, like in the early phase of design, as there is no sufficient knowledge of the process. Second, the CFD depends entirely on the choice of the geometry modelling (grid sizing), and in many cases the CFD models are not fine enough to solve little items of the process that are responsible for the turbulence of the process, for example (International Association of Oil and Gas Producers, 2010a). Third, the time spending on the simulations is very large, according to the complexity of the models and hence the analysis is sometimes only made for a few cases. Last, CFD needs expert knowledge and is costly (HABIB *et al*., 2014).

On the other hand, semi-empirical models for consequence analysis are also available and they are used worldwide, as they are easy to model and usually predict with good precision physical effects, especially in far field. Therefore, if the study requires information of the consequence far from the release - for example what would happen to a populated neighbourhood in case a leakage occurs in a tank of an industry -, semi-empirical models can be used. However, if it is necessary a higher precision in near field, CFD modelling is still the best way of obtaining accuracy, as it deals with numerical simulation and therefore can predict better the physical phenomenon. Another characteristic of empirical and semi-empirical models is the fact that they are usually more conservative than CFD modelling and thus provide conservative estimates.

Considering all the factors described above, it is of great advance in consequence analysis the possibility of having a simple computational tool to calculate consequences of an accident. This tool would be important for plant projects as well as for existing plants and it would estimate the sequence of an accident using already established models from the literature. Also, it could use probabilistic simulations in order to define which incidents lead to more danger outcomes, and the probability of each hazardous scenario.

Goal

The main objective of this work is to develop a computational tool namely, CASE (*Consequence Analysis Simulation Environment*) for dynamic analysis. The tool relies on CFD data as an add-on feature dealing with thousands of stochastic scenarios applying Monte Carlo technique. It also relies on semi-empirical and empirical modelling of the main physical effects of accidents, but it does not include Probit equations and the consequence calculation itself, which means that it does not include how the accident affect people (probability of fatalities). However, it does include the outcomes effects, which are the basis for the fatality probability study, such as fireball, pool fire, jet fire and explosion's effects.

In order to fulfil the main goal, specific goals are listed below:

1. Implement the discharge models for gas, liquid and two-phase releases;
2. Implement the dispersion models;
3. Implement TNT Equivalency and Multi-Energy models for vapour cloud explosion;
4. Implement jet and pool fire radiation models;
5. Implement BLEVE model (fireball);
6. Implement Monte-Carlo simulation with response surface add-on;

This dissertation

This work is divided in 5 chapters, according to the order summarized below, for better understanding of the study.

Chapter 1 presented a brief introduction of industrial accidents and the importance of studying accident scenarios to reduce and prevent them. Differences of the estimation of physical effects from accidents have been presented, especially regarding the use of empirical and semi-empirical models and CFD software. Finally, the goal of the work has been presented.

Chapter 2 accounts for the literature review. First, safety and CPQRA are explained. Then, works and models for all steps of an accident are exposed. Wide known models from the literature as well as new ones are presented. Finally, Monte Carlo simulation is presented.

Chapter 3 presents the methodology for the CASE software development. Models implemented in the tool are listed and the Monte Carlo methodology with CFD add-on is explained for the calculation of the most probable accident scenarios based on stochastic variables.

Chapter 4 shows the results obtained using the new tool developed in this work. Five accident scenarios have been studied to cover all models implemented in CASE for the physical effects, and one of them is studied as an accident scenario in an industrial refinery. A study of Monte Carlo simulation with CFD add-on is also performed, and the results are shown in this chapter. Discussion about the results is presented here.

Chapter 5 presents the conclusions of the work and suggestions for future works.

Chapter 2

Background

This chapter presents the literature review and the topics that support the development of the present work. First, the methodology of the CPQRA is explained, focusing mostly on the consequence analysis, which is the main goal of the work. A brief context of damage of accidents is also provided, especially the damages to humans. Then the most known consequence analysis' models for discharge, dispersion, and physical outcomes (pool fire, fireball, vapour cloud explosion and jet fire) are presented, as well as new models from the literature. The physical phenomena of the effects are also explained. Finally, Monte Carlo simulation is presented, as well as its use in process safety.

2.1 Safety and CPQRA

Processes are not completely safe. There are some processes however, that are inherently safe, which means that incidents are less likely to occur (LEES, 2005). Inherent (or intrinsically) safe processes are the ones that cause no hazard or danger. Almost all of the chemical process industry, however, is not one of those. Therefore, the designer of a plant or process must always select the most inherent safe process possible, considering always the financial matter.

The danger in a process plant is usually linked with some special characteristic of the substances present in the process. The toxicity, for example, is the extent of poising characteristic of the material. The effects of toxicity can be classified in two categories:

acute and chronic effects. The acute effect is a short-term effect, with symptoms that appear in short period, like burning skin after contact or paralysis. In contrast, chronic effects are developed after a long period of time, being cancer a clear example.

Besides toxicity, the flammability is also a hazard characteristic. A flammable material is a substance that is able to fire, with the appropriate concentration of fuel and oxidizer and (almost always) an ignition source. The concentrations in which a substance can ignite are in a range with the lower flammability limit (LFL) as the lowest frontier, and the upper flammability limit (UFL) as the upper frontier of the range. If a substance has a concentration higher than the UFL, even in contact with an ignition source it will not ignite, because the mixture fuel-oxidizer would be too rich to burn. In contrast, if a substance has a concentration below the LFL, it would also not burn, because the mixture would be too lean.

Considering that all chemical process industries do have at least one substance that can be either toxic or flammable, and that all organizations are legally and morally obligated to keep their employees and the general public in a safe condition, the study of the risks must be considered (LEES, 2005). An actual methodology to help evaluating the risks of the process and its safety was though only established after a number of accidents in chemical industries. The so called *Chemical Process Quantitative Risk Analysis* (CPQRA), which has evolved since the 1980s, was originated from a methodology that already existed in nuclear, electronics and aerospace industries (American Institute of Chemical Engineers - AICHE, 2000).

The CPQRA is a probabilistic tool that helps engineers define risks and therefore select, if necessary, mitigations actions in order to keep the risk in a reasonable range. Risk is a combination of frequency and consequence of a particular scenario. The consequence is expressed on how the accident can affect people, and the frequency is the probability of such accident to happen. Figure 1 shows how the CPQRA works.

Before calculating frequency and consequence, one crucial step of the risk analysis is the identification of hazardous scenarios. They happen due to incidents that might occur in the processing plant. An incident is usually defined as loss of containment or energy (AICHE, 2000), and it can be caused by rupture in a vessel or pipeline, valve leaving open

when it was not supposed to, run-away reactions, and so on. This step of the analysis is very important because it will define the scenarios that will be considered in the methodology. If an incident is not considered, than the risk analysis will not cover all possible scenarios and the risk estimative might be misleading. The idea of the enumeration of incidents is thus to identify as many incidents as possible, regardless the importance of them. It is important to bear in mind that a single incident can cause more than one incident outcome, which means more than one physical effect.

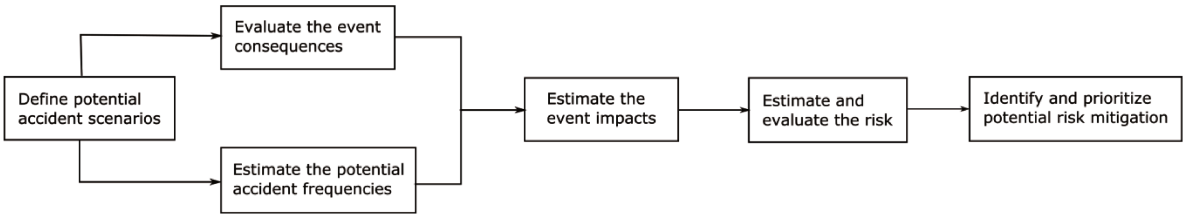

Figure 1. Framework of CPQRA (Adapted from AICHE, 2000).

Some methodologies can help enumerating the incidents, such as FMEA (Failure-Mode Effect Analysis), HAZOP and What-If Analysis, although none of them actually develops a list. After the list of incidents is concluded, a selection of some incidents from this first list must be done, as the effort of time and money to analyse all incidents makes it almost impossible to be done by industries. This work must be very cautious, as the critical incidents must remain in the smaller list just as the critical outcomes.

The next step of the CPQRA is the estimation of frequency and consequence. As they are both estimates, both have uncertainties. The uncertainty of the consequence calculation is due to simplifications of physical effects that are complex in real situations (PIKAAR *et al.*, 1990). On the other hand, frequency estimation has an inherent uncertainty, as it depends on the expertise of the engineer and hence speculations might be involved. That is why the consequence analysis is a more mature procedure than the frequency analysis.

Considering the mature of the consequence analysis, it is recommended to study it before calculating the frequency. Also, if a consequence is acceptable in any frequency, the analysis of the incident is already complete, which means that it is not necessary to obtain

the frequency (AICHE, 2000). This is a simplification of the risk analysis which is widely used in industries. In this case, the frequency can be established as a value of 1.0, and the next step is the modification of the process or part of it in order to reduce the consequences.

It is important to bear in mind that after any kind of modification in the process, the risk analysis must be done again, as new incident scenarios can become possible. The risk analysis is a live analysis, and it must follow the modifications of the process.

The entire methodology of CPQRA is usually performed in existing facilities, because in the project phase, not all information needed is available, therefore only a simpler CPQRA can be done. Information of the process usually follows the scheme showed in Figure 2 (AICHE, 2000).

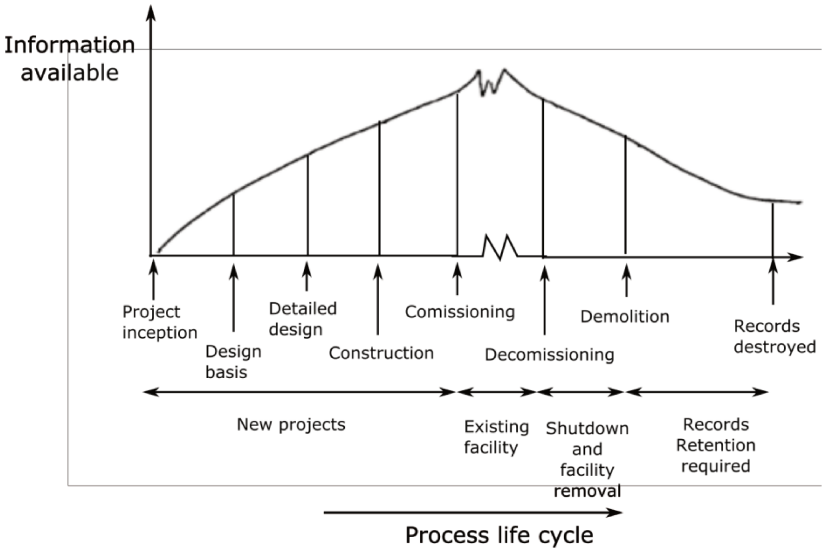

Figure 2. Information of the process during the process life cycle (adapted from AICHE, 2000).

Finally, the risk is estimated. In order to the value of the risk to have a meaning, the risk must be compared to other risks that are considered acceptable, such as the risk of riding a car, for example. In chemical industries, risks higher than 0.4 FAR (Fatal Accident Frequency Rate) should not be accepted. FAR is the number of fatalities based on 1000 employees working their entire life, which means that the tolerable limit is 4 deaths out of 100 people in their entire working life (LEES, 2005). Another methodology also used is the ALARP ("*As Low As Reasonably Possible*"). The principle of the methodology is that an

industry can have a risk in a region of acceptable risk, as long as it can demonstrate that the risk obtained is the lowest possible, considering the economic field.

2.2 Consequence Analysis

Accidents begin with an incident that can be the rupture of a pipeline, a hole in a tank, crack caused by corrosion, fire extern to the tank, escape reactions and so on. These incidents lead often to a leakage of the processing material and, depending on the properties of the material and the type of the accident, it is possible to evaluate how this substance will be discharged in the ambient. This is the first step of the accident.

In order to have a study on consequence analysis it is mandatory to first select the most appropriate discharge model of the incident, and the discharge models are based in the state of matter of the material, e.g. if is liquid, gas, solid or a mixture of both states. The discharge models provide data of the leakage flow rate.

The material discharged is then dispersed through the atmosphere, and this process is called dispersion. In that step of the accident, the material can suffer many kinds of dispersion, depending again on the state of matter, as, for example, the formation of a vapour cloud or a liquid pool.

Besides the dispersion model of the material, the possibility of a fire or explosion, when an ignition source exists, must be evaluated. It is also necessary to consider the possibility of happening an explosion, pool and jet fire, for instance. A framework of the procedure of the consequence analysis is shown in Figure 3.

All the models used in the consequence analysis are based on the mass, energy and momentum conservation's principles, which are the basis of chemical engineering. As described earlier, these models predict the physical effects and the incident outcomes from a specified incident. However, in order to determine the actual consequence on humans, consequences are expressed in deaths or injuries. In case physical structures are the mainly object of the study, the consequence must be expressed as monetary losses. There is also the possibility of verifying the consequence on the environment, by analysing for example soil contamination and impacts on plants and animals lives. However, this last analysis is

much more complex than the other two, as it depends on many properties of the environment.

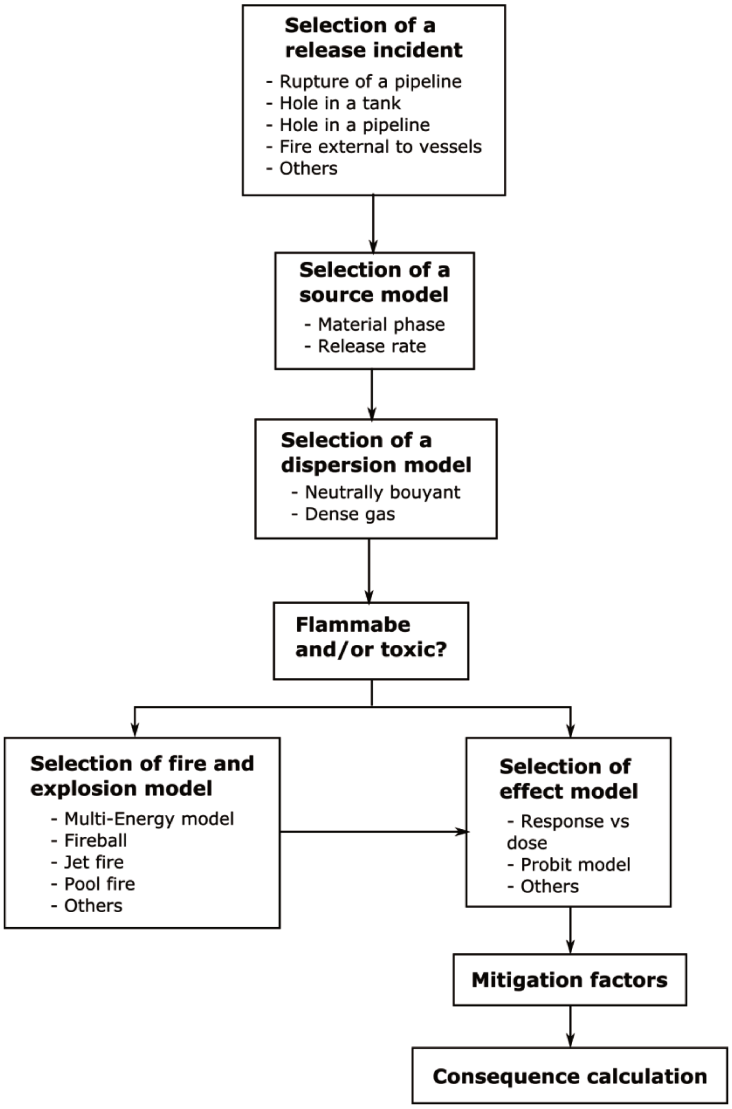

Figure 3. Framework of the Consequence Analysis (Adapted from AICHE, 2000).

The consequence estimation cannot be made using discrete functions, as it is a probabilistic distribution. This means that one cannot determine that a person will die only considering a certain concentration of toxic gas, for example, which means that a fixed input will not generate one single output (AICHE, 2000). The solution for estimating the consequences in terms of injuries or deaths is to use a probabilistic tool. The dose-response

is a statistical method to verify the response of an organism to many doses of toxic substances. The dose-response is made by administrating a certain dose of the substance in a test organism and verifying the consequences of the specific dose in it. If there is no consequence, the dose given is increased until changes in the organism are verified. The dose-response can give results in terms of quantity administered per unit of body weight, for example.

An important finding is that for a same dose of toxic substance, the response may be different for different humans. It is already known that characteristics such as age, genetics and health affect the response of a human (AICHE, 2000). Therefore, it is expected a range of responses for a determined dose, and this range is normally a Gaussian distribution, or almost a Gaussian distribution. After determining dose-response curves for a wide range of doses, the Gaussian distribution is transformed in a straight line by the use of Probit equations. Probit equations are used to calculate consequences of exposure to toxic materials, heat, radiation, pressure, as well as many other effects. Finally, the Probit value is converted to percentages, and the consequence in terms of deaths and injuries is then estimated.

2.3 Damages

The dose-response curves and the Probit equation are able to predict the percentage of injuries or deaths. However, it does not clarify what kinds of injuries are possible to obtain from a certain physical effect. This section presents some types of injuries from accidents in order to give a certain magnitude of the effects of accidents in humans.

The effects of the outcomes of accidents in people can be divided in terms of the most evident physical effect. If the most evident physical effect of the accident is thermal radiation (due to fires, for example), the pathological effect is the burning of the skin. It can be a first, second or third degree burn. In the worst case, the burned skin is absent of feeling because the nerves extremities are also burned. The age plays an important role not only because of the person's health, which is most likely to decrease in elderly, but also when it comes to determining the total duration of exposure to the radiation, therefore the damage that the thermal radiation causes in people. Humans tend to protect themselves from any

kinds of physical effects, however, children and older people tend to be less efficient to escape or look for sheltering. Hence, they are exposed to radiation a greater period of time than the average adult people. It is important to bear in mind, however, that more serious injuries as first and other degree burns occur only to people located very close to the fire.

Another physical effect that damages both structures and humans is the explosion. The importance of damages to structures by explosions is huge, as not only financial risks are observed, as well as human's injuries or even deaths, as the damages can cause missiles to be generated. This must be taken into consideration in plant design, as confined areas usually make the physical effect even greater and can enlarge the damages to people and buildings.

The pressure change caused by explosions (usually called overpressure) can also cause injury to the sensitive human organs like lungs and ear, as a primary effect (TNO, 1992). As described above, secondary effects are mainly caused by missiles. Finally, the tertiary effects are the ones where the human suffers a whole-body displacement and, because of the blast wave, is thrown away (TNO, 1992).

Different from the radiation damage, the explosion affects a wide region; therefore it is considered a more complex and problematic effect, as the damages have a greater vulnerable area.

2.4 Discharge models

According to the International Association of Oil and Gas Producers (2010a), the discharge models can be approached in two ways: a simpler approach, that calculates the initial discharge rate and assumes that this rate is constant during time, and a more complex approach, in which the release rate varies with time, which is more real. The second approach, according to the International Association of Oil and Gas Producers (2010a), is utilized in offshore processes and avoid some mistakes present in the simpler approach.

Another characteristic of the emission that must be taken into account is the aperture. There are basically two types of apertures: complete rupture and limited aperture. In the first case, a large hole occurs in a process' unit, and there is a fast release of a great

amount of material, which is the case of a complete rupture of a vessel, for example. The other case can be exemplified as a small hole in a pipeline.

All discharge models are based in the energy balance (AICHE, 2000). In this section the discharge models will be classified by the state of the substance, as it impacts the modelling of the leakage because of the differences in the properties and the transport of fluids.

2.4.1 Liquid discharge

If a substance has a temperature between its melting and boiling point, at a partial pressure or is a refrigerated liquefied gas below atmospheric pressure, the substance will be in liquid state (TNO, 2005). In a liquid release, it is the gradient of pressure that will provide the energy so that the leakage can occur, and the pressure will be converted in kinetic energy during the discharge (AICHE, 2000). As the density of the fluid is constant during the discharge of the material, Equation 2.4.1 of energy balance can be simplified through the direct resolution of the integral. Also, considering that there is not shaft work and that the fluid in question is pure, the Equation 2.4.1 is reduced to the Bernoulli Equation.

$$\int \frac{dP}{\rho} + \Delta\left(\frac{\bar{u}_f{}^2}{2\alpha g_c}\right) + \frac{g}{g_c}\Delta z + F = -\frac{W_s}{Q_m} \tag{2.4.1}$$

where P is the pressure (Pa), ρ is the density of the substance (kg/m³), $\bar{u}_f$ is the fluid velocity (m/s), g is the acceleration of gravity (m/s²), g_c is the gravitational constant force (m/s²), α is the unitless velocity profile correction factor, Δz is the difference in vertical height (m), F is the frictional loss term (m²/s²), W_s is the shaft work (J/s) and Q_m is the mass flow rate (kg/s).

Crowl and Louvar (2011) developed a model of liquid discharge based on Equation 2.4.1 of energy balance for limited aperture releases. All the simplifications above were made in the work, and they also considered the change in the elevation of the liquid negligible, so $\Delta z = 0$ and that the velocity of the fluid inside the process unit is also negligible. However, to better simplify the resultant equation, they represented the

frictional losses as a coefficient named discharge coefficient (C_1), which is defined as Equation 2.4.2.

$$\frac{\Delta P}{\rho} - F = C_1^2 \left(-\frac{\Delta P}{\rho}\right) \tag{2.4.2}$$

With the discharge coefficient substituted in Equation 2.4.1, it is possible to determine the average discharge velocity:

$$\left(\frac{\overline{u_f}^2}{2\alpha g_c}\right) = C_1^2 \left(-\frac{\Delta P}{\rho}\right) \tag{2.4.3}$$

$$\overline{u_f} = C_1 \sqrt{\alpha} \sqrt{\frac{2 g_c \Delta P}{\rho}} \tag{2.4.4}$$

Finally, it was defined a new discharge coefficient (C_d), and the mass flow rate was then defined as Equation 2.4.5:

$$Q_m = \rho \overline{u_f} A_h = A_h C_d \sqrt{2 \rho g_c \Delta P} \tag{2.4.5}$$

where A_h is the area of the hole (m²). It is important to highlight that in the case of a hole in a tank, the pressure of the tank depends on the pressure exerted by the amount of liquid above the hole (Figure 4). As this amount will decrease as the leakage occurs, so will the pressure, and, therefore, the liquid discharge rate will have a descendent behaviour, until there is no more liquid above the hole. Thus, in such cases, the discharge rate can be calculated as it is presented in the work of Crowl and Louvar (2011), where h_L is the liquid head above the hole (m).

$$Q_m = \rho \overline{u_f} A_h = \rho A_h C_d \sqrt{2 \left(\frac{g_c \Delta P}{\rho} + g h_L\right)} \tag{2.4.6}$$

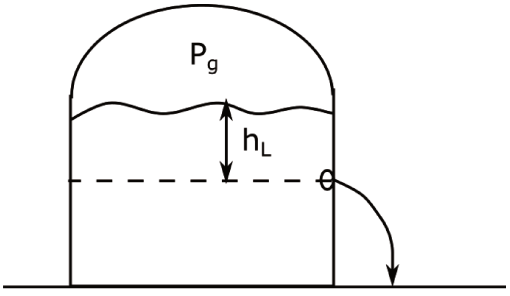

Figure 4. Liquid release through a hole in a vessel. The pressure in the tank depends on h_L, the height of liquid above the hole.

It is possible to have an iterative method in order to calculate the mass flow rate in a transient matter for each period of time of the leakage. One method is the one presented by TNO (2005). The first step of the procedure is to obtain the initial mass flow rate, with Equation 2.4.6. With this value, the decrease of mass inside the vessel (M) is obtained, as well as the decrease of liquid volume (V_L):

$$\delta M = -Q_m \, \delta t \tag{2.4.7}$$

$$\delta V_L = \delta M / \rho \tag{2.4.8}$$

The total new volume of liquid is:

$$V_{L,i+1} = V_{L,i} + \delta V_L \tag{2.4.9}$$

Equations are available to calculate the liquid height in the vessel as a function of the liquid volume and the size of the liquid surface for different vessels geometries. Crowl (1991) presented a generalized model to represent the liquid discharge as a function of time in different types of vessels, with constant and non-constant cross sectional area. The new liquid height is then calculated:

$$\delta h_L = \delta V_L / A_{L,i} \tag{2.4.10}$$

$$h_{L,i+1} = h_{L,i} + \delta h_L \tag{2.4.11}$$

where A_L is the cross sectional area of the liquid inside the vessel (m²). The value of the liquid height is used to calculate the next mass flow rate.

The discharge coefficient can have a defined value, according to the type of flow and hole. According to Lees (2005), the discharge coefficient assumes a value of 0.61 for holes and for Reynolds number greater than 30,000, for instance. However, if the value of the coefficient is unknown, it is always recommended to use the greater value (1.0) in order to maximize the flow.

2.4.2 Gas discharge

If the temperature of a substance is greater than its critical temperature, or if the temperature is below the critical temperature but the pressure is below the saturated vapour pressure, the state of the substance is gas. In order to model the discharge rate, it is necessary to know the type of release, because the models depend on this factor, as there

are differences in modelling when the leakage is due to a full bore rupture of a pipeline, for example, or a hole in a vessel. This means that the incident is again a crucial factor in the consequence analysis, as it is the heart of the selection of the models, even if there is still uncertainty in this stage of the analysis.

When an outflow of gas out of a vessel or pipeline to the atmosphere occurs, the gas rapidly depressurizes and therefore will expand. The expansion also causes the temperature and the density of the substance to decrease. All these changes must be considered in this stage of the accident. TNO (2005) presents an iterative numerical procedure to calculate these changes in a leakage from a hole in a vessel, and thus to determine the discharge flow rate of the substance. Considering a small step of time, the density of the vessel decreases as follows:

$$\delta\rho = -\left(\frac{Q_m}{V}\right)t \tag{2.4.12}$$

$$\rho_{i+1} = \rho_i + \delta\rho \tag{2.4.13}$$

$$t_{i+1} = t_i + \delta t \tag{2.4.14}$$

where V is the volume of the vessel (m³) and t is the discharge time (s). In order to obtain an equation to determine the decreasing of temperature inside the vessel, it is assumed reversible adiabatic outflow, thus the energy balance is:

$$\delta U = P.\delta V \tag{2.4.15}$$

The definition of the internal energy (U) according to its relationship between temperature and volume is shown in Equation 2.4.16 where C_V is the heat capacity at constant volume, J/kg.K (SANDLER, 1999).

$$U(T,V) = dU = C_V dT + \left[T\left(\frac{\partial P}{\partial T}\right)_V - P\right]dV \tag{2.4.16}$$

Considering ideal gas or simply neglecting the internal pressure of non-perfect gases, the relationship is simplified to:

$$\delta U = C_V(T)\delta T \tag{2.4.17}$$

Combining Equations 2.4.15 and 2.4.17 and using the definition of density, the change in temperature can be found as:

$$\delta T_i = \frac{P.\delta V}{C_V} = \frac{P_i}{C_V.\rho_i{}^2}\,\delta\rho \tag{2.4.18}$$

$$T_{i+1} = T_i + \delta T \tag{2.4.19}$$

Finally, as the gas is expanding and leaking from the hole, the amount of gas inside the vessel is reduced, and so is the pressure, according to the ideal gas law:

$$P_{i+1} = \frac{z_g.\rho_{i+1}.R_g.T_{i+1}}{MW} \tag{2.4.20}$$

Where R_g is the ideal gas constant (Pa.m³/mol.K), z_g is the compressibility factor and MW is the molecular weight of the substance (g/mol). In the case of discharge of gas in holes, the energy balance is integrated among the isentropic and adiabatic way and it is assumed, to calculus effect, that the gas is an ideal gas, and that there is no shaft work and no heat transfer (AICHE, 2000). For adiabatic gas flow, the relation shown by Equation 2.4.21 is valid:

$$PV^{\gamma} = P_1 V_1^{\gamma} \tag{2.4.21}$$

where γ is the heat capacity ratio (C_p/C_v). Using Equation 2.4.21 and the energy balance, Equation 2.4.22 is obtained:

$$Q_m = C_d.A_h.\psi.\sqrt{\rho_i.P_{0,i}.\gamma.\left(\frac{2}{\gamma+1}\right)^{(\gamma+1)/(\gamma-1)}} \tag{2.4.22}$$

where A_h is the hole area (m²), P_0 is the initial pressure inside the vessel (Pa) and ψ is an equation that depends on the type of flow. Equation 2.4.22 can be simplified to sonic velocities, because in such cases the flow is independent from the downstream pressure of the hole. The sonic flow (also known as the chocked flow) is reached when the downstream pressure is low enough so that the stream velocity of the fluid reaches the speed of sound, which is the maximum flow velocity possible (TNO, 2005). Mathematically speaking, the outflow is sonic when Equation 2.4.23 is valid:

$$\frac{P_0}{P_a} \geq \left(\frac{(\gamma+1)}{2}\right)^{\gamma/(\gamma-1)} \tag{2.4.23}$$

where P_a is the ambient pressure (Pa). Thus, for sonic outflow:

$$\psi^2 = 1 \tag{2.4.24}$$

and for subsonic outflow:

$$\psi^2 = \frac{2}{(\gamma-1)}.\left(\frac{(\gamma+1)}{2}\right)^{(\gamma+1)/(\gamma-1)}.\left(\frac{P_a}{P_0}\right)^{2/\gamma}.\left[1-\left(\frac{P_a}{P_0}\right)^{(\gamma-1)/\gamma}\right] \tag{2.4.25}$$

The iterative procedure for a full-bore ruptured pipeline is different from the emission of gas from a hole in a vessel. A full bore rupture is a total rupture of a pipeline, which generates a wave pressure that moves in the upstream (opposite) direction, as the pressure in the exact local of the rupture drops suddenly (TNO, 2005).

The Wilson empirical model is used to calculate such cases. The mass flow rate is calculated as follows:

$$Q_m(t) = \frac{Q_{m,0}}{(1+M_0/(t_B.Q_{m,0}))}.\left\{\frac{M_0}{t_B.Q_{m,0}}.exp\left(-\frac{t}{t_B}\right) + exp\left[-t.t_B\left(\frac{Q_{m,0}}{M_0}\right)^2\right]\right\} \quad (2.4.26)$$

where $Q_{m,0}$ is the initial mass flow rate (kg/s), M_0 is the initial total gas mass in the pipeline (kg) and t_B is the time constant (s). The initial mass flow rate is calculated with Equation 2.4.22, with the value of the discharge coefficient of 1.0. In order to calculate the time constant t_B, both sonic velocity of the gas and the Darcy friction factor must be determined. The sonic velocity of the gas, u_s (m/s), considering adiabatic expansion and a non-perfect gas is defined as shown in Equation 2.4.27:

$$u_s = \sqrt{\left(\frac{\mathcal{E}.z_g.R.T_0}{MW}\right)} \quad (2.4.27)$$

where ε is the internal roughness of the pipeline (m). The Darcy friction factor, f_D, can be calculated by the Colebrook-White equation used for high Reynolds number (TNO, 2005):

$$f_D = \left\{\frac{1}{-2.log(\mathcal{E}/(3.715.d_p))}\right\}^2 \quad (2.4.28)$$

where d_p is the pipe diameter (m). Finally, the time constant is given by Equation 2.4.29 where l_p is the pipe length (m) and the mass flow rate at any time can be calculated with Equation 2.4.26.

$$t_B = \frac{2}{3}.\frac{l_p}{u_s}.\sqrt{\frac{\gamma.f_D.l_p}{d_p}} \quad (2.4.29)$$

2.4.3 Two-phase discharge

The study of the two-phase discharge is extremely important, as the occurrence of two mutual phases in processes is really high. Any pressurized liquefied gas, for example, will flash during a release to the atmosphere, forming a two-phase flow.

As a pressurized liquefied gas is a liquid in thermodynamic equilibrium with its own vapour, the pressure must be the saturation pressure at a certain temperature (TNO, 2005). Following the same thought, as a pressurized liquefied gas is a two-phase system in equilibrium, its temperature must be along the saturation curve, between the critical and the triple point (Figure 5).

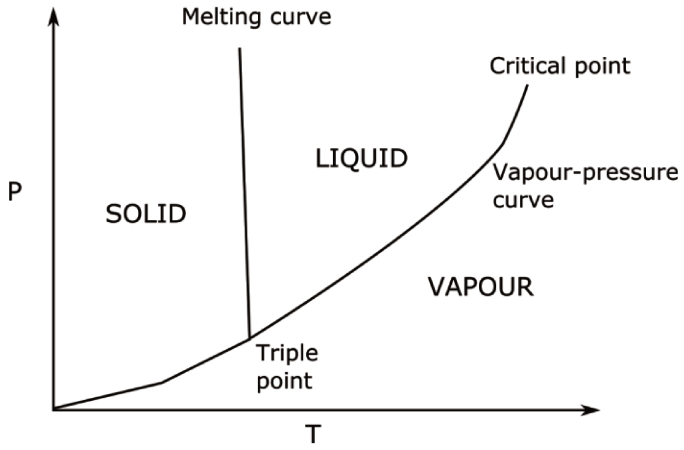

Figure 5. P-T phase diagram (Adapted from Sandler, 1999).

When launched to atmospheric pressure, a pressurized liquefied gas will suffer a flash process, which means that part of the liquid will become gas, and, this way, the leakage will occur in two phases. This occurs because of the sudden depressurization of the substance, which becomes superheated and tends to vaporise. The flashing process occurs initially as vaporisation nuclei. The bubble then starts to grow and bubble transport takes place (TNO, 2005). The bubble formation causes the "champagne-effect", in which the liquid tends to expand because of the bubbles.

As the release depends on the expansion of the liquid due to "champagne-effect", they must be considered when modelling a pressurized liquefied gas release. However, the "champagne-effect" is quite difficult to model as it is a complex phenomenon (TNO, 2005).

A complex analytical method developed by the American Institute of Chemical Engineers predicts the flow regime for two-phase flows. The model is called DIERS, which stands for Design Institute of Emergency Relief System. DIERS is a complex method but presents good agreements with data, therefore it is used for modelling. However, DIERS

was developed based on vertical right circular cylinders only. Fauske and Epstein (1988) also presented a model for predicting the two-phase flow, which is much simpler than the DIERS model and, according to Shepard (1994), the DIERS-model validates the Fauske correlation. Also, as the correlation was based on experimental data, it can be used for the modelling.

Fauske and Epstein (1988) first considered an all-liquid Bernoulli type flow, considering that the stagnation pressure is larger than the vapour pressure corresponding to the stagnation temperature. In this case, Equation 2.4.30 can be used to calculate the mass flow rate:

$$G_{sub} = C_d\sqrt{2\rho(P_0 + P_{sat})} \tag{2.4.30}$$

where G_{sub} is the subcooled mass flux (kg/m².s), C_d is the discharge coefficient, P_0 is the storage (or stagnation) pressure (Pa), P_{sat} is the saturation vapour pressure at ambient temperature (Pa) and ρ is the density of the liquid (kg/m³).

For saturated liquids, the equilibrium mass flux (G_{ERM}) in kg/m².s can be determined by:

$$G_{ERM} = \frac{h_{fg}}{v_{fg}}\left(\frac{1}{T.C_P}\right)^{1/2} \tag{2.4.31}$$

where h_{fg} is the enthalpy change in vaporisation (J/kg), v_{fg} is the specific volume change between liquid and vapour (m³/kg) and C_P is the heat capacity of the liquid (J/kg.K).

Fauske and Epstein (1988) have also taken into account the non-equilibrium effect in the two-phase flow. Based on experimental observations, they concluded that equilibrium was only reached for flow lengths greater than 0.1 m. For other lengths, as the length decreases, the liquid did not have time to flash, and the discharge would only be liquid. This observation was considered in the model by the definition of a non-equilibrium parameter N:

$$N = \frac{h_{fg}^2}{2\,\Delta P\,\rho {C_d}^2 v_{fg}^2 T C_P} + \frac{l_p}{L_c} \quad for\ 0 \le L \le L_c \tag{2.4.32}$$

where ΔP is the total available pressure drop (Pa), l_p is the pipe length (m), and L_c is the critical pipe length (m), usually 0.1 m.

The final mass flow rate is then obtained by Equation 2.4.33.

$$Q_m = A_h\sqrt{{G_{SUB}}^2 + \frac{{G_{ERM}}^2}{N}} \quad (2.4.33)$$

As in most cases, the CFD is also widely used to perform these calculations. As it deals with Navier-Stokes equations, as well as turbulence and energy balance, it is able to predict with accuracy the discharge rate for a two phase release, including the estimation of other parameters such as the velocity of both liquid and vapour phases and the droplet size. Calay and Holdo (2008), for instance, studied two phase discharge and dispersion in CFD. As CFD requires several initial boundary parameters for its calculation, they made use of empirical and semi-empirical correlations in order to determine them. The result of the use of empirical correlation as boundary conditions guidance was found to be satisfactory.

Other models are also used in two-phase discharge and dispersion. Witlox and Harper (2013) studied two phase dispersion in a Joint Industry Project of four phases. During this project, correlations for droplet size were proposed and validated with experiments. The correlation, which considered between other parameters the Weber number, was selected to be the default model of the latest version of *Phast*^{TM} (*Phast 6.7*), which is a commercial consequence analysis software (DNV-GL, 2015).

2.5 Flash and Evaporation

As already mentioned, a pressurized liquefied gas will suffer flashing process when released through the atmosphere. The resulting vapour will form a cloud and part of the liquid can also be present in this cloud, as an aerosol or as small droplets. If the discharge rate is high enough, it can also form a liquid pool in the surface next to the leakage.

If the liquid that leaks is not superheated, but it is still very volatile, the process that is most evident is the evaporation (AICHE, 2000). Thus, it is a great matter to determine the amount of liquid that will suffer flash or evaporation, in order to have an estimated value of the size of the formed cloud during these processes, which can eventually be either toxic or flammable. Figure 6 shows both cases: flash and evaporation phenomena.

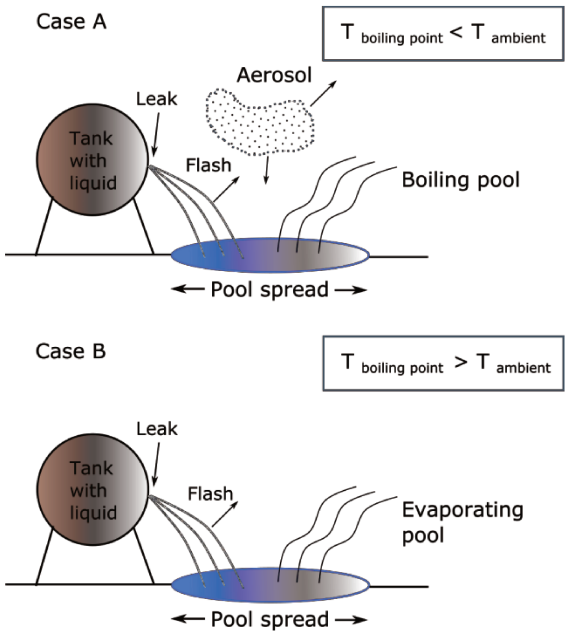

Figure 6. (A) Pressurized liquefied gas suffering flash and (B) liquid with high vapour pressure suffering evaporation (adapted from AICHE, 2000).

Crowl and Louvar (2011) developed a model to calculate the fraction of liquid mass that is vaporized in the flash, which is a function of the latent heat vaporization of the component, the initial and evaporation temperatures of the liquid and of its heat capacity. It is important to highlight that this value obtained is just an estimative of the total amount of material in the vapour cloud, since this value is influenced also by the amount of aerosol present in the cloud (AICHE, 2000).

The flashing process occurs so fast that it can be considered adiabatic, and therefore it is assumed that the energy of the superheated liquid vaporizes the liquid, lowering the temperature to a new boiling point. Equation 2.5.1 determines the fraction of liquid vaporised by flash:

$$f_v = \frac{C_P(T_0 - T_b)}{h_{fg}} \tag{2.5.1}$$

where f_v is the fraction of liquid vaporised, C_P is the heat capacity of the liquid, usually averaged over T_0 and T_b (J/kg.K), T_0 is the initial temperature of the liquid (K), T_b is the atmospheric boiling temperature of the liquid (K) and h_{fg} is the latent heat of vaporisation of the liquid at T_b (J/kg).

The presence of aerosol, which is more evident when the superheating of the liquid is not very high, affects directly in the characteristics of the vapour cloud formed. First, the density of the cloud increases, since the aerosol increases the amount of matter present in it. Second, it also decreases the temperature of the cloud until a value below the ambient temperature, which consequently increases the density of the cloud. Finally, a smaller temperature of the cloud can eventually condensate part of the humidity present in the air, which also affects the density of the cloud (AICHE, 2000).

In order to estimate the amount of aerosol formed, the common practice is to consider that it is the double of the amount of liquid that suffered the flashing process (AICHE, 2000).

In case of evaporation, the amount of liquid evaporated is determined by the amount of liquid in the pool formed in the surface and its energy balance. The area of the pool is, therefore, an important parameter to the calculation of the evaporated quantity of the substance. If there is a delimited space in which the liquid can flow and sufficient amount of liquid to fill this space, the area occupied by the liquid is simplified, because it is exactly the value delimited by such space. If there is not a physical delimitation, it is expected that the pool increases during time, considering that this increase is related directly with the roughness of the surface. In order to make the calculations of evaporation process easier, it is considered a constant liquid thickness in the pool, and this value is usually taken as 1 cm (AICHE, 2000). The vaporisation is given by the energy balance of the pool (Equation 2.5.2):

$$mC_p \frac{dT}{dt} = H_{flux} - L_{vap}\dot{m} \tag{2.5.2}$$

where m is the total mass of liquid in the pool (kg), T is the liquid temperature in the pool (K), t is the time (s), H_{flux} is the total heat flux (J/s), L_{vap} is the heat of vaporization of the liquid (J/kg) and $\dot{m}$ is the evaporation rate (kg/s).

The total heat flux accounts for the radiation, convection and conduction. Simplifications of Equation 2.5.2 can lead to simpler equations. For high volatile substances, it is possible to assume stationary state, and Equation 2.5.2 is reduced to:

$$\dot{m} = H_{flux}/L_{vap} \tag{2.5.3}$$

Considering only the heat transfer from the ground, the heat conduction can be obtained as:

$$q_g = \frac{k_s(T_g - T)}{(\pi \alpha_s t)^{1/2}} \quad (2.5.4)$$

where q_g is the heat flux from the ground (J/m².s), k_s is the thermal conductivity of the soil (J/m.s.K), T_g is the temperature of the ground (K), T is the temperature of the pool (K), α_s is the thermal diffusivity of the ground (m²/s) and t is the time after spill (s).

Assuming that the concentration of vapour in bulk surrounding gas is less than the saturation pressure gives:

$$Q_m = \frac{MW k_g A_{pool} P_{sat}}{R_g T_L} \quad (2.5.5)$$

where Q_m is the evaporation rate (kg/s), MW is the molecular weight of the substance (g/mol), k_g is the mass transfer coefficient (m/s), A_{pool} is the pool area (m²), P_{sat} is the saturation vapour pressure of the liquid (Pa), R_g is the ideal gas constant (Pa.m³/mol.k) and T_L is the temperature of the liquid (K).

The main issue of Equation 2.5.5 is the specification of the mass transfer coefficient. There are many correlations to calculate it, such as Equation 2.5.6:

$$k_g = k_g^0 \left(\frac{MW_0}{MW}\right)^{1/3} \quad (2.5.6)$$

where k_g^0 is a reference mass transfer coefficient (m/s) and MW_0 is the molecular weight of the reference (g/mol).

2.6 Dispersion models

After the leakage of a material, its dispersion in the ambient can occur in many different ways, but the dispersion is mainly considered as the dispersion of gas as a cloud through the atmosphere.

Seven factors are highly important in the cloud dispersion modelling: wind, atmospheric stability, ground conditions, source duration and its geometry, and momentum and buoyancy of the material. All factors affect directly the conditions of the dispersion of vapour clouds. The atmospheric stability is classified according the intensity of the

insulation, wind speed and vertical temperature gradient. During the day, for instance, the sun heats the surfaces and therefore the ground. This process makes the air just above the ground to get hotter. Unless the wind is able to remove the hotter air above the ground, the atmosphere would be classified as unstable, as vertical motions will occur, because the hotter air is below a layer of cold air (CROWL and LOUVAR, 2011). On the other hand, during the night this motion does not occur, which leads to a more stable atmosphere. From these factors, six categories of possible atmosphere stabilities were defined (A to F), called the Pasquill-stability classes, with the most stable class being the F class, and therefore the less stable class being the A class (AICHE, 2000). Figure 7 shows how each Pasquill stability categories are seen in terms of turbulence.

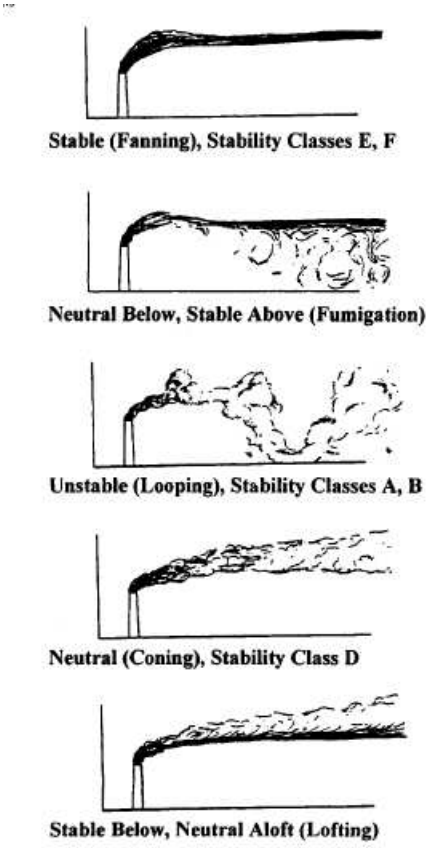

Figure 7. Pasquill stability classes (AICHE, 2000).

Atmospheric stability can be determined not only by the Pasquill-stability classes, but also by the Monin-Obukhov length. The Monin-Obukhov length can be calculated from routine meteorological data or from Pasquill stabilities categories (TNO, 2005). It takes

much information about the atmosphere in order to calculate the length by the first method: cloud cover, wind speed, temperature, roughness length, solar elevation and so one, so the second method could be a better estimative as it takes less effort. The Monin-Obukhov length is also important to calculate the wind speed profile along the height.

The turbulence of the air is also a determinant factor of the dispersion of a vapour or gas, as the presence of eddies are very effective in the dispersing process, 1000 times more effective than molecular diffusion (TNO, 2005). The turbulence can take place due to two main factors: first, because of the resistance of the earth's surface (represented by the earth's roughness), which causes a decrease of the wind speed near the surface. This causes flow instabilities and thus turbulence and it is called mechanical turbulence. The second factor is the heating of the surface, as already described above, namely thermal turbulence.

One important issue of the turbulence is the size of eddies. Eddies in the atmosphere can have hundreds of meters as well as millimetres. This influences hugely the dispersion of a vapour cloud. Large-sized eddies displace the puff without changing its size or geometry (TNO, 2005). However, eddies smaller than the dispersed puff tend to uniformly disperse the material and therefore increase the size of the puff. For a continuous release, the formed plume can also be influenced by eddies, as large ones can displace the centre-line of the plume and the concentration distribution.

The wind is also an important factor, as it influences the dilution of the cloud and also the stability of the atmosphere. The faster the wind, the faster the cloud will move in the wind direction, however, it will also suffer more dilution and the flammable gas cloud should have a greater volume, considering that the cloud is formed by a flammable substance. According to AICHE (2000), the wind speed is normally provided or calculated in a 10 meter height above the surface.

Another distinct characteristic of the dispersion phenomenon is the height of the release. The higher the release, the lower the concentration of the cloud near the ground, as it takes a longer distance for the cloud to reach the surface, and the cloud has more distance to mix with air. This is an important characteristic especially for toxic releases, as the concentration in the surface is the actual concentration that will affect humans and animals.

2.6.1 Neutral and positive buoyant

Neutral buoyant gases are the ones that have a density near the air density or lower concentration of gas (LEES, 2005). On the other hand, positive buoyant gases are the ones that have density or molecular weight lower than the air's, and also hot gases. The meaning of the positive buoyant cloud is that the inertial force and the buoyancy force act in the same direction. The most known and used model for the neutral and positive buoyant clouds dispersion is the Gaussian dispersion model. It has been verified by experiments that for a plume both crosswind and vertical concentrations distributions are almost Gaussian (LEES, 2005). Figure 8 shows the Gaussian dispersion for a continuous release from an elevated source.

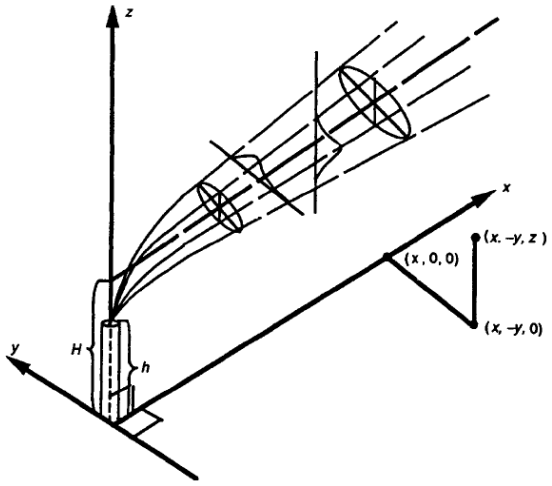

Figure 8. Gas dispersion model as a Gaussian distribution (AICHE, 2000).

Usually it is used the rectangular coordinates as seen in Figure 8 to obtain the concentration profile. The equation for diffusion of a gas is Equation 2.6.1:

$$\frac{dC}{dt} + u\frac{dC}{dx} + v\frac{dC}{dy} + w\frac{dC}{dz} = K_x\frac{d^2C}{dx^2} + K_y\frac{d^2C}{dy^2} + K_z\frac{d^2C}{dz^2} \qquad (2.6.1)$$

where x, y, z are the coordinates (m), K_x, K_y, K_z are the diffusion coefficients in x, y, z directions (m²/s), t is the time (s), u, v, w are the mean wind speeds in the x, y, z directions (m/s) and C is the concentration (kg/m³). Many works present different solutions of this equation and the main ones are described at Lees (2005). One of them is the Pasquill-Gifford model, which is one of the most important and known model for

dispersion using Gaussian model. For a puff (instantaneous release), the equation for the average concentration for a fixed coordinate system at the release point is shown below:

$$C(x,y,z) = \frac{Q}{(2\pi)^{3/2}\sigma_x\sigma_y\sigma_z}\, exp\left[-\frac{1}{2}\left(\frac{y}{\sigma_y}\right)^2\right].$$
$$\left\{exp\left[-\frac{1}{2}\left(\frac{z-H}{\sigma_z}\right)^2\right] + exp\left[-\frac{1}{2}\left(\frac{z+H}{\sigma_z}\right)^2\right]\right\}. exp\left[-\frac{1}{2}\left(\frac{x-ut}{\sigma_x}\right)^2\right] \quad (2.6.2)$$

and for a plume:

$$C(x,y,z) = \frac{Q_m}{2\pi\sigma_x\sigma_y u}\, exp\left[-\frac{1}{2}\left(\frac{y}{\sigma_y}\right)^2\right].\left\{exp\left[-\frac{1}{2}\left(\frac{z-H}{\sigma_z}\right)^2\right] + exp\left[-\frac{1}{2}\left(\frac{z+H}{\sigma_z}\right)^2\right]\right\} \quad (2.6.3)$$

where $C(x,y,z)$ is the concentration (g/m³), Q is the total mass released (g), Q_m is the mass flow rate (g/s), σ_x, σ_y and σ_z are the dispersion coefficients in the x, y and z directions (m), x is the downwind direction (m), y is the crosswind direction (m), z is the distance above ground (m), H is the release height above ground (m), u is the wind velocity (m/s) and t is the time (s). The dispersion coefficients are available in tables in the literature for both puff and plume, depending on the stability class of the atmosphere (Table 1 and Table 2, respectively).

Table 1. Dispersion coefficients for Pasquill-Gifford stability classes for puffs (AICHE, 2000), according to the downwind direction in meters ($\boldsymbol{x}$).

Pasquill-Gifford stability class	**σ_y or σ_x (m)**	**σ_z (m)**
A	$0.18x^{0.92}$	$0.60x^{0.75}$
B	$0.14x^{0.92}$	$0.53x^{0.73}$
C	$0.10x^{0.92}$	$0.34x^{0.71}$
D	$0.06x^{0.92}$	$0.15x^{0.70}$
E	$0.04x^{0.92}$	$0.10x^{0.65}$
F	$0.02x^{0.89}$	$0.05x^{0.61}$

Table 2. Dispersion coefficients for Pasquill-Gifford stability classes for plumes (AICHE, 2000), according to the downwind direction in meters (x).

Pasquill-Gifford stability class	σ_y or σ_x (m)	σ_z (m)
	Rural conditions	
A	$0.22x(1+0.0001x)^{-1/2}$	$0.20x$
B	$0.16x(1+0.0001x)^{-1/2}$	$0.12x$
C	$0.11x(1+0.0001x)^{-1/2}$	$0.08x(1+0.0002x)^{-1/2}$
D	$0.08x(1+0.0001x)^{-1/2}$	$0.06x(1+0.0015x)^{-1/2}$
E	$0.06x(1+0.0001x)^{-1/2}$	$0.03x(1+0.0003x)^{-1}$
F	$0.04x(1+0.0001x)^{-1/2}$	$0.016x(1+0.0003x)^{-1}$
	Urban conditions	
A-B	$0.32x(1+0.0004x)^{-1/2}$	$0.24x(1+0.001x)^{+1/2}$
C	$0.22x(1+0.0004x)^{-1/2}$	$0.20x$
D	$0.16x(1+0.0004x)^{-1/2}$	$0.14x(1+0.0003x)^{-1/2}$
E-F	$0.11x(1+0.0004x)^{-1/2}$	$0.08x(1+0.0015x)^{-1/2}$

A disadvantage of such model is that the concentration obtained by the calculation is an average time concentration. That means that some local concentrations can be greater than the calculated value, which is a relevant data when working with toxic or flammable materials.

The distance from the release in which one wants to know the concentration is a factor that must be taken into consideration, as well as the duration of the release, in order to define weather the release is instantaneous (and will form a puff) or continuous (plume).

If the distance from the release is too large, the release can be considered as a puff, because when it reaches the location of interest, it will appear as a great puff. Also, if the duration of the leak is short compared to the travel time, or even less than 10 minutes, it is also considered a puff (AICHE, 2000). Lees (2005) presents a criterion for defining the type of release, which was a work from Eisenberg *et al*. (1975). The criterion is based on

the dispersion coefficient in the downwind (x-axis in Figure 8) direction for a puff and it is stated as follows:

$$ut_c < 2\sigma_x \rightarrow Use\ puff\ model \quad (2.6.4)$$

$$ut_c > 5\sigma_x \rightarrow Use\ plume\ model \quad (2.6.5)$$

$$2\sigma_x < ut_c < 5\sigma_x \rightarrow Neither\ model\ entirely\ appropriate \quad (2.6.6)$$

where t_c is the time taken for total discharge (s).

It is also possible to determine isopleths for a certain concentration (Equation 2.6.7). Isopleths are interesting for knowing the frontier limits for a toxic gas, for example, or even for a flammable mass within its flammability limits.

$$y = \sigma_y \sqrt{2ln\left(\frac{C(x,0,0,t)}{C_{isopleth}}\right)} \quad (2.6.7)$$

where y is the off-centre distance to the isopleth (m), $C(x,0,0,t)$ is the downwind centreline concentration (g/m³) and $C_{isopleth}$ is the concentration at the isopleths (g/m³).

There are other models that perform the dispersion of a substance through the atmosphere, some of those more accurate than the ones showed above. A recent study performed by Kakosimos and Assael (2013), for example, developed a model for the simulation of toxic gas dispersion by using eddy simulation and finite element model.

However, there are still recent studies performed with Gaussian models. Lisboa *et al.* (2006) developed equations based on Gaussian models to predict odour dispersion. Jung *et al.* (2003) also used Gaussian models for predicting the behaviour of pollutant substances in Russia, and the conclusion was that the concentration predicted by plume and puff models agrees well with experiments.

2.6.2 Dense vapour cloud

For a gas be considered dense, its density must be greater than the density of the ambient in which the gas is dispersed, and this can be caused by a greater molecular weight than the ambient, by a gas temperature smaller than the ambient temperature or by the formation of aerosol in the cloud of gas. Examples of volatile substances that can be considered dense gases are: LPG (liquid petroleum gas), cyclohexane, chlorine, Freon, ammonia and hydrogen fluoride, as listed in TNO (2005).

According to TNO (2005), right after a dense gas has been released, four phases are observed regarding its dispersion (Figure 9). First, the fluid motion is mainly a function of the release conditions and the entrainment of air practically does not occur. The second phase corresponds to the gravity spreading phase. In this phase, the gravity force makes the cloud to move and therefore generates turbulence, which causes the entrainment of air, spreading the cloud. In this phase, the mixing with the atmosphere is due to self-generated eddies at the edge of the cloud. In the third phase, the turbulence is due to not only the gravity, but also the atmospheric turbulence itself. Finally, the fourth and last phase occurs when the cloud does not present a dense behaviour anymore because of its dilution with air, and so it can be considered as a neutrally buoyant gas.

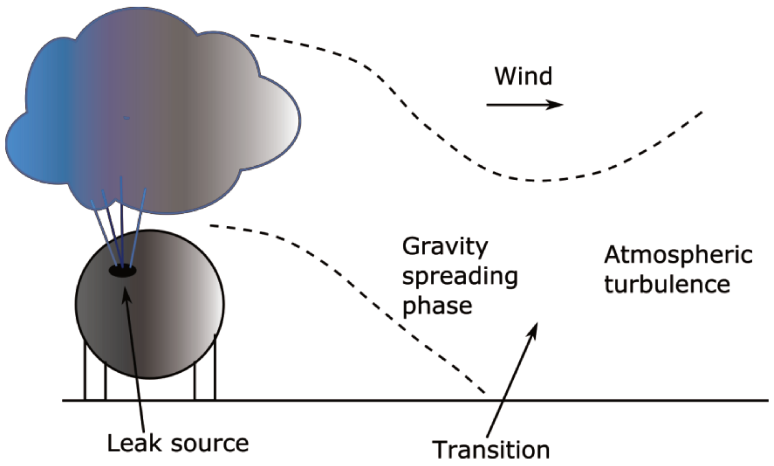

Figure 9. Dense gas dispersion behaviour after release puffs (adapted from AICHE, 2000).

The importance of studying dense gas dispersion, especially for toxic substances is because of its characteristic of remaining in the lower part of the atmosphere and its large spreading in the lateral direction, which means that it remains mainly in the region where humans can be affected. Because of the great difference of behaviour of a dense cloud compared to a neutral or positive buoyant cloud, it is not possible to use the Gaussian model in such cases. This model can only be used in such cases after the dilution of the cloud, when the atmospheric turbulence is predominant (AICHE, 2000).

Britter and McQuaid (1988) presented a model to estimate the concentration profile of a dense gas dispersion. The model from Britter and McQuaid consists of empirical

correlations with the following assumptions: the release is assumed to occur in ambient temperature, it was not considered the presence of aerosol or liquid droplet and the atmospheric stability does not impact the results, therefore it was not considered in the modelling. To start using the Britter and McQuaid model, first it is needed to prove that the model is suited for the study case, which depends on the type of release. Continuous dense gas releases are the ones that follow the rule:

$$\frac{uR_d}{x} \geq 2.5 \tag{2.6.8}$$

and instantaneous dense gas releases are the ones that correspond to the following equation:

$$\frac{uR_d}{x} \leq 0.6 \tag{2.6.9}$$

where R_d is the release duration (s). If the value is between 0.6 and 2.5, it is recommended to calculate the dispersion by both models and then use the maximum concentration obtained. The initial buoyancy is defined as:

$$g_0 = g(\rho_0 - \rho_a)/\rho_a \tag{2.6.10}$$

where g_0 is the initial buoyancy factor (m/s²), g is the gravity acceleration (m/s²), ρ_a is the density of the ambient air (kg/m³) and ρ_0 is the density of the released material (kg/m³).

The characteristic source dimension is, for continuous releases (Equation 2.6.11) and instantaneous releases (Equation 2.6.12):

$$D_c = \left(\frac{q_0}{u}\right)^{0.5} \tag{2.6.11}$$

$$D_i = V_0^{1/3} \tag{2.6.12}$$

where D_c and D_i are the characteristic source dimension (m), q_0 is the material volume flux (m³/s) and V_0 is the initial volume of released gas material (m³).

Finally, the criterion for the applicability of the Britter and McQuaid model is, for continuous releases and instantaneous releases, respectively:

$$\left(\frac{g_0 q_0}{u^3 D_c}\right)^{1/3} \geq 0.15 \tag{2.6.13}$$

$$\left(\frac{\sqrt{g_0 V_0}}{u\, D_i}\right)^{1/3} \geq 0.20 \tag{2.6.14}$$

If they are satisfied, the diagrams of Figure 10 (or Table 3 and Table 4) can be used to obtain the concentration C_m.

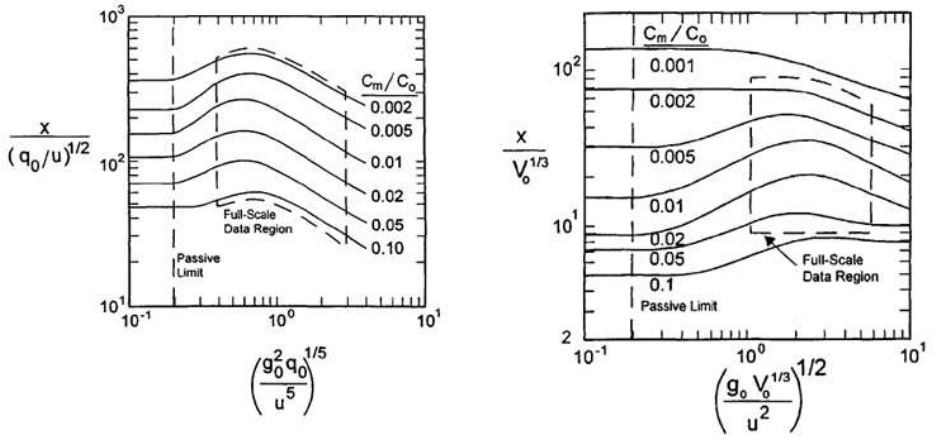

Figure 10. Britter and McQuaid charts for the calculation of the profile concentration of dense gases for (a) instantaneous and (b) puff releases (AICHE, 2000).

Table 3. Approximation of curves of the model of Britter and McQuaid for plumes (AICHE, 2000).

Concentration ratio C_m/C_0	**Valid range for** $\alpha = log\left[\frac{g_0^2 \cdot q_0}{(u)^5}\right]$	**Equations for** $\beta = log\left[\frac{x}{(\frac{q_0}{u})^{1/2}}\right]$
0.1	$\alpha \leq -0.55$	$\beta = 1.75$
0.1	$-0.55 < \alpha \leq -0.14$	$\beta = 0.24\alpha + 1.88$
0.1	$-0.14 < \alpha \leq 1.0$	$\beta = 0.50\alpha + 1.78$
0.05	$\alpha \leq -0.68$	$\beta = 1.92$
0.05	$-0.68 < \alpha \leq -0.29$	$\beta = 0.36\alpha + 2.16$
0.05	$-0.29 < \alpha \leq -0.18$	$\beta = 2.06$
0.05	$-0.18 < \alpha \leq -1.0$	$\beta = -0.56\alpha + 1.96$
0.02	$\alpha \leq -0.69$	$\beta = 2.08$
0.02	$-0.69 < \alpha \leq -0.31$	$\beta = 0.45\alpha + 2.39$
0.02	$-0.31 < \alpha \leq -0.16$	$\beta = 2.25$
0.02	$-0.16 < \alpha \leq 1.0$	$\beta = -0.54\alpha + 2.16$
0.01	$\alpha \leq -0.70$	$\beta = 2.25$
0.01	$-0.70 < \alpha \leq -0.29$	$\beta = 0.49\alpha + 2.59$
0.01	$-0.29 < \alpha \leq -0.20$	$\beta = 2.45$
0.01	$-0.20 < \alpha \leq 1.0$	$\beta = -0.52\alpha + 2.35$

Concentration ratio C_m/C_0	Valid range for $\alpha = log\left[\frac{g_0^2 \cdot q_0}{(u)^5}\right]$	Equations for $\beta = log\left[\frac{x}{(\frac{q_0}{u})^{1/2}}\right]$
0.005	$\alpha \leq -0.67$	$\beta = 2.40$
0.005	$-0.67 < \alpha \leq -0.28$	$\beta = 0.59\alpha + 2.80$
0.005	$-0.28 < \alpha \leq -0.15$	$\beta = 2.63$
0.005	$-0.55 < \alpha \leq 1.0$	$\beta = -0.49\alpha + 2.56$
0.002	$\alpha \leq -0.69$	$\beta = 2.60$
0.002	$-0.69 < \alpha \leq -0.25$	$\beta = 0.39\alpha + 2.87$
0.002	$-0.25 < \alpha \leq -0.13$	$\beta = 2.77$
0.002	$-0.13 < \alpha \leq 1.0$	$\beta = -0.50\alpha + 2.71$

Table 4. Approximation of curves of the model of Britter and McQuaid for puffs (AICHE, 2000).

Concentration ratio C_m/C_0	Valid range for $\alpha = log\left[\frac{g_0 . V_0^{\frac{1}{3}}}{(u)^2}\right]$	Equations for $\beta = log\left[\frac{x}{V_0^{1/3}}\right]$
0.1	$\alpha \leq -0.44$	$\beta = 0.70$
0.1	$-0.44 < \alpha \leq 0.43$	$\beta = 0.26\alpha + 0.81$
0.1	$0.43 < \alpha \leq 1.0$	$\beta = 0.93$
0.05	$\alpha \leq -0.56$	$\beta = 0.85$
0.05	$-0.56 < \alpha \leq 0.31$	$\beta = 0.26\alpha + 1.0$
0.05	$0.31 < \alpha \leq -1.0$	$\beta = -0.12\alpha + 1.12$
0.02	$\alpha \leq -0.66$	$\beta = 0.95$
0.02	$-0.66 < \alpha \leq -0.32$	$\beta = 0.36\alpha + 1.19$
0.02	$-0.32 < \alpha \leq 1.0$	$\beta = -0.26\alpha + 1.38$
0.01	$\alpha \leq -0.71$	$\beta = 1.15$
0.01	$-0.71 < \alpha \leq 0.37$	$\beta = 0.34\alpha + 1.39$
0.01	$0.37 < \alpha \leq 1.0$	$\beta = -0.38\alpha + 1.66$
0.005	$\alpha \leq -0.52$	$\beta = 1.48$
0.005	$-0.52 < \alpha \leq 0.24$	$\beta = 0.26\alpha + 1.62$
0.005	$0.24 < \alpha \leq 1.0$	$\beta = -0.30\alpha + 1.75$
0.002	$\alpha \leq 0.27$	$\beta = 1.83$
0.002	$0.27 < \alpha \leq 1.0$	$\beta = -0.32\alpha + 1.92$
0.001	$\alpha \leq -0.10$	$\beta = 2.075$
0.001	$-0.10 < \alpha \leq 1.0$	$\beta = -0.27\alpha + 2.05$

2.7 Flammable mass

For flammable materials, an important parameter after defining the concentration profile of a vapour cloud is to determine how much of the total mass of the cloud can ignite in case an ignition source exists. The mass that can catch fire is only the one between the flammable limits. The lower (LFL) and upper (UFL) flammability limits are concentrations of fuel that determine the limit frontier of flammable concentrations.

It is important to point out that the total flammable mass within the flammability limits changes as the dispersion time grows. For an instantaneous release, for example, initially low amount of mass is flammable, because the concentration of the fuel is too high and there is no sufficient air entrainment. As the air begins to mixture with the cloud, the amount of mass within the flammability limits increase, until a certain time where the cloud is so diluted that it is no longer flammable (Figure 11).

Lees (2005) presents a model to calculate the total flammable mass of a cloud for a puff (Equations 2.7.1 and 2.7.2) and for a plume (Equation 2.7.3).

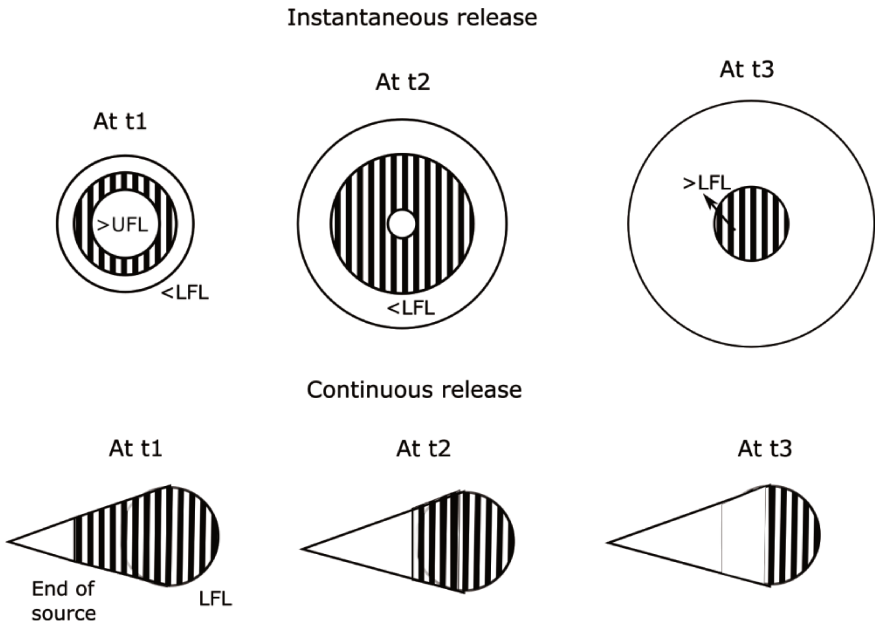

Figure 11. Flammable regions for puffs (instantaneous) and plumes (continuous) clouds at different times after the release of the material (adapted from WOODWARD, 1998).

$$\frac{Q_{flam}}{Q} = erf\left[\left(ln(\frac{C_{cc}}{C_{LFL}})\right)^{1/2}\right] - erf\left[(ln(C_{cc}/C_{UFL}))^{1/2}\right] - \frac{2C_{LFL}}{C_{cc}\sqrt{\pi}}\left[(ln(C_{cc}/C_{LFL}))^{1/2}\right] + \frac{2C_{UFL}}{C_{cc}\sqrt{\pi}}\left[\left(ln(\frac{C_{cc}}{C_{UFL}})\right)^{1/2}\right] \quad if\ C_{cc} > C_{UFL} \tag{2.7.1}$$

$$\frac{Q_{flam}}{Q} = erf\left[(ln(C_{cc}/C_{LFL}))^{1/2}\right] - \frac{2C_{LFL}}{C_{cc}\sqrt{\pi}}\left[\left(ln(C_{cc}/C_{LFL)}\right)^{1/2}\right] \ if\ C_{cc} < C_{UFL} \tag{2.7.2}$$

$$Q_{flam} = \left(\frac{1}{\pi.D}\right)^{1/f} \cdot \frac{f}{f+1} \cdot \left(\frac{Q_m}{u}\right)^{(f+1)/f} \cdot \left(\frac{1}{{C_{LFL}}^{1/f}} - \frac{1}{{C_{UFL}}^{1/f}}\right) \tag{2.7.3}$$

where Q_{flam} is the flammable mass (mg), C_{cc} is the concentration in the centre of the cloud (mg/m³), C_{LFL} is the lower flammability limit concentration (mg/m³), C_{UFL} is the upper flammability limit concentration (mg/m³), u is the wind speed (m/s), Q_m is the mass flow rate (mg/s) and f and D are meteorological parameters of Marshall's equation for the Pasquill stability classes (Table 5).

In case is important to also know the flammable volume, it must be calculated with Equation 2.7.4:

$$V_{flam} = \frac{Q_{flam}}{\rho C_s} \tag{2.7.4}$$

where C_s is the stoichiometric concentration with air (%vol), which can be found in literature (TNO, 2005).

Table 5. Meteorological parameters of Marshall's equation (LEES, 2005).

Pasquill	**Parameters**	
Stability Class	***D***	***f***
A	3.06×10^{-3}	2.4
B	1.38×10^{-3}	1.9
C	8.9×10^{-3}	1.8
D	6.0×10^{-3}	1.7
E	3.88×10^{-3}	1.7
F	1.43×10^{-3}	1.7

2.8 Gas Explosion

According to AICHE/CCPS (1994), quoted by AICHE (2000), the definition of explosion is: "*release of energy that causes a transient change in the density and in the pressure of the gas and in the velocity of the air that surrounds the point of explosion*".

Basically an explosion is a phenomenon that happens when a pre-mixed gas cloud of fuel and air meets an ignition source, causing rapid increase in pressure. However, not every pre-mixed cloud will explode in the presence of an ignition source. For that to happen, the cloud must have a concentration within its flammability limits, which means that the concentration must be higher than the lower flammability limit (LFL), and also lower than the upper flammability limit (UFL).

Flammability limits have been mostly determined by empirical relations that fit experimental results, and they are used worldwide, despite the lack of theory involved. Benedetto (2013) presented an approach to calculate the flammability limits using thermodynamics. He took in consideration the fact that the flame does not propagate outside the limits because the heat from the reaction cannot compensate the losses of heat of the flame due to convection and radiation. Thus, the unburnt gases are not pre-heated so they cannot reach the ignition temperature, and the flame does not propagate. The result of his study is that the flammable limits determined experimentally depend highly on the experimental apparatus and conditions, and therefore suggests the use of the thermodynamic model to determine their values.

The flame of an explosion is the region where the combustion reaction takes place. When an explosion occurs, the products of the combustion are formed. Because the reaction is exothermic, the temperature will increase and the gas will expand by a factor of 8 or 9 (BJERKETVEDT *et al.*, 1997). This expansion causes a shock wave to be formed, in the direction of the unburnt gases, which are pushed ahead of the flame. This movement causes turbulence, especially in the presence of obstacles. Finally, the turbulence tends to wrinkle the flame front, which enlarges the surface area of the reaction, causing the burning rate to increase. A diagram of this positive feedback loop is presented in Figure 12.

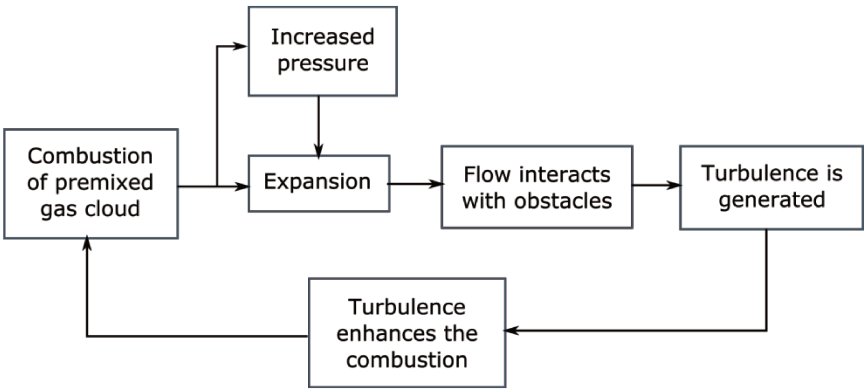

Figure 12. Explosion mechanism (adapted from BJERKETVEDT *et al.*, 1997).

There are two types of explosions: detonation and deflagration. A detonation is an explosion where the blast wave is immediately followed by the flame (reaction zone), and the blast wave propagates with a supersonic velocity (greater than the speed of sound). Detonation causes higher overpressures than deflagrations, and therefore also greater damages. It can be either caused by an explosion of a high explosive charge (TNT, for example) or by the transition of a deflagration to a detonation due to the great level of confinement and obstacles in the ambient where the explosion takes place. In a deflagration, on the other hand, the blast wave propagates ahead of the flame with a velocity below sonic velocity.

The importance of studying explosions is the possibility of predicting the value of the resultant overpressure and whether there is the possibility of forming missiles or not, as both can damage the industrial plant, the environment surrounding the plant and have direct connection in risk and accidents' effects, as already mentioned in Section 2.3.

The overpressure is also known as the peak side-on overpressure. The name is explained through the phenomenon of the blast wave, which is characterized by the positive phase duration, the positive impulse and the negative duration phase. The first phase takes place right after the blast wave is generated and it is the greatest peak of overpressure from the explosion. The duration of this phase is called positive phase duration time, which ends when the pressure reaches the ambient pressure, and the impulse is the area under the curve of this phase. After the peak of overpressure, the pressure tends to decay more than the ambient pressure. The shape of idealized blast waves is shown in Figure 13, according to

the type of explosion (deflagration or detonation). Most models characterize the explosion by the positive phase, which means that usually the negative phase is not evaluated (VAN DEN BERG and LANNOY, 1993).

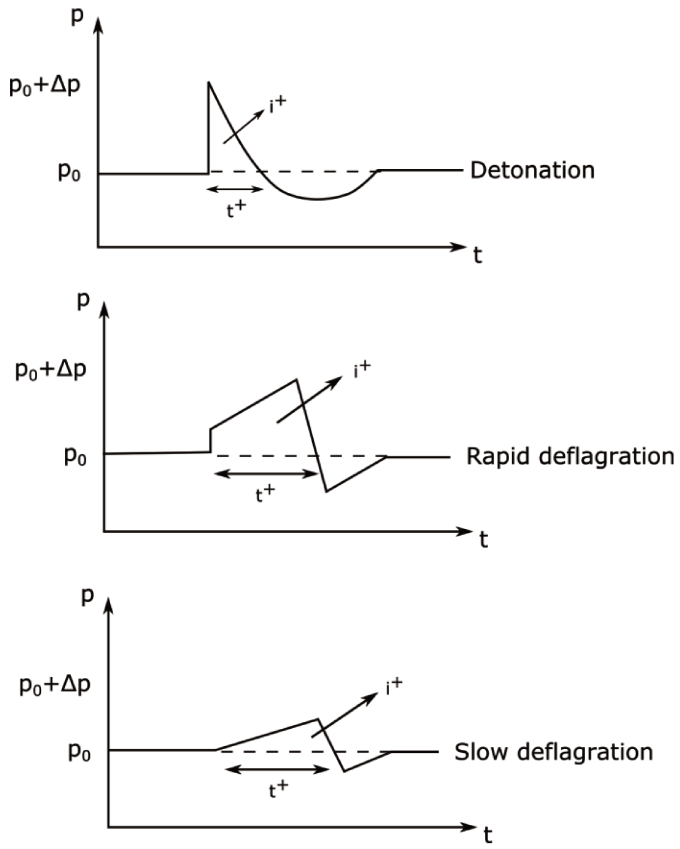

Figure 13. Blast wave profile overpressure (adapted from VAN DEN BERG and LANNOY, 1993).

2.8.1 Vapour Cloud Explosion (VCE)

Vapour cloud explosion occurs when the vapour cloud formed after the leakage is between the lower and upper flammability limits of the material and it suffers ignition. Mostly VCE are deflagrations, but they can be transformed to detonations if the congestion and obstacles degrees are high, causing great turbulence. This phenomenon is known by the DDT (Deflagration to Detonation Transition). Lenoir and Davenport (1993) published a list with all reported VCE accidents in the 1980's decade. It was observed that although the number of VCEs had been reduced, it represented 37% of number of property losses greater

than $50 million. In addition, from the 10 largest property losses, 7 of them were caused by VCE. This information shows the importance of studying VCEs.

As already mentioned, a vapour cloud explosion phenomenon is very complex and depends on many parameters, which makes the analysis hard. Not only congestion and obstacles degree are crucial for determining the magnitude of the explosion, but several other characteristics influence it, such as energy of ignition source, local of ignition source, type of fuel, total amount of flammable material, presence of venting and local and size of the venting. All play an important role in the phenomenon of explosion.

An ideal explosion model would be the one that takes into account all of these parameters in the calculation of the overpressure generated by the explosion. However, as the phenomenon is very complex, it is almost impossible to develop such model. In order to obtain an estimative of the overpressure, simpler approaches have been made during the development of explosion models, and the models here presented are the most used ones in consequence analysis.

The simplest model still used nowadays and present in consequence analysis simulators like *Phast*^{TM} (DNV-GL, 2015) is the TNT equivalence model. This model is based on the comparison between the fuel of interest and TNT. The flammable mass of the fuel that will generate the VCE is converted to an equivalent in mass of TNT, as stated by the Equation 2.8.1 below:

$$W = \frac{\eta_{TNT} \cdot Q_{flam} \cdot E_c}{E_{c,TNT}} \tag{2.8.1}$$

where W is the equivalent in mass of TNT (kg), Q_{flam} is the total flammable mass of the fuel (kg), E_c is the heat of combustion of the fuel (kJ/kg), $E_{c,TNT}$ is the heat of combustion of TNT (4437-4465 kJ/kg) and η_{TNT} is an empirical explosion efficiency (usually from 2 to 20%).

The model also defines a scaled distance (Equation 2.8.2):

$$Z = \frac{x_{blast}}{W^{1/3}} \tag{2.8.2}$$

where Z is the scaled distance (m/kg³) and x_{blast} is the distance from the blast (m). Finally, charts are used to estimate overpressures, as shown in Figure 14. For

computational studies, the curves in the chart of Figure 14 have been adjusted for a function, and the result is shown in Table 6.

Despite being used until nowadays and provide a quick and conservative estimative of the overpressure, the TNT model has also disadvantages. First, it compares the VCE of gases, which is almost always a deflagration, with the explosion of TNT, which is a detonation. It means that it does not take into account the differences between both types of VCE, some of them shown in Figure 13. Also because of that, its estimative usually provides higher values of overpressures than the real values in the near field, and lower values in the far field, mainly because of the detonation phenomenon. This means that usually the overpressure is overestimated in the near field and underestimated in the far field. Second, the TNT model is very dependent on the explosion efficiency parameter, which is hard to determine.

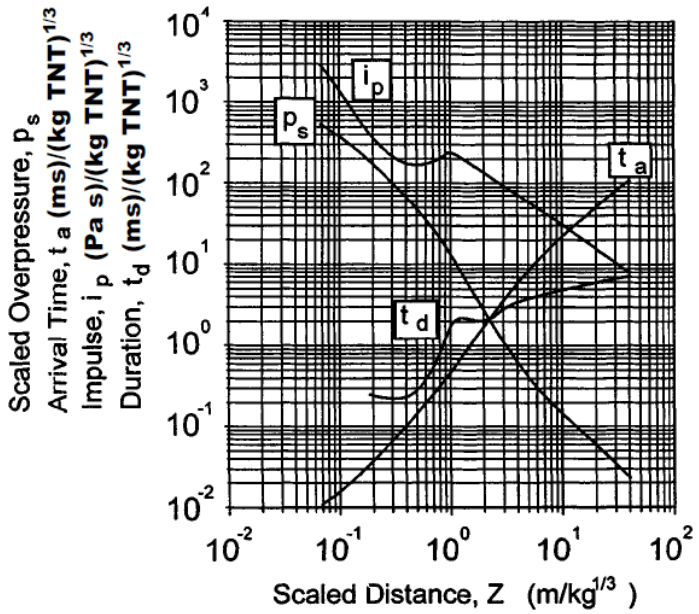

Figure 14. Blast characteristics for TNT model (AICHE, 2000).

Table 6. Parameters for the blast characteristic for the TNT Equivalency model (AICHE, 2000).

Parameter	Range	Function: $log\phi = \sum_{i=0}^{n} c_i(a + b.\log Z)^i$ (where ϕ is the function of interest)		
		Overpressure (kPa)	Impulse (Pa.s)	Duration time (ms)
	1	$0.0647 \leq Z \leq 40$	$0.0647 \leq Z \leq 0.955$	$0.178 \leq Z \leq 1.01$
	2		$0.0955 \leq Z \leq 40$	$1.01 \leq Z \leq 2.78$
	3			$2.78 \leq Z \leq 40$
	1	-0.21436278915	2.06761908721	1.92946154068
a	2		-1.94708846747	-2.12492525216
	3			-3.53626218091
	1	1.35034249993	3.076032966	5.25099193925
b	2		2.40697745406	9.2996288611
	3			3.46349745571
	1	2.78076916577	2.52455620925	-0.614227603559
c_0	2		1.67281645863	0.315409245784
	3			0.686906642409
	1	-1.6958988741	-0.502992763686	0.130143717675
c_1	2		-0.384519026965	-0.0297944268976
	3			0.0933035304009
	1	-0.154159376846	0.171335645235	0.134872511954
c_2	2		-0.0260816706301	0.030632955288
	3			-0.0005849420883
	1	0.514060730593	0.0450176963051	0.0391574276906
c_3	2		0.0059579875382	0.0183405574086
	3			-0.00226884995013
	1	0.0988554365274	-0.0118964626402	-0.00475933664702
c_4	2		0.014544526107	-0.0173964666211
	3			-0.00295908591505

Parameter	Range	Function: $log\phi = \sum_{i=0}^{n} c_i(a + b.\log Z)^i$ (where ϕ is the function of interest)		
		Overpressure (kPa)	Impulse (Pa.s)	Duration time (ms)
c_5	1	-0.293912623038		-0.00428144598008
	2		-0.00663289334734	-0.00106321963633
	3			0.0014029868929
c_6	1	-0.0268112345019		
	2		-0.00284189327204	0.00562060030977
	3			
c_7	1	0.109097496421		
	2		0.0013644816227	0.0001618217499
	3			
c_8	1	0.00162846756311		
	2			-0.0006860188944
	3			
c_9	1	-0.0214631030242		
	2			
	3			
c_{10}	1	0.0001456723382		
	2			
	3			
c_{11}	1	0.00167847752266		
	2			
	3			

An improved model was described in a work of Van den Berg (1985) and is known as the TNO Multi-Energy model. The model assumes a hemispherical cloud with stoichiometric concentration and a constant flame speed. The main purpose of the model is to include some external factors that influence the generated overpressure of a VCE. One of

them is the confinement of the cloud and the presence of obstacles. As many degrees of confinement can exist, it was defined 10 blast strengths that depend not only on the degree of confinement, but also on the nature of the fuel involved. Number 1 blast is an insignificant strength, and 10 is a gaseous detonation. Another interesting idea of the method is the fact that it is possible to have more than one centre of explosion for the same cloud, and only the flammable mass inside the obstructed area participates in the explosion. This is an interesting feature of the model, as parts of the cloud can produce blasts of different strengths.

In order to calculate the overpressure with TNO Multi-Energy model, first the Sachs-Scaled distance is obtained from Equation 2.8.3:

$$R = \frac{x_{blast}}{(E/P_a)^{1/3}} \tag{2.8.3}$$

where R is the Sachs-Scaled distance, x_{blast} is the distance from the blast (m), E is the total heat of combustion (J) and P_a is the ambient pressure (Pa). The total heat of combustion E is calculated as follows:

$$E = V_{flam}.E_c \tag{2.8.4}$$

where V_{flam} is the flammable volume of the cloud (m³) obtained by the dispersion modelling and E_c is the heat of combustion, which is approximated to 3.5×10^6 J/m³ for all hydrocarbons. The dimensionless peak side-on overpressure is then obtained by a chart (Figure 15), and the actual overpressure is the multiplication of the dimensionless overpressure by the ambient pressure.

Alonso *et al.* (2006) used the curves from the Multi-Energy method to develop equations called "characteristic curves" that fitted the curves. With these equations it is possible to relate overpressure and impulse to the distance from the blast, which is very useful for computational studies.

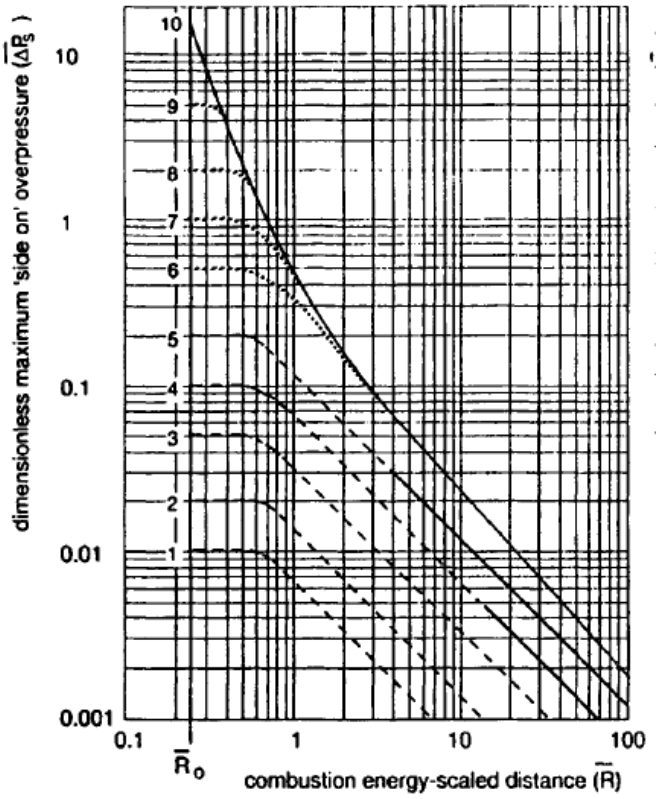

Figure 15. Dimensionless peak side-on overpressure of TNO Multi-Energy model according to the blast strengths (AICHE, 2000).

The advantages of this model is that it is much more realistic than the TNT model, as it considers that unconfined explosions do not occur, the degree of confinement and admits more than one centre of explosion for a single cloud. The main disadvantage is that it depends on the choice of the blast strength. Works have been done in order to make this choice easier. Raman and Grillo (2005) applied the TNO Multi-Energy method in two configurations of offshore installations and calibrated the blast strengths with CFD data. The CFD result was carried out and after that it was studied the Multi-Energy method. The volume of the cloud that participates in the explosion was calculated with the use of the layout plant, and the blast strength which gave the nearest value as the CFD result was established. Finally, it was concluded that the rule developed by Kinsella (1993) works well in determining which blast strength is the most adequate for each case (Table 7).

Table 7. Blast strength rule for the Multi-Energy model (Raman and Grillo, 2005).

Category	High congestion	Low congestion	Parallel plane confinement	Unconfined (grated deck)	Multi-Energy initial blast strength
1	√		√		5 – 7
2	√			√	4 – 5
3		√	√		3 – 5
4		√		√	2 - 3

Pitblado *et al.* (2014) developed a guide on how to better use the TNO Multi-Energy model. They specified rules for a series of factors, like the flammable cloud volume and composition, and also defined which equipments and structures should be considered as a congested volume for the overpressure calculation of an explosion. Also, in order to define if a certain volume of cloud can originate a blast centre, it was defined a minimum separation distance of 9.1 m between congested volumes that might have each one a blast centre.

Finally, the Baker-Strehlow is another VCE model used nowadays. This model was developed from a series of numerical studies using a modified form of *CLOUD* program to calculate the blast wave of a spherical source region containing fuel-air mixture and assuming that this mixture is centrally ignited and the flame that propagates has a constant velocity (STREHLOW *et al.*, 1979). The studies were conducted to determine the nature of the blast during propagation of the flame and also when the flame had stopped propagating. With the results, it was possible to develop correlations for the overpressure considering the flame speed, which was represented in Mach number.

Strehlow *et al.* (1979) also verified the overpressure for non-constant flame velocities, and the conclusion obtained was that the acceleration of the flame does not increase the overpressure, compared to the overpressures obtained with constant flame velocity. The meaning of the result is that the study with constant flame velocity gives a conservative overpressure. A relationship between Mach number, reactivity and obstacle density was obtained in the work, and the value of the Mach number is then used to obtain the side-on overpressure.

It is quite obvious that none of the models here revised are able to address the overpressure of an explosion considering all factors that influence the phenomenon. Works

however have been made to improve the study. Mercx *et al.* (2000), for example, developed a correlation for calculating the overpressure considering the boundary conditions, the mixture reactivity, the scale and the degree of confinement and obstruction. Although it takes into account many factors, the application of the correlation showed that parameter combination is not always straightforward, and that some parameters still need further research (MERCX *et al.*, 2000).

Matos *et al.* (2014) studied vapour cloud explosions concerning confined or partially confined spaces in the presence of vent. Vents are usually used to prevent an overpressure to exceed a limited value, thus the right design of the vent area and location are crucial. Their study was focused mainly on the influence of obstacles in overpressure calculation of an explosion of large scale. The principle of the correlation developed by them was a theoretical approach. In this approach, the maximum overpressure was considered to occur when the maximum unburned gas flow rate through the vent equals the maximum rate of consumption of unburned gas in the flame region (MATOS *et al.*, 2014). An interesting characteristic of such approach is that the study is able to model the reaction rate using the flamelet concept, which is a very sophisticated combustion model. Also, it uses the volume blockage ratio as a parameter of the model, representing the obstruction.

The kinetics energy as a function of the volume blockage ratio was obtained according to *FLACS* simulations, and after using that function the correlation results were compared to experimental data. Results showed that the correlation agrees well with experimental data, but the function of the kinetics energy obtained could not predict well the behaviour for all cases, which demonstrated that it is probably a function of other parameters as well, not only the volume blockage ratio.

Lautkaski (2012) studied the effects of gas explosions in ducts, in order to predict the vent area. In the study, a revision of semi-empirical correlations for venting gas explosion was carried out, and a new correlation was proposed, in order to reduce the errors of modelling. The comparison of this new correlation with test data showed that errors were in fact reduced, and it gave the most precise predictions.

Li *et al.* (2014) proposed a correlation for estimating the overpressure of a VCE based on guidance for the application of the Multi-Energy method, namely GAME. The

correlation is a relation of volume blockage ratio, maximum distance of flame propagation, average obstacle diameter and the laminar flame speed of the gas. Results from the correlation were compared to those from CFD simulations, and it was verified that it was not able to provide good results when dealing with practical problems. Therefore, a new correlation was proposed, taking into account other parameters such as the confinement ratio. The last correlation was found to predict better the overpressure compared to CFD simulations than the first one.

CFD is another wide used method to estimate the parameters of VCE. CFD simulators solve fundamental equations of fluid flow (Navier-Stokes equations), as well as combustion and turbulence models, which means that CFD treatments usually have much higher agreement with experiments than empirical or semi-empirical correlations. To solve these equations, usually the software uses a finite volume method as a discrete form (LEES, 2005). It is undeniable that CFD modelling is much more accurate than other models as it takes in account the plant design and information about the weather and other factors that can influence the VCE.

Tauseef *et al.* (2011) carried out a study of VCE in a LPG tank farm using CFD. First, calculations were made in order to verify which values of parameters such as wind speed would lead to greater flammable mass and, therefore, a greater overpressure in case a VCE takes place (worst scenario). After defining such parameters and also the boundary conditions, the vapour cloud explosion was obtained. Results were compared with calculations made with Multi-Energy and Baker-Strehlow models.

Finally, it was concluded that the turbulence model chosen in the CFD study had a good influence on the result and the other two models did not present the same behaviour as they do not take in consideration the turbulence effect as deep as CFD.

2.9 Fires

A fire can be caused by accidents like fireballs, pools and jets when caught on fire. In order for a fire to take place, three factors are required: ignition source, fuel and oxidizer, the last one being usually the oxygen present in air. A fire is basically the region where the combustion reaction takes place.

The major hazard from fires is the thermal radiation, which can cause damages to people and structures as discussed in Section 2.3. It is important to state that, although fires can cause serious damages, the extent of which thermal radiation can be hazardous is lower than the extension of a blast wave, for example.

2.9.1 BLEVE and fireball

The BLEVE (*boiling liquid expanding vapour explosion*) is a sudden release of a great mass of pressurized material with high temperature to the atmosphere (AICHE, 2000). Many incidents can cause a BLEVE, but the most common example is fire external to a vessel. When a fire occurs near a vessel that contains a liquefied pressurized gas, the vessel receives the radiation and the liquid absorbs parts of the radiation as heat. As the process goes on, the vapour pressure inside the vessel tends to rise, until the pressure reaches the set-point pressure of the relief valve, which begins to operate. As the valve works and releases the liquid vapour to the atmosphere, the liquid level inside the vessel tends to be reduced. The liquid can cool the vessel's wall, but the vapour cannot do that, therefore the lower the level of liquid, the lower the cooling of the wall. After a certain period of time, parts of the wall which receive the heat directly are no longer cooled as there is almost no more liquid inside the vessel. The walls are heated and as they are projected to work until a certain temperature, it ruptures (ABBASI and ABBASI, 2007). The vapour inside the vessel expands so much that the vessel's walls are not able to content the substance. The vessel suffers a sudden rupture, as the volume of the liquid can be raised up until 200 times (AICHE, 2000), which causes a high pressure wave, tank fragments and eventually - if the liquid is flammable – fireball.

It is important to bear in mind though that not only fire external to tank can cause BLEVE, but also other types of accidents such as corrosion, missile hit, manufacturing defects, and so one. Basically all accidents that can cause a sudden rupture of a vessel with pressurized liquefied gas can cause a BLEVE.

Although much attention has been taken over the years in VCE, BLEVE can cause as much losses as a VCE and that is why it should be studied. Abbasi and Abbasi (2007) pointed out that the BLEVE accident that occurred at an LPG plant in Mexico City in 1984

was one of the biggest accidents in chemical process industry, with over 650 lost lives. One of the factors that are determinant in the hazard of BLEVE is the great possibility of a domino effect, in which a consequence of one accident can lead to an incident of another accident. This is actually common in BLEVE accidents, because of the missiles generated, which can damage other vessels inside a process plant, leading to a series of accidents.

One model for calculating the properties of a fireball resulted from a BLEVE is presented in TNO (2005). The first step of the method is to calculate the total amount of pressurized liquefied gas released if the vessel fails (Equation 2.9.1).

$$Q_{flam} = f_{PLG}.V.\rho \tag{2.9.1}$$

where Q_{flam} is the mass of flammable material (kg), f_{PLG} is the fraction of the volume of the pressure tank filled with pressurized liquefied gas, V is the volume of the tank (m³) and ρ is the density of the substance in the pressure tank (kg/m³). With the mass of flammable material it is possible to calculate the radius and the duration of the fireball:

$$r_{fb} = 3.24\ {Q_{flam}}^{0.325} \tag{2.9.2}$$

$$t_{fb} = 0.852\ {Q_{flam}}^{0.26} \tag{2.9.3}$$

and the lift of height of the fireball (m):

$$H_{bleve} = 2.r_{fb} \tag{2.9.4}$$

In order to calculate the radiation flux from fireball at a certain receiver, it is important to bear in mind that although heat radiation is assumed to be uniform, it actually varies over its surface. The first step is to calculate the distance from the receiver to the centre of the fireball (Figure 16). In Figure 16, H_{bleve} is the height from the surface to the centre of the fireball, x_{bleve} is the horizontal distance from the receiver to the axis of the fireball (m) and X is the distance from the receiver to the centre of the fireball (m).

$$X = \left({x_{bleve}}^2 + {H_{bleve}}^2\right)^{1/2} \tag{2.9.5}$$

The view factor is given by Equation 2.9.6.

$$F_p = \left(\frac{r_{fb}}{X}\right)^2 \tag{2.9.6}$$

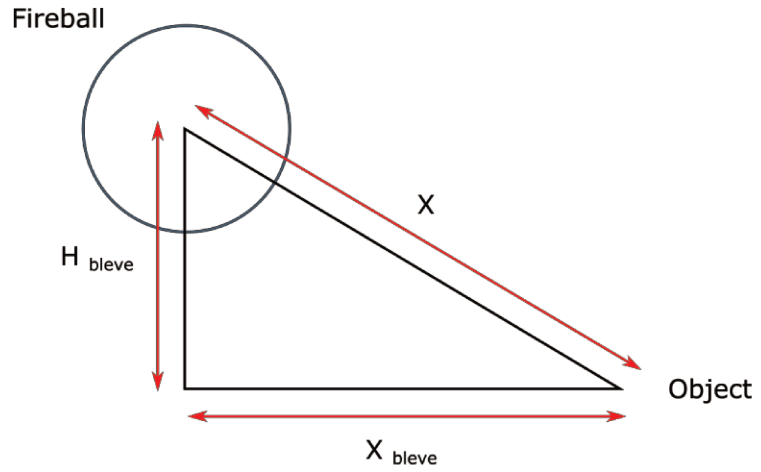

Figure 16. Dimensions for the fireball modelling (adapted from TNO, 2005).

The fraction of heat radiated by a fireball is obtained with Equation 2.9.7:

$$F_s = 0.00325\, P_{SV}^{0.32} \tag{2.9.7}$$

where P_{SV} is the vapour pressure inside the vessel (Pa). The net available heat for radiation:

$$\Delta H = \Delta H_c - \Delta H_v - C_P.\Delta T \tag{2.9.8}$$

where ΔH is the net available heat (J/kg), ΔH_c is the heat of combustion of the material at its boiling point (J/kg), ΔH_v is the vaporization heat of the material at its boiling point (J/kg), C_P is the specific heat capacity at constant pressure (J/kg.K) and ΔT is the temperature difference between flame and ambient temperature (assume 1700 K).

The surface emissive power (SEP) in J/(m².s) is calculated by Equation 2.9.9:

$$SEP = \frac{\Delta H.Q_{flam}.F_s}{4.\pi.r_{fb}^2.t_{fb}} \tag{2.9.9}$$

The actual path length of the radiation from a fire ball is:

$$x_{path} = X - r_{fb} \tag{2.9.10}$$

and the partial pressure of water vapour can be calculated as stated in Equation 2.9.11 (MUDAN, 1984):

$$P_w = 101325.RH.exp\left(14.4114 - \frac{5328}{T_a}\right) \tag{2.9.11}$$

where P_w is the water partial pressure (Pa), RH is the relative humidity of the ambient and T_a is the ambient temperature (K).

The atmospheric transmissivity, τ_a, accounts for the absorption of part of the radiation by the atmosphere, and is calculated with Equation 2.9.12.

$$\tau_a = 2.02 \left(P_w . x_{path}\right)^{-0.09} \quad (2.9.12)$$

Finally, the heat flux, E_r (W/m²), can be obtained at a certain distance from the fireball:

$$E_r = SEP . F_p . \tau_a \quad (2.9.13)$$

AICHE (1994) also presented a model to determine the heat flux from fireball. The first step of the model presented is to define the maximum fireball diameter ($D_{max,fb}$), considering the total flammable mass involved in the accident Q_{flam} (Equation 2.9.14).

$$D_{max,fb} = 5.8\, Q_{flam}^{1/3} \quad (2.9.14)$$

The duration of the fireball, t_{fb}, is then determined according to the total amount of flammable mass (Equations 2.9.15 and 2.9.16).

$$t_{fb} = 0.45\, Q_{flam}^{1/3} \;\; if\; Q_{flam} < 30{,}000\; kg \quad (2.9.15)$$

$$t_{fb} = 2.6\, Q_{flam}^{1/6} \;\; if\; Q_{flam} > 30{,}000\; kg \quad (2.9.16)$$

The centre height of the fireball is calculated as shown in Equation 2.9.17:

$$H_{bleve} = 0.75\, D_{max,fb} \quad (2.9.17)$$

Then the heat flux at the surface of the fireball can be determined by Equation 2.9.18.

$$SEP = \frac{\Delta H . Q_{flam} . F_s}{\pi . D_{max,fb}^2 . t_{fb}} \quad (2.9.18)$$

To calculate the total heat flux of the fireball from a receiver at a certain distance from the fireball, the view factor must be taken into account (Equation 2.9.19).

$$F_p = \frac{x_{bleve} . (D_{max,fb}/2)^2}{\left(x_{bleve}{}^2 + H_{bleve}^2\right)^{3/2}} \quad (2.9.19)$$

Finally, the heat flux at the receiver is determined the same as in Equation 2.9.13.

Torok *et al.* (2011) used this methodology to study the Feyzin accident to improve Romanian legislation. It was concluded that the most severe effect of a fireball caused by BLEVE is the thermal radiation.

Other models for estimating BLEVE's physical effects can be found in literature. Genova *et al.* (2008) presented in their work an empirical correlation for calculating the overpressure caused by BLEVE. The correlation is based on thermodynamic study and the driven force, which is the excess of heat stored in the liquid. Gong *et al.* (2004) also provides a simplified BLEVE model for PLG that takes into account the stratification layer. Results were compared to a small-scaled experiment and showed good agreement.

2.9.2 Pool fires

Pool fires are generated initially as liquid pools that are formed due to the release of a material in its liquid state. In order to liquid pool become a pool fire, it is necessary an ignition source. This ignition source can be the vapour cloud itself, if the liquid material is stocked with temperature beyond its boiling point or, if the liquid is stocked below its boiling point, the ignition source can be the flammable vapour formed by the evaporation of the liquid. In both cases, the flash fire must initially occur, in the vapour phase, and then the ignition of the liquid phase.

According to Mudan (1984), the ideal model of pool fires would be the one that has an analysis of the mixing dynamics and the chemical process of combustion. However, as such mechanism is not all well-defined, mainly because of the turbulent diffusion of flames and the non-equilibrium kinetics of soot formation, most models for pool fire are semi-empirical.

There are two different approaches for the calculation of the heat flux from a pool fire. The solid plume radiation model considers that the combustion heat is radiated through the visible surface area of the flame, and the flame is simplified to a cylinder. According to AICHE (2000), the problem of using this approach is that for large pool fires, a great amount of soot is generated and it obscures the radiating flame and also absorbs much of the radiation, decreasing the heat flux as the diameter of the pool increases.

The second approach is the point source radiation model. As the name suggest, the model considers that the flame is radiated from a single point that disperses the energy equally in the radial direction, like a sphere.

In both approaches the rate of liquid pool level decrease must be calculated:

$$\dot{y}_{max} = 1.27.10^{-6}\frac{\Delta H_c}{\Delta H^*} \quad (2.9.20)$$

where $\dot{y}_{max}$ is the vertical rate of liquid level decrease (m/s), ΔH_c is the heat of combustion (J/kg) and ΔH^* is the modified heat of vaporization (J/kg), which is given by:

$$\Delta H^* = \Delta H_v + \int_{T_a}^{T_{BP}} C_P dT \quad (2.9.21)$$

where ΔH_v is the vaporization heat of the liquid at ambient temperature (J/kg), T_{BP} is the boiling point temperature of the liquid (K), T_a is the ambient temperature (K) and C_P is the heat capacity of the liquid (J/kg.K).

The mass burning rate m_b (kg/m².s) is calculated simply by multiplying the vertical rate of liquid decrease by the density of the liquid:

$$m_b = \dot{y}_{max}.\rho \quad (2.9.22)$$

The pool diameter is another important parameter for pool fire. The burning rate tends to decrease with the spreading of the pool for laminar flow regime, but with further increase of the diameter, the burning velocity begins to increase, as the burning becomes turbulent and is almost not influenced by the pool diameter (MUDAN, 1984).

For a continuous leak, the equilibrium condition occurs when the total burning rate equals the spill rate, which gives the following condition:

$$D_{pool} = 2\left(\frac{V_s}{\pi.\dot{y}_{max}}\right)^{1/2} \quad (2.9.23)$$

where D_{pool} is the equilibrium diameter of the pool (m) and V_s is the liquid spill rate (m³/s). And in case the leak is instantaneous:

$$D_{pool} = 2\left(\frac{{V_s}^3.g}{{\dot{y}_{max}}^2}\right)^{1/8} \quad (2.9.24)$$

where g is the gravity acceleration (m/s²). The flame height is calculated as follows:

$$\frac{H_{flame}}{D_{pool}} = 42\left(\frac{m_B}{\rho_a\sqrt{gD_{pool}}}\right) \quad (2.9.25)$$

where ρ_a is the density of the ambient air (kg/m³). For the solid plume model, the emissive power E_{av} (W/m²) is given by Equation 2.9.26 and the view factor (F_{21}) is given by Figure 17.

$$E_{av} = 140.e^{-0,12.D_{pool}} + 20.(1 - e^{-0,12.D_{pool}}) \quad (2.9.26)$$

And finally, the radiation flux at the receiver (W/m²) is calculated as follows:

$$E_r = E_{av}.F_{21}.\tau_a \quad (2.9.27)$$

where τ_a is obtained from Equation 2.9.12.

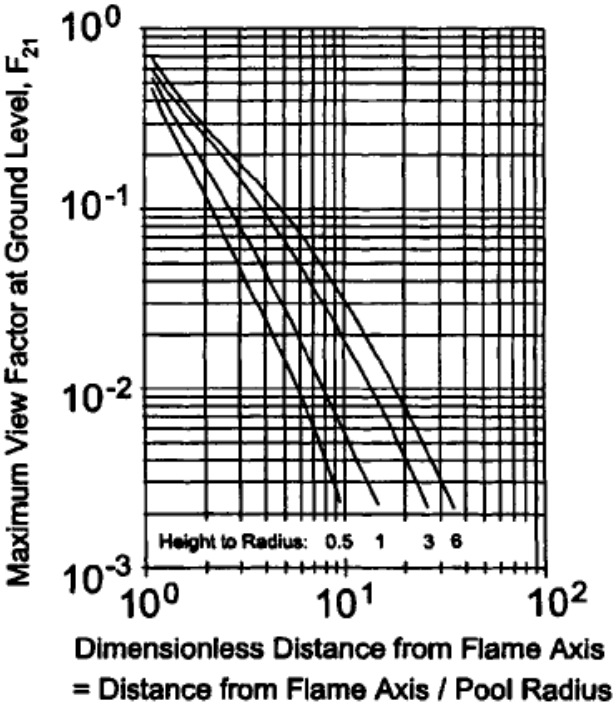

Figure 17. Relationship between pool distances and the view factor (AICHE, 2000).

For the point source model, the view factor is calculated as:

$$F_p = \frac{1}{4\pi X^2} \quad (2.9.28)$$

where X is the distance from the point source (which is usually consider as half the height of the flame) to the receiver (m).

The thermal flux at the receiver (W/m²) can be finally calculated with Equation 2.9.29.

$$E_r = \eta_{rad}.m_b.\Delta H_c.F_p.A_{pool}.\tau_a \quad (2.9.29)$$

where η_{rad} is the fraction of heat of combustion radiated (typically 0.15 to 0.30), A_{pool} is the total area of the pool (m²) and ΔH_c is the heat of combustion of the liquid (J/kg).

Another model for calculating the heat flux from a pool fire is presented in TNO (2005). The model considers drag and tilt of the flame and the pool, which means that the

wind is considered in the model and plays an important role in the calculation of the heat flux.

The first step of the model is to determine the initial outflow velocity:

$$v_0 = C_{d.}(2.g.h_L)^{0.5} \quad (2.9.30)$$

where h_L is the liquid head above hole (m). The next step is to determine both acceleration constant (Equation 2.9.31) and the dimensionless parameters β and τ_{max} (Equations 2.9.32 and 2.9.33).

$$ac_c = (C_d.A_h/A_{tank})^2.g \quad (2.9.31)$$

$$\beta = \frac{acc_c.\delta_{pool}.\rho_0}{v_0.m_b} \quad (2.9.32)$$

$$\tau_{max} = Log\left(\frac{1+\beta}{\beta}\right) \quad (2.9.33)$$

where A_h is the area of the hole (m²), A_{tank} is the cross sectional area of the vessel (m²), δ_{pool} is the pool thickness (m) and m_b is the mass burning rate (Equation 2.9.22). Then, the maximum time of the pool fire t_{max} is estimated, as well as the parameter Φ_{max}:

$$t_{max} = \frac{\tau_{max}.\rho_0.\delta_{pool}}{m_b} \quad (2.9.34)$$

$$\Phi_{max} = 1 + \beta.(1-\tau_{max}) - (1+\beta).\exp(-\tau_{max}) \quad (2.9.35)$$

Finally, the pool radius and diameter can be determined according to Equation 2.9.36.

$$\mathrm{D}_{pool} = 2.r_{pool} = \sqrt{\frac{\Phi_{max}.\rho_0.A_h.v_0}{m_b.\pi}} \quad (2.9.36)$$

The total release time and the duration of the fire are presented in Equations 2.9.37 and 2.9.38, respectively.

$$\mathrm{R}_d = \left(\frac{A_{tank}}{C_d.A_h}\right).\sqrt{\left(\frac{2.h_L}{g}\right)} \quad (2.9.37)$$

$$\mathrm{t}_{pool} = R_d + \delta_{pool}.\rho_0/m_b \quad (2.9.38)$$

The wind speed is also taken into account in this model. The dimensionless wind velocity u' is calculated by dividing the wind speed by the characteristic wind velocity (Equation 2.9.39):

$$\mathrm{u}_c = \left[\left(g.m_b.\mathrm{D}_{pool}\right)/\rho_a\right]^{1/3} \quad (2.9.39)$$

where ρ_a is the density of the ambient air (kg/m³).

The next step is to determine the mean fire length (Equation 2.9.40) and the flame tilt angle (Equation 2.9.41).

$$L_{flame} = 55.D_{pool}.\left(\frac{m_b}{\rho_a.(g.D_{pool})^{\frac{1}{2}}}\right)^{0.67}.u'^{-0.21} \quad (2.9.40)$$

$$tan\Theta_{tilt}/cos\Theta_{tilt} = 0.666.(Fr_{10})^{0.333}.(Re)^{0.117} \quad (2.9.41)$$

where Re is the Reynolds number and Fr_{10} is the Froude number.

According to the flame presentation (cylindrical or conical), the elongated diameter of the pool is determined:

$$D_{elong} = D_{pool}1.6.(Fr_{10})^{0.061}\ for\ conical\ flames \quad (2.9.42)$$

$$D_{elong} = D_{pool}1.5.(Fr_{10})^{0.069}\ for\ cylindrical\ flames \quad (2.9.43)$$

The surface emissive power in this model is presented in Equation 2.9.44:

$$SEP = \frac{\eta_{rad}.m_b.\Delta H_c}{1+4.\frac{L_{fire}}{pool}}.(1-\varsigma) + SEP_{soot}.\varsigma \quad (2.9.44)$$

where η_{rad} is the fraction of heat of combustion radiated, ς is the fraction of the surface of the flame covered by soot and SEP_{soot} is the surface emissive power of soot (J/m².s).

Before determining the heat flux, the view factor must be estimated using Equations from 2.9.45 to 2.9.55.

$$a_{ratio} = L_{fire}/r_{pool} \quad (2.9.45)$$

$$b_{ratio} = x_{pool}/r_{pool} \quad (2.9.46)$$

$$A_{view} = ({a_{ratio}}^2 + (b_{ratio}+1)^2 - 2.a_{ratio}.(b_{ratio}+1) + sin\Theta_{tilt})^{1/2} \quad (2.9.47)$$

$$B_{view} = ({a_{ratio}}^2 + (b_{ratio}-1)^2 - 2.a_{ratio}.(b_{ratio}-1) + sin\Theta_{tilt})^{1/2} \quad (2.9.48)$$

$$C_{view} = \left(1 + \left({b_{ratio}}^2 - 1\right).cos\Theta_{tilt}\right)^{1/2} \quad (2.9.49)$$

$$D_{view} = \sqrt{(b_{ratio}-1)/(b_{ratio}+1)} \quad (2.9.50)$$

$$E_{view} = (a_{ratio}.cos\Theta_{tilt})/(b_{ratio} - a_{ratio}.sin\Theta_{tilt}) \quad (2.9.51)$$

$$G_{view} = \sqrt{\left({b_{ratio}}^2 - 1\right)} \tag{2.9.52}$$

$$F_{view,vertical}.\pi = -E_{view}.tan^{-1}D_{view} + E_{view}\left[\frac{{a_{ratio}}^2 + (b_{ratio}+1)^2 - 2.b_{ratio}(1+a_{ratio}.sin\Theta_{tilt})}{A_{view}.B_{view}}\right] tan^{-1}\left(\frac{A_{view}.D_{view}}{B_{view}}\right).\frac{cos\Theta_{tilt}}{C_{view}} + \left[tan^{-1}\left(\frac{a_{ratio}.b_{ratio} - {F_{view}}^2.sin\Theta_{tilt}}{F_{view}.C_{view}}\right) + tan^{-1}\left(\frac{{F_{view}}^2.sin\Theta_{tilt}}{F_{view}.C_{view}}\right)\right] \tag{2.9.53}$$

$$F_{view,horizontal}.\pi = tan^{-1}\left(\frac{1}{D_{view}}\right) + \frac{sin\Theta_{tilt}}{C_{view}}\left[tan^{-1}\left(\frac{a_{ratio}.b_{ratio} - {F_{view}}^2.sin\Theta_{tilt}}{F_{view}.C_{view}}\right) + tan^{-1}\left(\frac{{F_{view}}^2.sin\Theta_{tilt}}{F_{view}.C_{view}}\right)\right] \left[\frac{{a_{ratio}}^2 + (b_{ratio}+1)^2 - 2.(b_{ratio}+1+a_{ratio}b_{ratio}.sin\Theta_{tilt})}{A_{view}.B_{view}}\right] tan^{-1}\left(\frac{A_{view}.D_{view}}{B_{view}}\right) \tag{2.9.54}$$

$$F_p = \sqrt{{F_{view,horizontal}}^2 + {F_{view,horizontal}}^2} \tag{2.9.55}$$

where x_{pool} is the distance from the receiver to the axis of the pool (m).

Finally, the heat flux at the receiver is shown in Equation 2.9.56.

$$E_r = SEP.F_p.\tau_a \tag{2.9.56}$$

Ditch *et al.* (2013) studied pool fires in order to develop a new empirical correlation that could be validated for all practical conditions. Their work consisted on mathematical treatment of the energy balance in a pool fire. The correlation obtained had the pool diameter, fuel heat of gasification and sootiness of the flame as parameters of the equation. Experiments were made to validate the empirical correlation obtained, and the comparison showed roughly 9% error, which demonstrates good agreement.

Numerical simulations are also widely used to model pool fires, despite the complexity and the limitation to simulate physical phenomena such as soot formation. Wen-he *et al.* (2013), for instance, used software *Fluent* to determine the radiation hazard of a pool fire generated by a 10 million cubic meters oil tank.

Vasanth *et al.* (2014) studied the radiation effect of multiple pool fires, a physical phenomenon that occurred in accidents such as Buncefield (UK, 2005) and Jaipur (India, 2009). Multiple pool fires are pool fires that occur close enough so that they influence each other. CFD was used to model the effect and simulations were validated with experimental

data. Finally, it was concluded that the pool diameter plays an important role in thermal radiation, as well as the distance between pools.

2.9.3 Jet fires

Just like in cases where there is a formation of flame, in jet fires the most important consequence is also the thermal radiation effect caused by the combustion reaction. Jet fires are formed when the ignition occurs right after the substance stars to leak. According to Badri *et al.* (2013), a jet fire is "*a turbulent diffusion flame resulting from the combustion of a fuel continuously released with significant momentum in a particular direction*". The jet momentum plays an important role in the shape and position of the jet flame.

AICHE (2000) presented an approach for determining the radiation flux from a jet fire to a receiver at a certain distance from the fire. As the effect is the same as for pool fires, there are many similarities in the modelling. The length of the visible turbulent flame is calculated as Equation 2.9.57 below:

$$\frac{H_{flame}}{d_{hole}} = \frac{5.3}{C_T}\sqrt{\frac{T_f/T_j}{\alpha_T}\left[C_T + (1 - C_T)\frac{MW_a}{MW_f}\right]} \tag{2.9.57}$$

where H_{flame} is the length of the flame (m), d_{hole} is the diameter of the hole (m), C_T is the fuel mole fraction concentration in a stoichiometric fuel-air mixture, T_f is the adiabatic flame temperature (K), T_j is the jet temperature (K), α_T is the mols of reactant per mole of product for a stoichiometric fuel-air mixture, MW_a is the molecular weight of air (g/mol) and MW_f is the molecular weight of the fuel (g/mol).

The transmissivity and the view factor are calculated respectively by Equations 2.9.12 and 2.9.28. Thus, the radiant flux at the receiver is given by Equation 2.9.29.

Hankinson and Lowesmith (2012) studied the fraction of heat radiated for jet fires. They proposed a study to verify the significance of this parameter and the possibility of using a value of fraction of radiation derived from one method in another model, for both far and near fields. Point source and solid flame models were analysed, and the conclusion was that the parameter obtained by one method is only applicable to another if adjustment is made. Also, near field studies showed higher disagreement than far field studies.

2.10 Monte Carlo Simulation

Monte Carlo simulation is a methodology for verifying the results of a function based on the uncertainty of the input parameters (NRG, 2005). The name Monte Carlo is because of the similarity between the method and the gambling games in casinos.

The technique consists in building a probabilistic model of the system, translating the model to a computer, estimating the probabilistic distribution of the input data and interpreting the output probability distribution (NRG, 2005). In order to build a probabilistic model of the system, it is usually used a random number generator that provides the sample of the input. For each input, the output is then calculated and the probabilistic distribution of the output is determined. These results are considered experimental data when the number of simulations is high, because they represent the actual problem.

The application of Monte Carlo simulation is very wide, from engineering to finances. In risk analysis, it can be used for the fault tree methodology and even estimating the risk. Zhang *et al.* (2013) developed in their work a probabilistic evacuation model using the Monte Carlo analysis in order to determine a probabilistic distribution of the human behaviour in case of fire emergency. Arunraj *et al.* (2013) also used Monte Carlo simulation in order to model the uncertainty of the risk analysis. They combined Monte Carlo simulation and Fuzzy theory to obtain the probabilistic distribution of the risk, considering that it is a combination of consequence and frequency.

The Monte Carlo analysis can also be used to determine which incident leads to a great accident, by using Monte Carlo technique for determining a probabilistic variable that affects the whole accident scenario, as the hole diameter of an incident, for example. This way it could be determined which size of hole generates the greatest and most probable damage, considering the incident outcome or accident effect.

Chapter 3

Methodology

This chapter presents the methodology used for the development of CASE. For each model, a list of steps that have been implemented in the tool is presented here. The Monte Carlo simulation and CFD add-on methodologies are presented and explained.

For each model, a series of steps were determined in order to obtain the main parameters of the consequence and to make CASE easier to use and develop. The methodology for the development of CASE is shown in Figure 18. CASE has been programmed in *Fortran* programming language and it works both in *Windows* and *Linux* operating systems.

CASE needs initial parameters about the substance, atmosphere and release that should be provided by the user. One of the most important data is the state in which the substance is stored. This information is crucial for the calculation, because the models will be chosen depending on the state of matter of the substance.

If the substance is gas, the discharge rate will be calculated for full bore ruptured pipeline or vessels, in a transient matter. The discharge rate or the total amount of substance released is then used as an input for the dispersion models (puff, plume or dense gas). In this step, the concentration of the cloud is obtained as well as the flammable mass, according to the LFL and UFL of the material. Finally, explosion models are used to

calculate the overpressure in case the cloud meets an ignition source. Jet fire is also calculated directly from the discharge rate.

For liquid releases, the transient discharge rate is also calculated for release of material through hole in a vessel and the liquid released forms a pool. The evaporation of the pool is considered to form a vapour cloud that is dispersed through the atmosphere and can explode. The pool can also catch fire.

Finally, for two-phase releases, the flashing process should be considered. The material is released and is flashed when depressurizes, forming vapour. The vapour will form a cloud that can ignite, which is the same procedure for liquids and gases as well. The pool of liquid formed could catch fire. Fireball is also considered in two phase releases, if a BLEVE occurs, but its calculation does not depend on any other models. Table 8 shows a list of all models implemented in CASE.

Concerning the Monte Carlo simulation and CFD add-on, the methodology is to use the Monte Carlo method to study stochastic variables. A set of initial discharge rates is listed according to its probability for a specific sector of the installation chosen for the CPQRA analysis. Random numbers are generated according to Monte Carlo, and each of those numbers defines which initial discharge rate to use in each simulation.

Next, based on the probabilistic distribution of the wind direction and speed, the flammable volume for each discharge rate would be calculated with response surfaces based on CFD simulations. In this case, the flammable volume is a function of the angle between wind and leakage and the ventilation rate, which is a function of wind speed and discharge rate (FERREIRA and VIANNA, 2014). The overpressure of a possible explosion is also determined by the use of response surfaces, according to the work of Vianna and Cant (2012). Finally, it would be possible to have an exceedance probability curve to verify the frequency of a range of overpressures. Detailed information about this methodology can be seen in Section 3.7.

Table 8. Empirical and semi-empirical models implemented in CASE for consequence analysis.

Step of the accident	**Model**
Discharge	Gas through a hole: TNO (2005) Gas through a full bore ruptured pipeline: TNO (2005) Liquid through a hole: TNO (2005) Two-phase: Fauske and Epstein (1988)
Flash and Evaporation	Crowl and Louvar (2011)
Dispersion	Neutrally or positive buoyant: Pasquill-Gifford Dense gas: Britter and McQuaid (1988)
Explosion	TNT Equivalency Multi-Energy (VAN DEN BERG, 1983) with the use of characteristic curves of Alonso *et al*. (2006)
Pool fire	Mudan (1984) – point source model TNO (2005)
Jet fire	Mudan (1984)
Fireball (BLEVE)	AICHE (1994) TNO (2005)

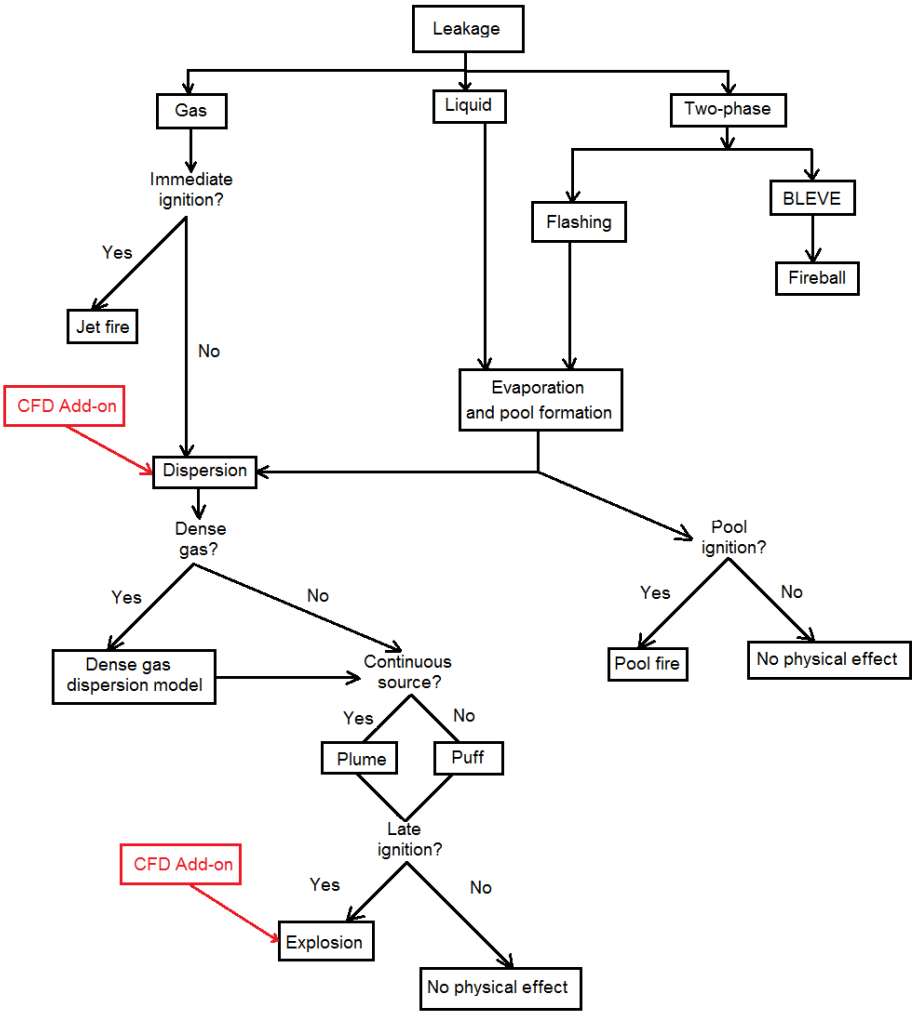

Figure 18. Framework of CASE.

3.1 Discharge

As the discharge models differ for each state of the substance (liquid, gas or two-phase) and each release type (hole in a vessel or full bore ruptured pipeline, for example), the computational tool was also done separately.

3.1.1 Liquid discharge through hole in a vessel

Table 9 shows the input needed for the modelling of liquid discharge through hole in a tank.

Table 9. Input data for liquid discharge calculation through hole in tanks.

Parameter	Nomenclature	International System Unit
Pressure above liquid	P_0	Pa
Temperature of the vessel	T_0	K
Hole diameter	d_{hole}	m
Discharge coefficient	C_d	-
Pressure outside the vessel	P_a	Pa
Density of the liquid	ρ_0	kg/m³
Volume of the vessel	V	m³
Length of the vessel	L_{vessel}	m
Filling degree of the vessel	$\emptyset$	-
Leak height	H	m

The sequence of steps that has been implemented in CASE for obtaining the mass flow rate for any time for a transient liquid discharge through hole in a vessel is listed below:

Step 1: Calculate the diameter of the tank:

$$d_{tank} = \sqrt{\frac{4.V}{\pi.L_{vessel}}} \tag{3.1.1}$$

Step 2: Calculate the superficial area of the tank:

$$A_s = \frac{\pi {d_{tank}}^2}{4} \tag{3.1.2}$$

Step 3: Calculate the area of the hole:

$$A_h = \frac{\pi d_{hole}^2}{4} \tag{3.1.3}$$

Step 4: Determine the total mass of liquid in the vessel:

$$M = \rho.V.\emptyset \tag{3.1.4}$$

Step 5: Determine the total volume of liquid in the vessel:

$$V_L = V.\emptyset \tag{3.1.5}$$

Step 6: Determine the liquid height in the vessel:

$$h_L = \frac{V_L}{A_s} \tag{3.1.6}$$

Step 7: Calculate the initial mass discharge (Equation 2.4.6).

Step 8: For the next time step, calculate decrease of mass that remains in the pipeline (Equation 2.4.7).

Step 9: Calculate the decrease in the volume of liquid inside the vessel (Equation 2.4.8).

Step 10: Calculate the new volume of liquid in the tank (Equation 2.4.9).

Step 11: Calculate the decrease of liquid height in the tank (Equation 2.4.10).

Step 12: Calculate the new liquid height in the tank (Equation 2.4.11).

Step 13: Calculate the mass discharge (Equation 2.4.6).

Step 14: Repeat steps 7-11 until the mass discharge rate is zero.

3.1.2 Gas discharge through hole in a vessel

First, all the input necessary for the model need to be provided by the user (Table 10). The sequence of steps that were implemented in CASE for obtaining the mass flow rate for any time for a transient gas discharge is listed below:

Step 1: Calculate the density of the substance inside the vessel:

$$\rho = \frac{P_0.MW}{R_g T_0} \tag{3.1.7}$$

Step 2: Determine the total mass of gas in the vessel by multiplying the volume of the vessel by the density of the gas.

Step 3: Calculate the area of the hole (Equation 3.1.3).

Step 4: Calculate the ratio of the initial and final (ambient) pressure.

Step 5: Verify which type of flow is (sonic or subsonic) using Equation 2.4.23.

Step 6: Determine the value of ψ using Equations 2.4.24 or 2.4.25.

Step 7: Calculate the initial mass discharge (Equation 2.4.22).

Step 8: For the next time step, calculate the total mass that remains in the vessel:

$$m = (m_{initial} - Q_m).\Delta t \tag{3.1.8}$$

Step 9: Calculate the density decrease using Equation 2.4.12.

Step 10: Calculate the new density (Equation 2.4.13).

Step 11: Calculate the temperature decrease (Equation 2.4.18).

Step 12: Calculate the new temperature (Equation 2.4.19).

Step 13: Calculate the new pressure inside the vessel (Equation 2.4.20).

Step 14: Verify which type of flow is (sonic or subsonic) using Equation 2.4.23.

Step 15: Determine the value of ψ using Equations 2.4.24 or 2.4.25.

Step 16: Calculate the mass discharge (Equation 2.4.22).

Step 17: Repeat steps 8-16 until the mass discharge rate is zero.

Table 10. Parameters necessary for the calculation of the discharge rate of a gas release through a hole.

Parameter	Nomenclature	International System Unit
Pressure of the vessel	P_0	Pa
Temperature of the vessel	T_0	K
Hole diameter	d_{hole}	m
Discharge coefficient	C_d	-
Pressure outside the vessel	P_a	Pa
Molecular weight of the substance	MW	g/mol
Heat capacity ratio	γ	-
Specific heat at constant volume of the gas	C_V	J/kg.K
Volume of the vessel	V	m³

3.1.3 Gas discharge for a full bore ruptured pipeline

Table 11 shows the input needed for the modelling. The sequence of steps that were implemented in CASE for obtaining the mass flow rate for any time for a transient gas discharge after a full bore rupture of a pipeline is listed below:

Step 1: Calculate the density of the substance inside the vessel:

$$\rho = \frac{P_0.MW}{R_g T_0} \tag{3.1.9}$$

Step 2: Calculate the area of the pipeline:

$$A_p = \frac{\pi d_p^2}{4} \tag{3.1.10}$$

Step 3: Determine the total mass of gas in the pipeline:

$$M_0 = A_p . l_p . \rho \quad (3.1.11)$$

Step 4: Calculate the ratio of the initial and final (ambient) pressure.

Step 5: Verify which type of flow is (sonic or subsonic) using Equation 2.4.23.

Step 6: Determine the value of ψ using Equations 2.4.24 or 2.4.25.

Step 7: Calculate the initial mass discharge (Equation 2.4.22)

Step 8: For the next time step, calculate the total mass that remains in the pipeline:

$$m = (m_{initial} - Q_m) . \Delta t \quad (3.1.12)$$

Step 9: Calculate the sonic velocity of the gas using Equation 2.4.27.

Step 10: Calculate the Darcy friction factor (Equation 2.4.28)

Step 11: Calculate the time constant (Equation 2.4.29)

Step 12: Calculate the new mass discharge rate for any time after the rupture using Equation 2.4.26.

Table 11. Input data for determining the release rate of gas discharge caused by a full bore rupture of a pipeline.

Parameter	Nomenclature	International System Unit
Pressure of the pipeline	P_0	Pa
Temperature of the pipeline	T_0	K
Pipe length	l_p	m
Pipe diameter	d_p	m
Internal roughness of the pipe	$\mathcal{E}$	m
Discharge coefficient	C_d	-
Pressure outside the vessel	P_a	Pa
Molecular weight of the substance	MW	g/mol
Heat capacity ratio	γ	-

3.1.4 Two-phase discharge through hole in a pipe

First, all the input necessary for the model need to be provided by the user (Table 12).

Table 12. Parameters necessary for the calculation of discharge rate of a two-phase release through a hole in a pipe.

Parameter	Nomenclature	International System Unit
Pressure of the pipe	P_0	Pa
Temperature of the pipe	T	K
Discharge coefficient	C_d	-
Area of the hole	A_h	m²
Pressure outside the pipe	P_a	Pa
Heat capacity of the liquid	C_p	J/kg.K
Pipe length	l_p	m
Saturation vapour pressure at ambient temperature	P_{sat}	Pa
Density	ρ	kg/m³
Enthalpy change in vaporisation	h_{fg}	J/kg
Specific volume change between liquid and vapour	v_{fg}	m³/kg
Atmospheric boiling temperature of the liquid	T_B	K

The sequence of steps implemented in CASE for obtaining the mass flow rate for a two-phase discharge is listed below:

Step 1: Calculate the subcooled mass flux (Equation 2.4.30).

Step 2: Calculate the equilibrium mass flux (Equation 2.4.31).

Step 3: Calculate the non-equilibrium parameter (Equation 2.4.32).

Step 4: Calculate the mass flow rate (Equation 2.4.33).

Step 5: Calculate the fraction of liquid vaporized (Equation 2.5.1).

3.2 Dispersion

The dispersion has been implemented separately as long as puff, plume and dense gas dispersion are concerned. In this section, the flammable mass is also calculated.

3.2.1 Puff dispersion

Table 13 shows the input needed for the modelling.

Table 13. Input data for the calculation of the puff (instantaneous) dispersion of a neutral or positive buoyant cloud.

Parameter	Nomenclature	International System Unit
Total mass released	Q	kg
Leak height	H	m
Pasquill stability class	$A-F$	-
Wind speed	u	m/s
Step	$step$	m
Lower flammability limit	C_{LFL}	kg/m³
Upper flammability limit	C_{UFL}	kg/m³

The sequence of steps that were implemented in CASE for obtaining the concentration profile of the cloud as a puff is listed below:

Step 1: Determine the distance of the cloud centre at a given time t after the release:

$$D_{cc} = u.t \tag{3.2.1}$$

Step 2: Determine the distance from the centre:

$$D_{centre} = -step.(number\ of\ steps) \tag{3.2.2}$$

Step 3: Determine the distance:

$$x = D_{cc} + D_{centre} \tag{3.2.3}$$

Step 4: Calculate the values of the dispersion coefficients (Table 1).

Step 5: Calculate the concentration at the centre of the cloud (Equation 2.6.2).

Step 6: Calculate the isopleths for the lower flammability limit (Equation 2.6.7).

Step 7: Determine the next distance from the centre:

$$D_{centre,i+1} = D_{centre,i} + step \tag{3.2.4}$$

Step 8: Determine the next distance:

$$x_{i+1} = D_{centre,i+1} + D_{cc} \tag{3.2.5}$$

Step 9: Repeat steps 5-7.

Step 10: Repeat steps 8-10 until the concentration at the centre of the cloud is zero.

Step 11: Calculate the flammable mass in the cloud (Equation 2.7.1 or 2.7.2).

3.2.2 Plume dispersion

Table 14 shows the input needed for the modelling.

Table 14. Input data for the calculation of the plume (continuous) dispersion of a neutral or positive buoyant cloud.

Parameter	Nomenclature	International System Unit
Release rate	Q_m	kg
Leak height	H	m
Pasquill stability class	$A - F$	-
Wind speed	u	m/s
Step	$step$	m
Lower flammability limit	C_{LFL}	kg/m³
Upper flammability limit	C_{UFL}	kg/m³

The sequence of steps that were implemented in CASE for obtaining the concentration profile of the cloud as a plume is listed below:

Step 1: Determine the distance downwind:

$$x_{i+1} = x_i + step \tag{3.2.6}$$

Step 2: Determine the time:

$$t = \frac{x}{u} \tag{3.2.7}$$

Step 3: Calculate the values of the dispersion coefficients (Table 2 for rural conditions).

Step 4: Calculate the concentration at the centre of the cloud (Equation 2.6.3).

Step 5: Calculate the isopleths for the lower flammability limit (Equation 2.6.7).

Step 6: Repeat steps 1-6 until the concentration at the centre of the cloud is zero.

Step 7: Calculate the flammable mass in the cloud (Equation 2.7.3) using the parameters presented in Table 5.

3.2.3 Dense gas dispersion

Table 15 shows the input needed for the modelling.

Table 15. Input data for the calculation of dense gas dispersion of a negative buoyant cloud.

Parameter	Nomenclature	International System Unit
Release rate	Q_m	kg
Release duration	R_d	s
Initial density of the material	ρ_0	kg/m³
Density of ambient air	ρ_a	kg/m³
Wind speed	u	m/s

The sequence of steps that were implemented in CASE for obtaining the concentration for a dense gas is listed below:

Step 1: Determine the initial buoyancy factor (Equation 2.6.10).

Step 2: Determine if the release is continuous or instantaneous using the criterion of Equations 2.6.8 and 2.6.9. If the release is instantaneous, go to step 3. If the release is continuous, go to step 5.

Step 3: Calculate the initial volume of dense gas material:

$$V_0 = \frac{Q}{\rho} \tag{3.2.8}$$

Where Q is the total mass released (kg).

Step 4: Calculate the criterion for dense cloud for instantaneous releases (Equation 2.6.12). If the criterion is satisfied, go to step 7. If it is not satisfied, use a puff model.

Step 5: Calculate the initial plume volume flux:

$$q_0 = \frac{Q_m}{\rho} \tag{3.2.9}$$

Where Q_m is the discharge rate (kg/s).

Step 6: Calculate the criterion for dense cloud for continuous releases (Equation 2.6.11). If the criterion is satisfied, go to step 7. If it is not satisfied, use a plume model.

Step 7: Calculate the concentrations based on the charts of the Britter and McQuaid model.

Step 8: Repeat steps 2-7 for different downwind distances.

Step 9: Calculate the flammable mass in the cloud (Equation 2.7.1 or 2.7.2 or 2.7.3).

3.3 VCE

The VCE models were implemented separately. It is the user's decision which one to use.

3.3.1 TNT Equivalency method

Table 16 shows the input needed for the modelling.

Table 16. Input data for the calculation of the overpressure and impulse of a vapour cloud explosion with the TNT Equivalency method.

Parameter	Nomenclature	International System Unit
Mass of flammable gas in the cloud	Q_{flam}	kg
Distance from the explosion	x_{blast}	m
Heat of combustion of the flammable gas	E_c	J/kg
Heat of combustion of TNT	$E_{c,TNT}$	Jkg
Explosion efficiency	η_{TNT}	-

The sequence of steps that were implemented in CASE for obtaining the overpressure of an explosion for a determined distance from the blast centre is listed below:

Step 1: Calculate the equivalent mass of TNT (Equation 2.8.1).

Step 2: Calculate the scaled distance (Equation 2.8.2).

Step 3: Calculate the overpressure with the parameters listed in Table 6.

Step 4: Repeat steps 2-3 for different distances from the explosion centre.

3.3.2 TNO Multi-Energy method

Table 17 shows the input needed for the modelling.

Table 17. Input data for the calculation of overpressure and impulse of a vapour cloud explosion with the TNO Multi-Energy method.

Parameter	Nomenclature	International System Unit
Mass of flammable gas in the cloud	Q_{flam}	kg
Distance from the explosion	x_{blast}	m
Stoichiometric concentration with air	C_s	%vol
Heat of combustion of the flammable gas	E_c	J/kg
Ambient pressure	P_a	Pa
Blast strength	$1-10$	-

The sequence of steps that were implemented in CASE for obtaining the overpressure of an explosion for a determined distance from the blast centre is listed below:

Step 1: Calculate the flammable volume (Equation 2.7.4).

Step 2: Calculate the charge heat of combustion (Equation 2.8.4).

Step 3: Calculate the Sachs-scaled distance (Equation 2.8.3).

Step 4: Calculate the overpressure with the equations provided by Alonso (2006).

Step 5: Repeat steps 2-3 for different distances from the explosion centre.

3.4 Jet Fire

The jet fire has been modelled in order to obtain the radiation flux at any time during the release of the material. Table 18 shows the input needed for the modelling.

The sequence of steps that were implemented in CASE for obtaining the radiant flux caused by a jet fire is listed below:

Step 1: Calculate the length of the flame (Equation 2.9.57).

Step 2: Calculate the view factor (Equation 2.9.28).

Step 3: Calculate the water partial pressure (Equation 2.9.11).

Step 4: Calculate the transmissivity (Equation 2.9.12).

Step 5: Calculate the flux at the receiver (Equation 2.9.29).

Step 6: Repeat step 5 for each time of the discharge rate.

Table 18. Input data for the calculation of the radiation flux of a jet fire.

Parameter	Nomenclature	International System Unit
Distance from the flame	X	m
Diameter of the hole	d_{hole}	m
Fuel mole fraction concentration at stoichiometric fuel-air mixture	C_T	-
Adiabatic flame temperature	T_f	K
Jet temperature	T_j	K
Fraction of heat of combustion radiated	η_{rad}	-
Mols of reactant per mole of product for a stoichiometric fuel-air mixture	α_T	-
Molecular weight of air	MW_a	g/mol
Molecular weight of fuel	MW_f	g/mol
Relative humidity	RH	-
Ambient temperature	T_a	K

3.5 Pool Fire

3.5.1 Point source model (AICHE, 2000)

Table 19 shows the input needed for the modelling of pool fire of point source model presented in AICHE (2000). The sequence of steps that were implemented in CASE for obtaining the radiant flux caused by a pool fire is listed below:

Step 1: Calculate the modified heat of vaporization (Equation 2.9.21).

Step 2: Calculate the vertical rate of liquid level (Equation 2.9.20).

Step 3: Calculate the mass burning rate (Equation 2.9.22).

Step 4: Calculate the liquid spill rate:

$$V_s = \frac{Q_m}{\rho} \tag{3.5.1}$$

Step 5: Calculate the diameter of the pool (Equation 2.9.23 or 2.9.24).

Step 6: Calculate the flame height (Equation 2.9.25).

Step 7: Calculate the view factor (Equation 2.9.28).

Step 8: Calculate the water partial pressure (Equation 2.9.11).

Step 9: Calculate the transmissivity (Equation 2.9.12).

Step 10: Calculate the area of the pool:

$$A_{pool} = \frac{\pi D_{pool}^2}{4} \tag{3.5.2}$$

Step 11: Calculate the thermal flux at the receiver (Equation 2.9.29).

Table 19. Input data for determining the radiation flux of a pool fire, based on the point source model.

Parameter	Nomenclature	International System Unit
Discharge rate	Q_m	kg/s
Heat of combustion	ΔH_c	J/kg
Heat capacity of the liquid	C_p	J/kg.K
Vaporization heat of the liquid at ambient temperature	ΔH_v	J/kg
Ambient temperature	T_a	K
Boiling point temperature of the liquid	T_{BP}	K
Density of the liquid	ρ	kg/m³
Density of air	ρ_a	kg/m³
Fraction of heat of combustion radiated	η_{rad}	-
Relative humidity	RH	-
Distance from the receiver to the pool	x_{pool}	m

3.5.2 Model presented in TNO (2005)

Table 20 shows the input needed for the modelling of pool fire as it is presented in TNO (2005).

Table 20. Parameters necessary for the calculation of the radiation flux caused by a pool fire.

Parameter	Nomenclature	International System Unit
Hole diameter	d_{hole}	m
Volume of the vessel	V	m³
Length of the vessel	L_{vessel}	m
Discharge coefficient	C_d	-
Liquid head above the hole	h_L	m
Pool thickness	δ_{pool}	m
Density of the liquid	ρ	kg/m³
Mass burning rate	m_b	kg/s
Density of air	ρ_a	kg/m³
Wind speed	u	m/s
Heat of combustion	ΔH_c	J/kg
Fraction of the surface of the flame covered by soot	ζ	-
Surface emissive power of soot	SEP_{soot}	J/(m².s)
Fraction of heat of combustion radiated	η_{rad}	-
Ambient temperature	T_a	K
Relative humidity	RH	-
Distance from the receiver to the pool	x_{pool}	m

The sequence of steps that were implemented in CASE for obtaining the radiant flux caused by a pool fire is listed below:

Step 1: Calculate the area of the hole (Equation 3.1.3).

Step 2: Calculate the surface area of the vessel (Equation 3.1.2).

Step 3: Calculate the outflow velocity (Equation 2.9.30).

Step 4: Calculate the acceleration constant (Equation 2.9.31).

Step 5: Calculate the dimensionless parameter β (Equation 2.9.32).

Step 6: Calculate the dimensionless parameter τ_{max} (Equation 2.9.33).

Step 7: Calculate the maximum duration time of the pool fire (Equation 2.9.34).

Step 8: Calculate the parameter Φ_{max} (Equation 2.9.35).

Step 9: Calculate the diameter and radius of the pool (Equation 2.9.36).

Step 10: Calculate the total release time and the duration of the fire (Equation 2.9.37 and Equation 2.9.38).

Step 11: Calculate characteristic wind velocity (Equation 2.9.39).

Step 12: Calculate non-dimension wind velocity by dividing the wind speed by the characteristic wind velocity.

Step 13: Calculate the mean fire length (Equation 2.9.40).

Step 14: Calculate the flame tilt angle (Equation 2.9.41).

Step 15: Calculate the elongated diameter of the pool (Equation 2.9.42 or 2.9.43).

Step 16: Calculate the surface emissive power (Equation 2.9.44)

Step 17: Calculate the view factor (Equations from 2.9.45 to 2.9.55).

Step 18: Calculate the heat flux at the receiver (Equation 2.9.56).

3.6 BLEVE (Fireball)

3.6.1 Model presented in TNO (2005)

BLEVE has been modelled in order to obtain the radiation flux caused by the fireball. Table 21 shows the input needed for the modelling.

The sequence of steps that were implemented in CASE for obtaining the radiant flux caused by a fireball is listed below:

Step 1: Calculate the mass of flammable material (Equation 2.9.1).

Step 2: Calculate the radius and the duration of the fireball (Equations 2.9.2 and 2.9.3).

Step 3: Calculate the lift of height of the fireball (Equation 2.9.4).

Step 4: Calculate the distance from the receiver to the centre of the fireball (Equation 2.9.5).

Step 5: Calculate the view factor (Equation 2.9.6).

Step 6: Calculate the fraction of heat radiated by a fireball (Equation 2.9.7).

Step 7: Calculate the net available heat for radiation (Equation 2.9.8).

Step 8: Calculate the SEP (Equation 2.9.9).

Step 9: Calculate the actual path length of the radiation (Equation 2.9.10).

Step 10: Calculate the water partial pressure (Equation 2.9.11).

Step 11: Calculate the transmissivity (Equation 2.9.12).

Step 12: Calculate the flux at the receiver (Equation 2.9.13).

Table 21. Input data for the calculation of the radiation flux of a fireball after a BLEVE based on the model presented in TNO (2005) and the model presented in AICHE (2000).

Parameter	Nomenclature	International System Unit
Volume of the tank	V	m³
Fraction of the volume of the tank with material	f_{PLG}	-
Density of the substance in the tank	ρ	kg/m³
Distance from the receiver to the axis of the fireball	x_{bleve}	m
Vapour pressure inside the vessel	P_{SV}	Pa
Heat of combustion of the material at its boiling point	ΔH_c	J/kg
Vaporization heat of the material at its boiling point	ΔH_v	J/kg
Specific heat capacity of the material	C_p	J/kg.K
Temperature difference between flame and ambient temperature	ΔT	K
Relative humidity	RH	-
Ambient temperature	T_a	K

3.6.2 Model presented in AICHE (1994)

The sequence of steps for determining the heat flux from a fireball is:

Step 1: Calculate the mass of flammable material (Equation 2.9.1).

Step 2: Calculate the maximum diameter and the duration of the fireball (Equations 2.9.14 and 2.9.15 or 2.9.16).

Step 3: Calculate the centre height of the fireball (Equation 2.9.17).

Step 4: Calculate the fraction of heat radiated by a fireball (Equation 2.9.7)

Step 5: Calculate the SEP (Equation 2.9.18).

Step 6: Calculate the view factor (Equation 2.9.19).

Step 7: Calculate the actual path length of the radiation (Equation 2.9.10).

Step 8: Calculate the water partial pressure (Equation 2.9.11).

Step 9: Calculate the transmissivity (Equation 2.9.12).

Step 10: Calculate the flux at the receiver (Equation 2.9.13).

3.7 Monte Carlo simulation and CFD add-on

According to Figure 1, the first step of the Chemical Process Quantitative Risk Analysis is the definition of potential accident scenarios. The first step is perhaps the most crucial one, because it will select the scenarios that will be studied. According to the Publication Series on Dangerous Substances (PGS, 2005), it is not necessary to assess the risks of all installations of a plant, but is important to consider all facilities that contribute to the risk, which means facilities that have a specific amount of dangerous substance and that have hazard process conditions. Therefore, the selection of the scenarios must be done first by dividing the plant into separate sections. These sections must be divided in order that if an incident happens in one section, it would not lead to a significant release in other sections. Then, two variables must be calculated: the indication number, which calculates the intrinsic hazard of an installation and depends on the amount of substance present in the section, and the selection number, that measures the hazard of the section at a specific location (PGS, 2005). Based on these parameters, the section of the plant is selected for the risk analysis or not.

The Monte Carlo simulation can then be used in each of these sections selected to determine the probability of different accident scenarios. To analyse that, information about the frequency of incidents and ignition probability must be available for the section selected. Such information is usually available for plants according to the history data of the plant. However, if needed, PGS (2005) also contains information about the loss of containment frequency based on the type of reactors, pipelines and other devices, and also about the ignition probabilities based on the state of the substance. International Association of Oil and Gas Producers (2010b) also presents information about the ignition probability, based on the release rate, the state of the substance and the area in which the facility is located (rural, industrial or urban).

In this study, Monte Carlo simulation has been used to verify the probability and frequency of each vapour cloud explosion scenario based on the probability of the following input variables: discharge rate, wind direction, wind speed and leakage direction. It is important to bear in mind that this methodology should be used for each section of the plant which has been selected to the CPQRA, as already explained.

There are many methods for generating random numbers. In this study, the random numbers for this analysis are generated based on the multiplicative congruential pseudo-random number generator (DOWNHAM and ROBERTS, 1967). This method basically consists of setting a random number as the rest of a division between two numbers (Equation 3.7.1):

$$random_{i+1} = a.random_i \; MOD \; m \tag{3.7.1}$$

where a is the multiplier, m is the modulus and the first random number is called the seed. In this study, the value of the random number must be between 0 and 1, because it represents the probability of an input data. However, this methodology does not limit this range, therefore the random number was again divided by the modulus, in order to have values according to the specification needed.

As already mentioned, four probabilistic variables would be represented by the random number: discharge rate, wind speed, wind direction and leak direction. A set of discharge rates should have each one its own probability. Small discharge rates should have higher probability than great ones, as it is more likely to have small incidents than large ones. Because of that, the discharge rates have been divided into smaller ranges, to cover all possible scenarios with greater accuracy. Based on the study of the International Association of Oil and Gas Producers (2010b), discharge rates smaller than 1 kg/s have been considered small discharge rates. Medium discharge rates are the ones smaller than 10 kg/s but greater than or equal to 1 kg/s. Finally, large discharge rates are the ones greater than 10 kg/s. The information is summarized in Table 22.

In fact, each Monte Carlo study has been performed for a single category (small, medium or large). For each of these categories, four discharge rates – each one with its own occurrence probability - are set in the Monte Carlo simulation, to make the analysis more precise, just as shown in Figure 19 for small releases.

Table 22. Ranges for the discharge rate distribution of each category (International Association of Oil and Gas Producers (2010b).

Range	From (kg/s)	To (kg/s)
Small	0.10	1.00
Medium	1.00	10.00
Large	10.00	1000.00

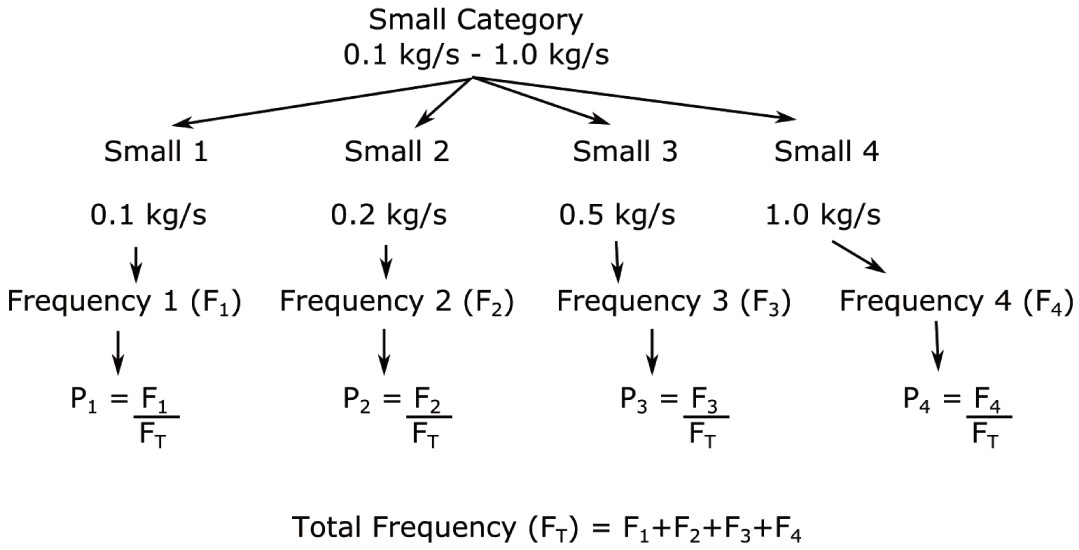

Figure 19. Discharge rates and their probabilities (P) based on the frequency of occurrence for the small category.

For each random number and each category studied, the discharge rate with a probability with the closest value to the random number is the one chosen for this scenario. Same analysis is done with the wind speed, wind direction and the leakage direction, which means that the wind speed, wind direction and leak direction with the smallest difference between the random number and the probability would be the ones selected for the calculations. Hence, all input would be selected according to the smallest difference between the probability and the random number, as shown in Figure 20.

The next step is the calculation of the flammable volume using the stochastic variables selected with the random number. Such calculation is based on the study of Ferreira and Vianna (2014). With CFD data obtained for an offshore facility, they

developed response surface curves for calculating the flammable volume, based on two independent variables: a non-dimensional variable that accounts for the effect of wind speed and discharge rate (R), and the angle between the leakage and the wind directions (φ). Four response surfaces were proposed, each of them for one quadrant of the variable φ, according to Figure 21. Both independent variables are dependent upon the input data selected based on the random number, and therefore the flammable volume could be determined for each random number (Figure 20).

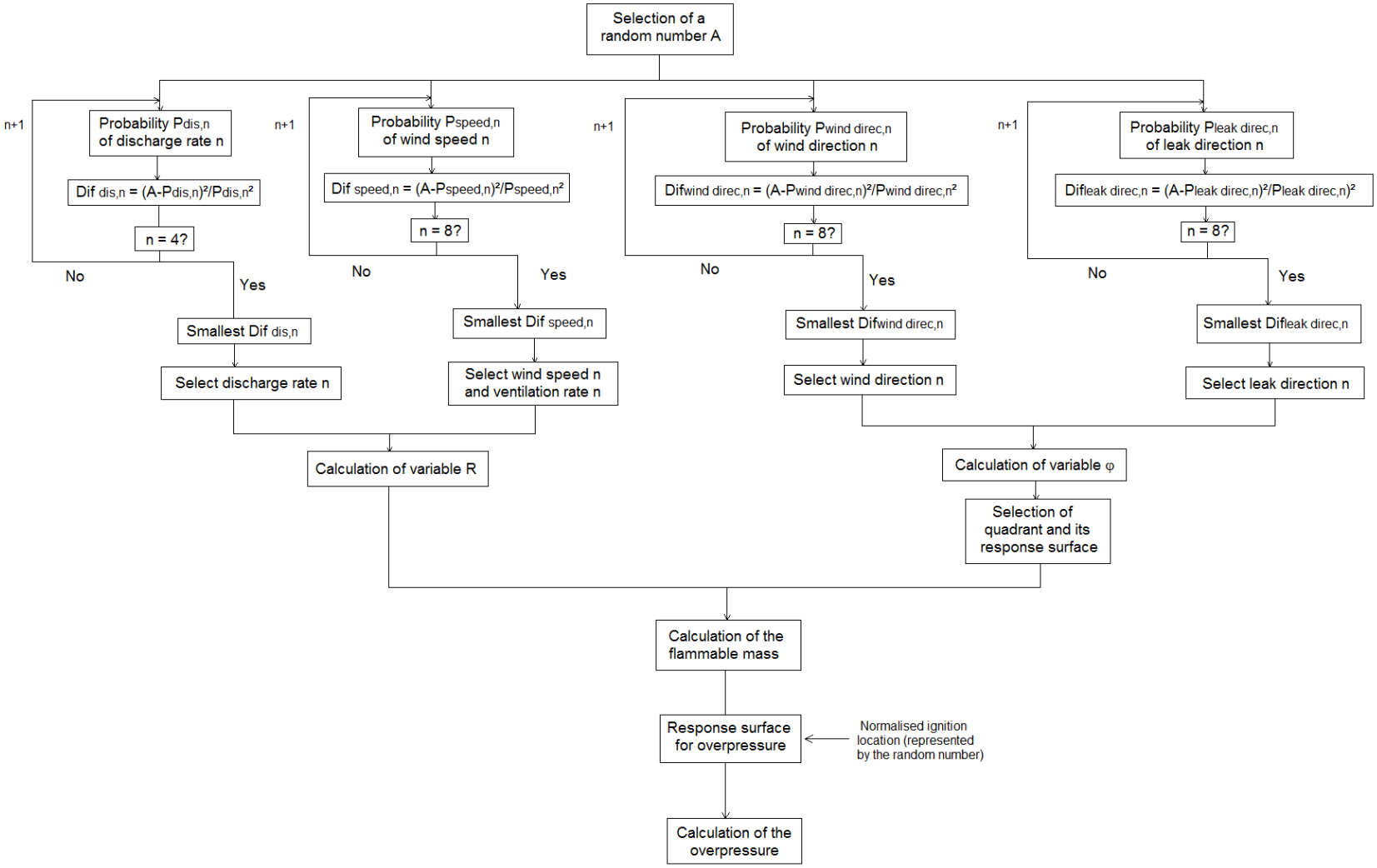

Figure 20. Monte Carlo simulation and CFD add-on methodology for one Monte Carlo simulation.

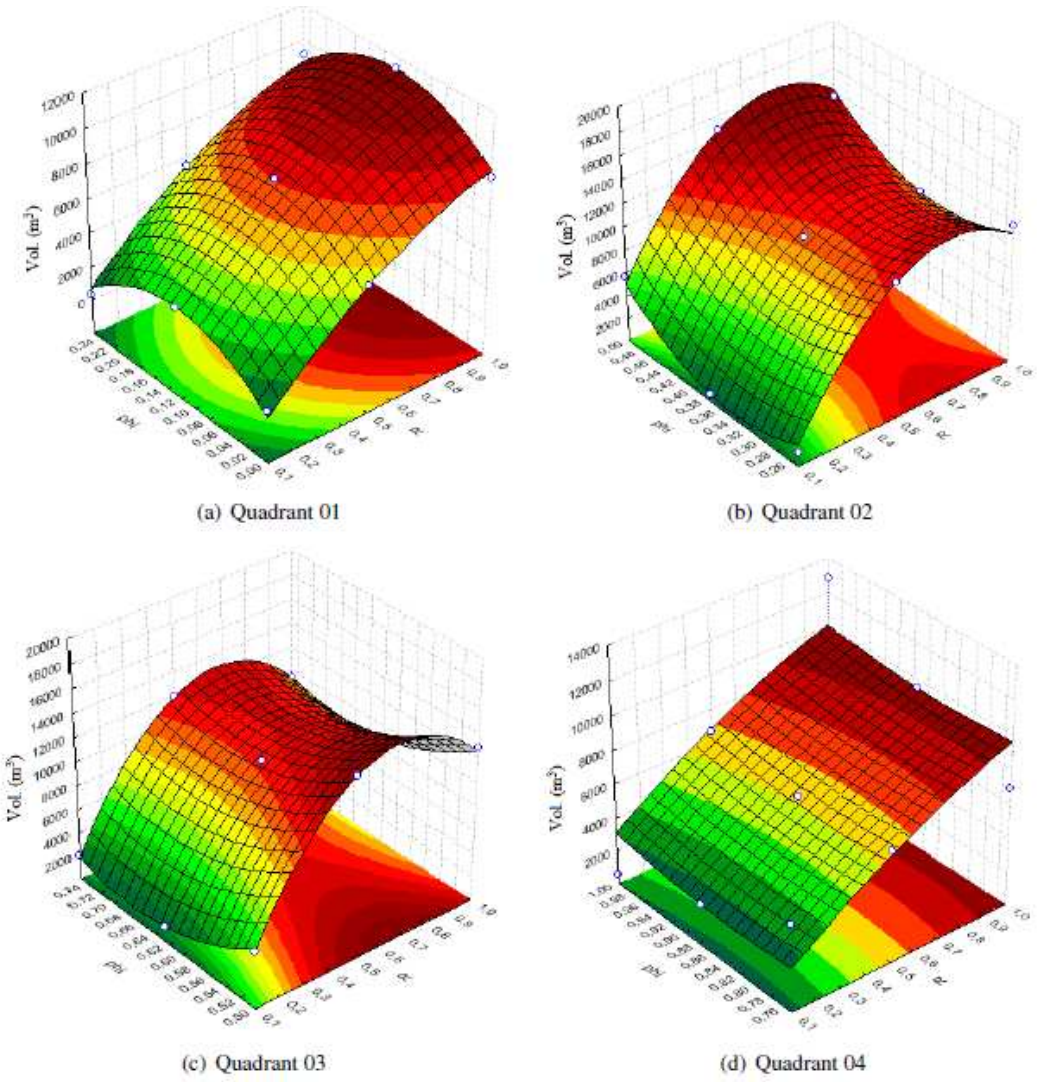

Figure 21. Response surfaces of flammable volume for (a) Quadrant 1, (b) Quadrant 2, (c) Quadrant 3 and (d) Quadrant 4 (FERREIRA and VIANNA, 2014).

A study of the overpressure caused by an explosion has also been taken into account. Vianna and Cant (2012) also developed a response surface curve based on CFD analysis, and the study has been focused on the determination of the overpressure of an explosion (Figure 22). It is based on two variables which are very important for explosion modelling: the normalised ignition and the normalised flammable volume of the sector.

Figure 22 shows the methodology used for obtaining the response surface and the response surface itself. First, CFD cases have been simulated in order to generate data for the response surface development. Then, the response surface has been developed according to CFD results and it has been validated with a different set of data than the one used to generate it. Finally, if the validation is good, the response surface can be used to calculate the overpressure. As shown in Figure 22, the results of the response surface match the CFD results with good precision. The flammable volume determined by the use of response surfaces from Ferreira and Vianna (2014) served as an input for the response surface modelling of overpressure. Therefore, for each random number, a value of overpressure is obtained.

Table 23 shows an example of ten Monte Carlo simulations performed for small leakages. As already explained, for each random number (each simulation), a specific discharge rate is chosen for the scenario according to the smallest difference between the random number and the discharge rate probability. In the first simulation, for example, 1.0 kg/s discharge rate has been chosen. Next, the same analysis is done for the wind speed, wind direction and leak direction. The wind and leak directions are represented by the parameter φ, which accounts for the angle between them. The discharge and the ventilation rates are used to determine the value of variable R, which is a non-dimensional variable for the effect of ventilation and discharge rate. Then, the flammable volume is calculated with these two variables according to the response surfaces for each quadrant. Finally, the flammable volume is an input for the overpressure calculation, which is performed using the response surface of Vianna and Cant (2012).

Considering the total number of Monte Carlo simulations performed, it is possible to determine the probability of certain ranges of overpressures to occur with the results from the Monte Carlo analysis. CASE determines ranges of 0.5 bar for the overpressure results, from 0 bar to 20 bars. According to the total value of overpressure results inside a range and the total number of simulations performed, it calculates the probability of such scenario to occur.

Table 23. Ten Monte Carlo simulation results for small leakages category. Parameters φ and R are normalised.

Simulation	Discharge rate (kg/s)	Wind speed (m/s)	φ	R	Flammable volume (m^3)	Overpressure (bar)
1	1.0	15	0.5	0.1276	5829.553	0.0
2	0.1	9	0.125	0.0221	1790.727	1.2109
3	0.2	3	0.0	0.20	34384.98	0.067
4	0.2	6	0.125	0.0663	1803.326	0.3622
5	1.0	24	0.75	0.0913	5111.131	0.0176
6	0.1	9	0.125	0.0221	1790.727	1.6019
7	1.0	12	0.375	0.1509	0.0	0.0
8	0.5	9	0.125	0.1104	1792.907	0.535
9	0.1	9	0.125	0.0221	1790.727	1.362
10	0.1	9	0.125	0.0221	1790.727	0.7333

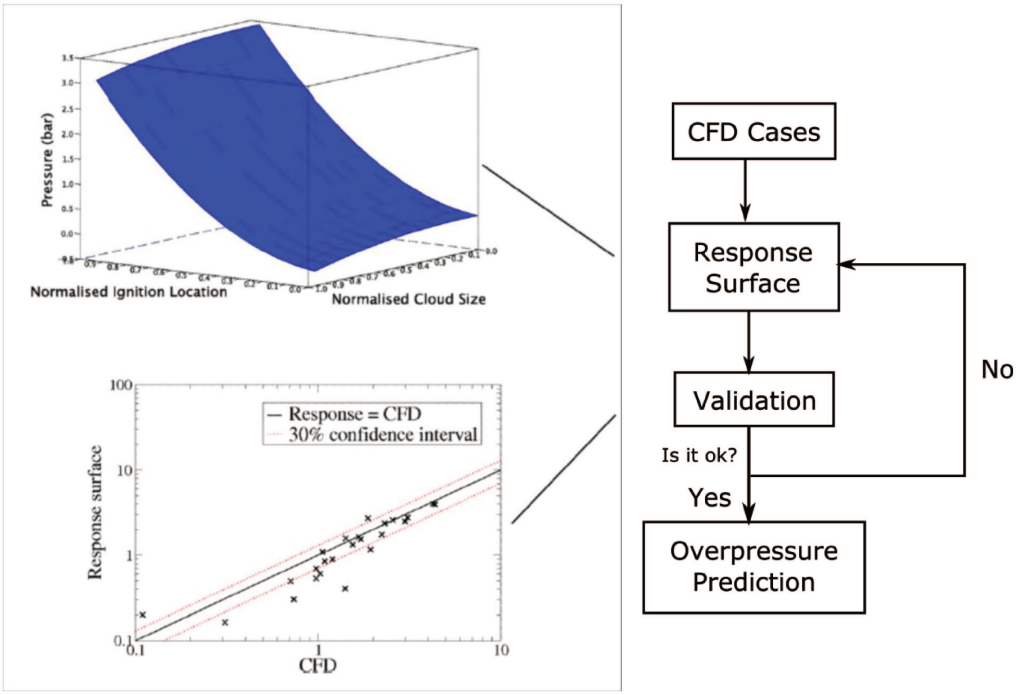

Figure 22. Response surface of overpressure of explosions and the outline of the response surface methodology (VIANNA and CANT, 2012).

Chapter 4

Results

This chapter presents the results obtained in this work after the simulations performed by the new tool CASE. Five accident scenarios have been studied and the results obtained by CASE were compared with the ones from the literature. The behaviour of each model and physical effect is discussed, as well as the results obtained. A study of the vulnerable area of an industrial plant after a gas release is performed. Finally, the Monte Carlo study has been performed according to the methodology previously presented, and the analysis of the results is done.

All models implemented in CASE have been studied in order to verify the consistency of the results obtained by CASE. The results obtained by CASE have been compared with examples from the literature and the behaviour of each step of the accident has been analysed. Five scenarios of possible accidents have been studied with CASE, and the results are shown in this section. In addition, a Monte Carlo simulation has also been performed. As already mentioned, the Monte Carlo simulation has been used to analyse stochastic variables based on surface responses obtained by CFD simulations. Such study provided analysis of flammable volume and overpressure caused by a VCE.

As already mentioned, the following steps of the consequence analysis have been studied and implemented in the tool:

1. Discharge rate:

a. Gas release through hole in a vessel;
b. Gas release through a full bore ruptured pipeline;
c. Liquid release through hole in a vessel;
d. Two-phase constant release.

2. Dispersion:
    a. Puff and plume models for neutral and positive buoyant clouds;
    b. Dense gas.
3. Explosion:
    a. TNT Equivalency Model;
    b. TNO Multi-Energy Model.
4. Jet fire.
5. Pool fire.
6. BLEVE (fireball).
7. Monte Carlo simulation and CFD add-on

4.1 First scenario: hydrogen release through a hole in a vessel

The first scenario accounts for a hydrogen leakage through a hole in a vessel. In order to verify the computational tool, the chosen scenario is a discharge example from the literature (TNO, 2005). With the same scenario, dispersion and explosion have also been analysed. For the dispersion calculation, it has been established a constant discharge rate (plume), according to the criterion shown in Equations 2.6.4 to 2.6.6 with a value exactly as the total mass discharge rate divided by the total release duration time. The input data for the discharge modelling are specified in Table 24, and the input for dispersion and explosion are presented in Table 25. The release rate previously calculated by the discharge model is used in the dispersion calculation.

Table 24. Data used for the calculation of the discharge rate of hydrogen through hole in a vessel.

Properties	Value
Volume of the vessel (m^3)	100
Diameter of the hole (m)	0.1
Molecular weight of hydrogen (g/mol)	2.02
Initial pressure (kPa)	5000.0
Initial temperature (K)	288.15
Ambient pressure (kPa)	100.0
Heat capacity ratio of hydrogen	1.4
Cv - Specific heat at constant volume of the gas (J/kg.K)	10114.4
Discharge coefficient	0.62

Table 25. Input for dispersion, jet fire and explosion calculation of the first scenario - hydrogen release through hole in a vessel.

Dispersion (plume)		Explosion	
Properties	**Value**	**Properties**	**Value**
Initial release rate (kg/s)	15.31	Stoichiometric concentration (%vol)	30.0
Leak height (m)	0.0	Efficiency of explosion	0.05
Pasquill stability class	F	Blast Strength	7
Wind speed (m/s)	2.0	Heat of combustion of TNT (J/kg)	4.69×10^6
		Heat of combustion of hydrogen (J/kg)	1.2×10^8
		LFL (%vol)	4.0
		UFL (%vol)	75.0

Figure 23 shows the discharge rate changing with time for the first scenario. It can be observed that both CASE and the literature present the same behaviour. Such behaviour is already expected as the pressure inside the vessel tends to decrease during the leak, and the same happens to the amount of gas inside the vessel. As the difference between the pressure inside the vessel and the ambient pressure is the gradient for the discharge, the discharge rate will also decrease. The total amount of material (394.79 kg) inside the vessel is released in 109 seconds.

The concentration profile obtained by CASE for a plume considering a constant leak rate agrees well with the result obtained from calculation based on the literature. Figure 24 shows the isopleths for the lower flammability limit of hydrogen for both CASE and the literature's calculation.

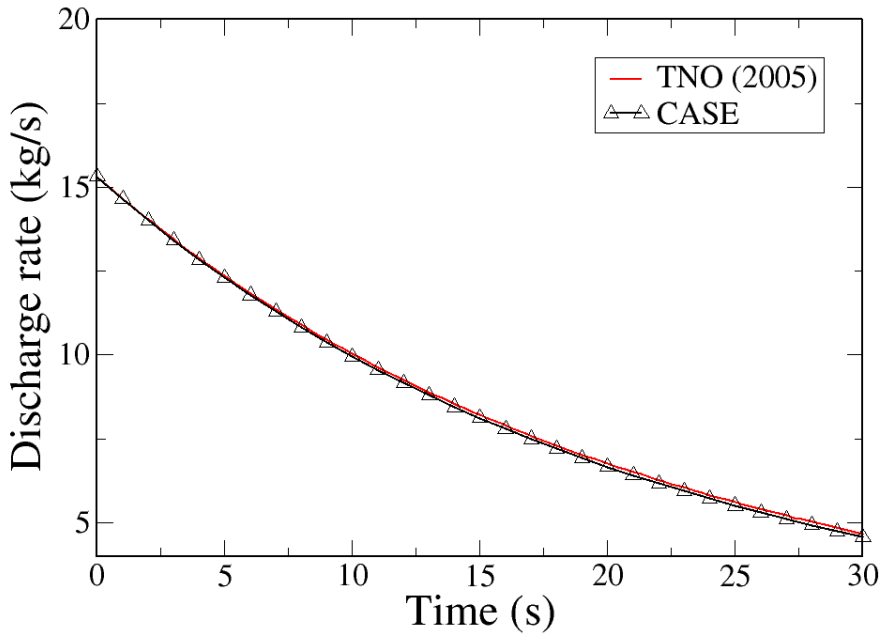

Figure 23. Discharge rate for the first scenario of hydrogen release through a hole in a vessel, based on CASE and TNO (2005) results.

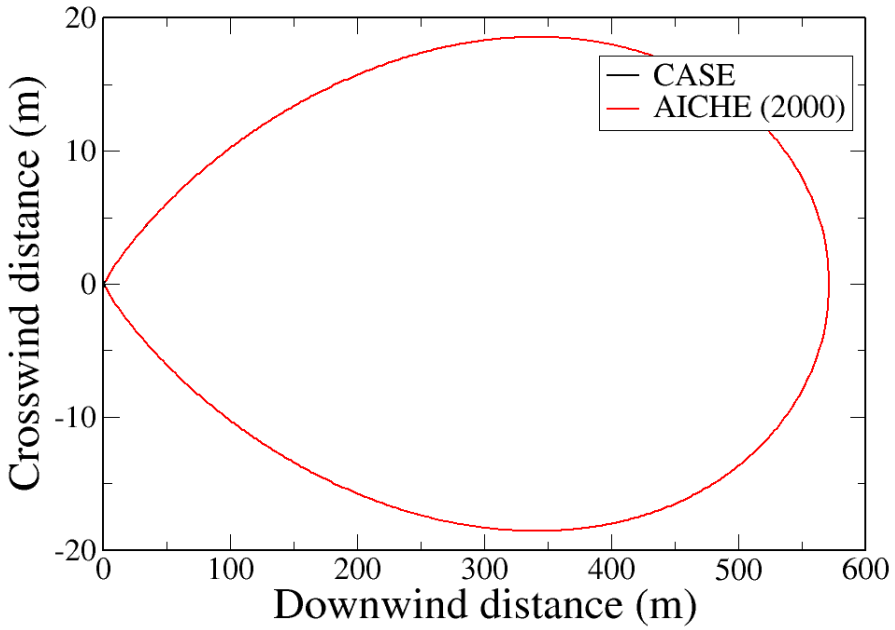

Figure 24. Isopleth for LFL of the plume generated by the hydrogen release of the first accident scenario studied. Comparison between CASE and AICHE (2000) results.

The results for the explosion are based on the data from Table 25, after calculating the total flammable mass of the cloud. Analysis of Figure 25 shows a significant difference between models in the near field. This is due to coarse estimation of the equivalent mass of dynamite as it does depend on the efficiency of the explosion. Also, such behaviour of the TNT Equivalency model is already expected as commented in Section 2.8.1. On the other hand, both models agree well in the far field, but the TNT Equivalency method does decrease faster than the Multi-Energy method, which is also expected. As the Multi-Energy approach considers the decay of released energy with increasing distance from the source, the good agreement for such cases is expected.

The values of overpressure obtained in this scenario show the magnitude of the damage of the explosion. Table 26 shows the damage estimates for common structures for overpressures. Analysis of Table 26 demonstrates that the result obtained in this scenario can cause a serious damage, even if the near field is not considered because of the limitations of the TNT model. The overpressure obtained from a distance from the blast of 200 m, for example, is 19.7 kPa (Multi-Energy model) and 6.46 kPa (TNT Equivalency

model). An overpressure of 19.7 kPa can cause serious structural damages, and even the value obtained by the use of the TNT Equivalency model can cause partial demolition of houses.

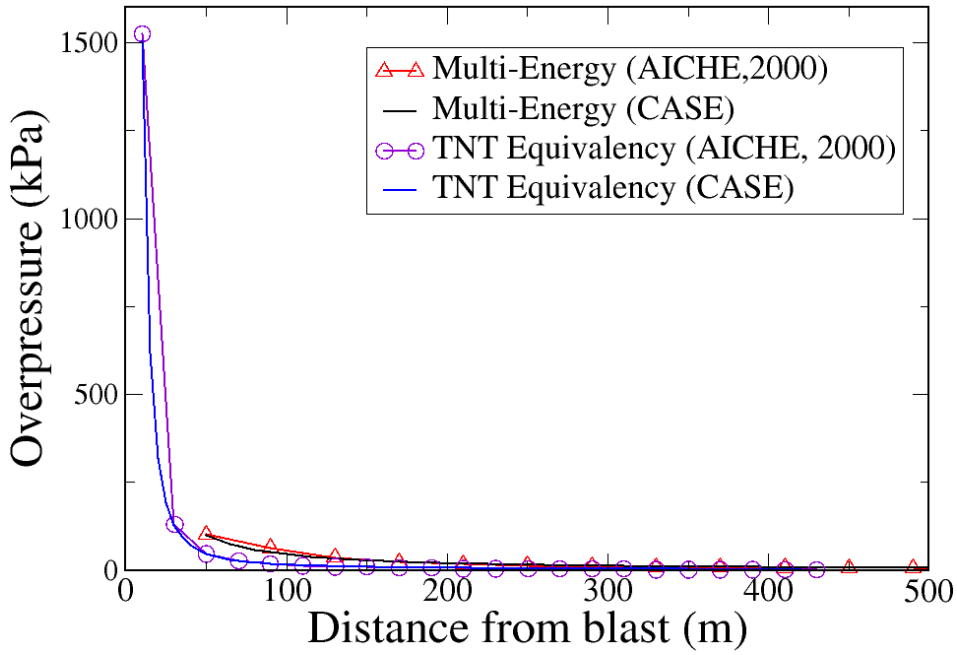

Figure 25. Explosion result for the first scenario regarding the two models available in CASE (TNT Equivalency and Multi-Energy) according to the distance from the blast centre. Comparison between the results obtained by CASE and by calculations based on AICHE (2000).

When considering the damage caused to humans by the increase in pressure, the first and main damage is located in the lungs. This organ is really affected when the pressure differential between the inside and the outside increases, because the thorax is pressed inwards (TNO, 1992). In this analysis, not only the magnitude of the overpressure is important, but the phase duration and the position of the person also play an important role. For a short period of time, the total impulse is very important when determining the damage to humans, and the position of the person (whether the person is down or standing up, or near an obstructed area) may change the actual pressure exerted.

Companhia Ambiental do Estado de São Paulo (CETESB, 2011) states that an overpressure greater than 30 kPa represents 75% probability of fatality. Therefore, in this

scenario, the 75% probability of fatality would occur until a distance of 140 meters from the blast, considering the results from the Multi-Energy model.

Table 26. Damage estimates for common structures for different overpressures (AICHE, 2000).

Overpressure (kPa)	Damage
0.14	Annoying noise
1.03	Typical pressure for glass breakage
2.07	95% probability of no serious damage below this value
6.9	Partial demolition of houses
15.8	Lower limit of serious structural damages
34.5 – 48.2	Nearly complete destruction of houses
68.9	Probable total destruction of buildings

A study of how the blast strength influences the overpressure calculation of the Multi-Energy model has also been evaluated in CASE (Figure 26). As expected, strengths 1 to 3 provided the smallest values of overpressures. As the blast strength increases, the overpressure tends to achieve higher values, which makes sense as the strengths represent the obstacle and the confinement degree of the studied scenario, hence the turbulence effect. As already mentioned, the more obstacles there is, and therefore the greater strength, the greater is the overpressure.

However, the difference in overpressure for different blast strengths is more significant in the near field. In far field the difference almost disappears as the blast loses its strength when the distance from the blast centre grows.

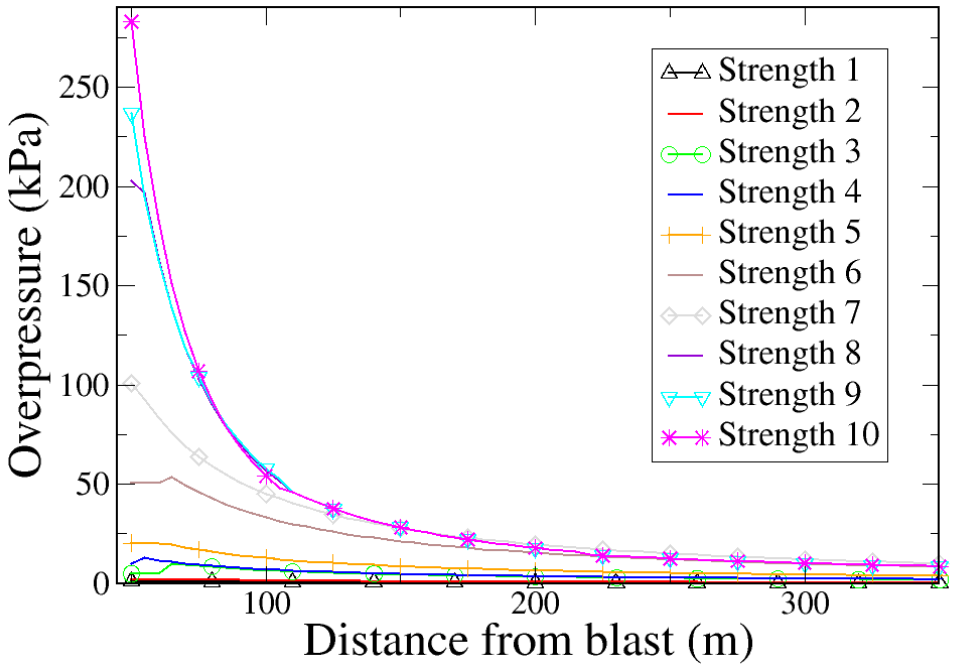

Figure 26. Different overpressure profiles for each blast strength from the Multi-Energy model, according to the distance from the blast and obtained by CASE.

A similar analysis can be done for the efficiency of explosion (η_{TNT}) of the TNT Equivalency model (Figure 27). The greater the efficiency, the greater the overpressure is, because the efficiency is used in the calculation of the equivalent mass of TNT. Such difference is more visible in the near field, which is a similar behaviour as the blast strengths of Multi-Energy method. Figure 27 shows that small changes in the efficiency of explosion can provide greater changes in the outcome, which reinforces the importance on the estimation of the parameter.

The output provided by CASE for this scenario is shown in Appendix A for all accident effects studied.

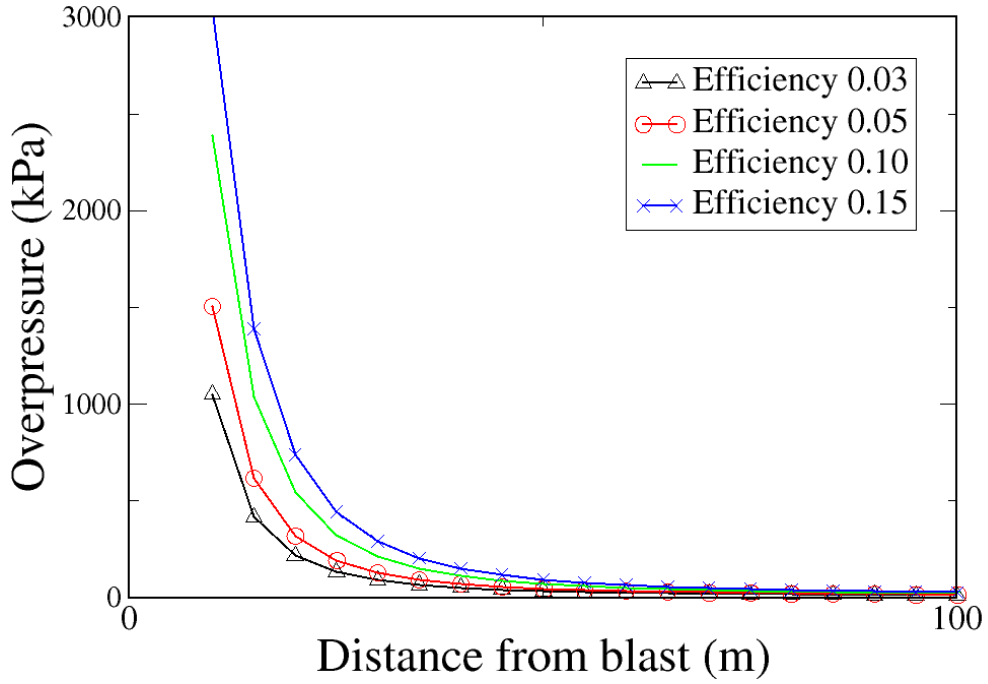

Figure 27. Different overpressure profiles for different values of the explosion efficiency parameter of the TNT Equivalency model, according to the distance from the blast and obtained by CASE.

4.2 Second scenario: methane discharge through a full bore ruptured pipeline

The second scenario is a transient leak of methane due to a full bore rupture of a pipeline. The input data are the ones described in Table 27. CASE agrees fairly well with the literature (Figure 28), and the behaviour is expected to be the decreasing of discharge rate, as already mentioned in Section 4.1.

Table 27. Input for the release behaviour of the second scenario of a full-bore ruptured pipeline of methane.

Properties	**Value**
Pipe length (m)	1.0×10^{5}
Pipe diameter (m)	1.219
Internal roughness of the pipeline (m)	3.0×10^{-5}
Pressure of the pipeline (kPa)	6850.0
Temperature of the pipeline (K)	288.15
Molecular weight of methane (g/mol)	16.04
Ambient pressure (kPa)	100.0
Heat capacity ratio of methane	1.31
Discharge coefficient	1.0

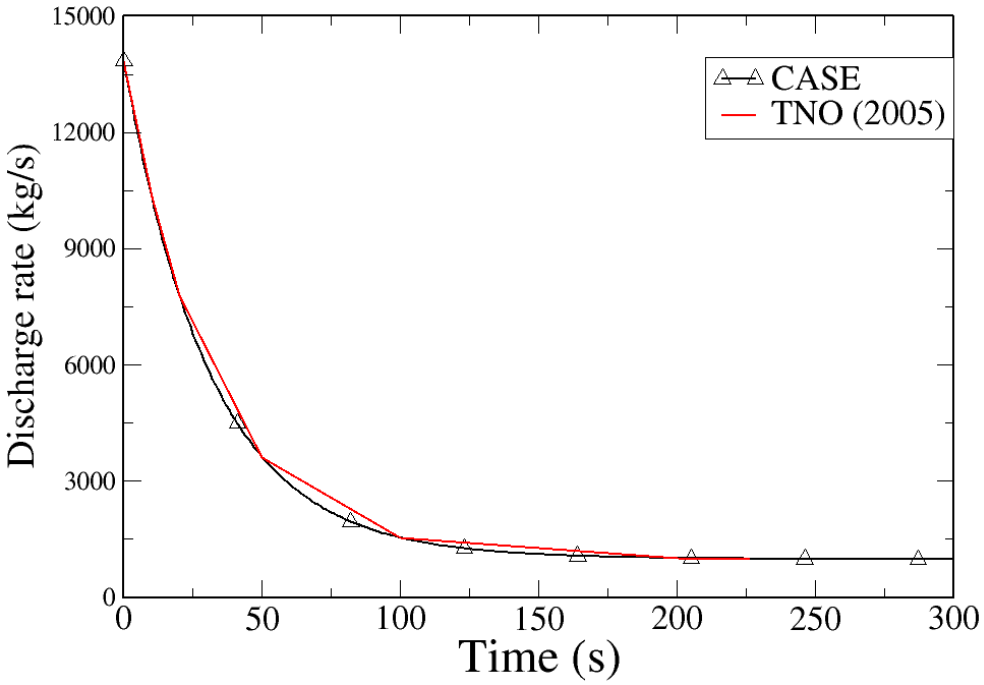

Figure 28. Discharge rate of methane after a full bore rupture in the pipeline. Comparison between the results obtained by CASE and TNO (2005).

4.3 Third scenario: liquid discharge through a hole in a vessel

The third scenario accounts for a liquid discharge through a hole in a vessel. Table 28 presents the input data, in which acrylonitrile is released through a 0.1 m hole. As the other two scenarios, it agrees well with the literature (Figure 29).

The behaviour of the liquid discharge differs from the gas discharge (Figure 23 and Figure 28) because of the size of the vessel, which is much larger in the third scenario (6600 m³). Despite such difference, both discharge models provide a descending behaviour, which is expected as the gradient for the liquid and gas discharge reduces with time.

Table 28. Input for the discharge calculation of the third scenario (liquid leakage of acrylonitrile from a hole in a vessel).

Properties	**Value**
Volume of the vessel (m³)	6600
Diameter of the hole (m)	0.1
Pressure above liquid (Pa)	101325
Initial temperature (K)	288.15
Ambient pressure (Pa)	101325
Filling degree of the vessel	0.80
Leak height (m)	0.0
Discharge coefficient	0.62
Density of the liquid (kg/m³)	812.5

The evaporation of the liquid being discharged has also been determined, as well as the pool formation and the dispersion of the cloud formed by evaporating the pool, with the data presented in Table 29. As the molecular weight of acrylonitrile (53.06 kg/mol) is higher than the molecular weight of air (28.96 kg/mol), it is expected a dense gas behaviour in the dispersion of the cloud. The dense gas dispersion has been calculated by CASE for

the lower flammability limit of acrylonitrile (2.42 %vol), and the result is shown in Table 30.

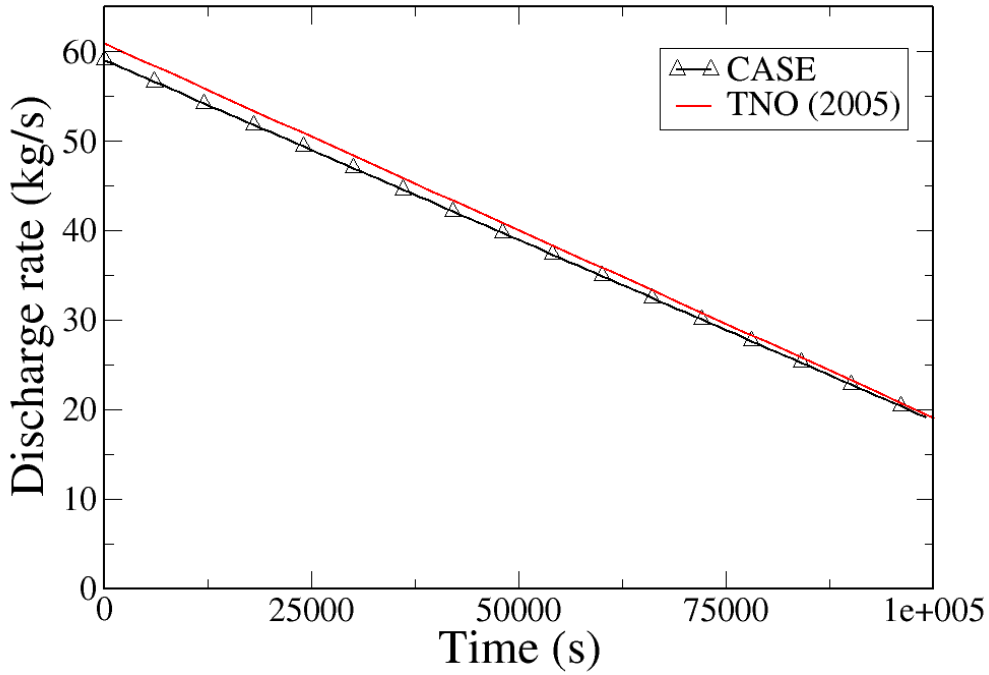

Figure 29. Discharge rate for the third scenario of acrylonitrile (liquid) release through hole in a vessel of 6600 m³. Comparison between CASE and TNO (2005) results.

As already mentioned, the pool fire outcome has also been verified for the acrylonitrile leakage. The pool fire radiation flux has been studied in CASE for both models presented in the Methodology section, for different distances from the receiver (Figure 30). Figure 30 depictures the results from both models after their implementation in the computational tool CASE. Both models present a similar decreasing behaviour, which is expected because of the nature of the pool fire. Different from the overpressure in explosions, the radiation flux in pool fire or even in jet fire are more directional, which means that for a victim to occur, the person must be very near the jet or the pool. In contrast, the outcome of an explosion can make victims even if the person is not near the explosion blast centre.

Table 29. Input for the pool evaporation and pool fire calculations after the acrylonitrile leakage through hole in a vessel.

Properties	**Value**
Temperature of the ground (K)	298.0
Thermal diffusivity of the soil (m^2/s)	4.2×10^{-7}
Thermal conductivity of the soil (W/m.K)	0.9
Boiling point temperature (K)	350.0
Kinematic viscosity (m^2/s)	4.5×10^{-7}
Heat of combustion (J/kg)	3.18×10^{7}
Heat of vaporization (J/kg)	6.34×10^{5}
Heat capacity (J/kg.K)	2029.7
Pool thickness (m)	1.0
Temperature of the pool (K)	290.0
Wind speed (m/s)	2.0
Ambient temperature (K)	198.0
Relative humidity of ambient	0.5
Fraction of energy converted to radiation	0.4
Fraction of soot	0.05
Surface emissive power of soot (W/m^2)	30.0

Table 30. Results of the dispersion of the acrylonitrile cloud after a release through hole in a vessel (plume dense gas cloud). Flammable mass result based on the LFL concentration (concentration of interest).

Concentration of interest (%vol)	Distance to reach the concentration (m)	Flammable mass (kg)
2.42	0.8	103.71

CETESB (2011) states that for a risk analysis, it must be considered 100% probability of fatality for a radiation flux greater than 35kW/m² for a pool fire. In the scenario studied, therefore, victims would occur in a radius of roughly 12.5 meters from the pool fire, considering the TNO model. The model of Mudan (1984) shows that such distance is increased to about 25 meters. The radiation flux then decreases quite fast until it reaches almost zero.

Differences between the two models of pool fire implemented in CASE can also be verified in Figure 30. There are mainly two differences between the models: the first one is that the model presented in TNO (2005) takes into account the tilt and drag of the pool caused by the wind. The second is that it also considers the formation of soot, a phenomenon which absorbs part of the radiation and decreases the heat flux. These differences are probably the cause of the deviation between models.

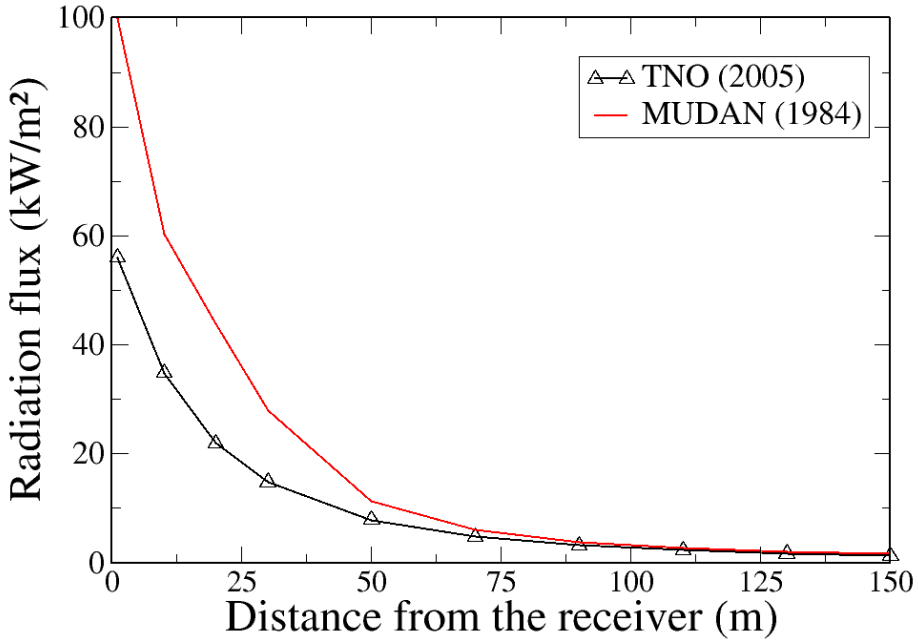

Figure 30. Radiation flux from pool fire caused by a liquid discharge and later ignition of the pool, according to the distance from the receiver. Results obtained by CASE using two different models presented in TNO (2005) and Mudan (1984).

4.4 Fourth scenario: methane leakage through a hole in a vessel

The fourth scenario is the study of a jet fire in case methane is released and instantaneously ignited. In addition, discharge, dispersion and explosions results have also been verified. Table 31 presents the data for calculating all the steps of the accident.

Figure 31 shows the discharge behaviour for the scenario, which agrees well with the literature and present a similar behaviour from the first scenario of hydrogen gas release. The next result (Figure 32) shows the dispersion of the cloud as a plume, and Figure 33 shows the overpressure outcome. The overpressure behaviour is similar to the one of the first scenario (Figure 25), but in this case, the overpressure is much smaller than the other one. Such difference can be explained by the fact that the range of flammability of hydrogen is much greater than the one of methane, which means that more concentrations of the cloud would be between the flammability limits.

Finally, the jet fire radiation effect has been verified for a distance at 15 meters from the receiver (Figure 34). As the radiation flux of a jet fire is proportional to the discharge rate, such decreasing behaviour is expected. CASE modelling agrees well with the same scenario calculated by the literature. As already mentioned, according to CETESB (2011), a radiation flux greater than 35kW/m² represents 100% probability of fatality. Therefore, for this scenario and for a receiver at 15 meters from the jet fire, fatalities would occur in the first 65 seconds after the release.

Table 31. Input for the calculation of all steps of an accident (discharge and dispersion) and accident outcomes for gas release (explosion and jet fire) for the fourth scenario (methane release through hole in a vessel).

Properties	**Value**
Volume of the vessel (m^3)	100
Diameter of the hole (m)	0.1
Molecular weight of methane (g/mol)	16.04
Molecular weight of air (g/mol)	28.96
Initial pressure (kPa)	5000.0
Initial temperature (K)	288.15
Ambient pressure (kPa)	100.0
Heat capacity ratio of methane	1.31
Cv - Specific heat at constant volume of the gas (J/kg.K)	1685.63
Discharge coefficient	0.62
Wind speed (m/s)	2.00
Atmospheric stability class	F
Temperature of the flame (K)	2200
Distance from the flame (m)	15
Fraction of energy converted to radiation	0.2
Heat of combustion of the material (J/kg)	5.0×10^7
C_T	0.095
α_T	1.0
Lower and upper flammability limits (%vol)	5.0-15.0

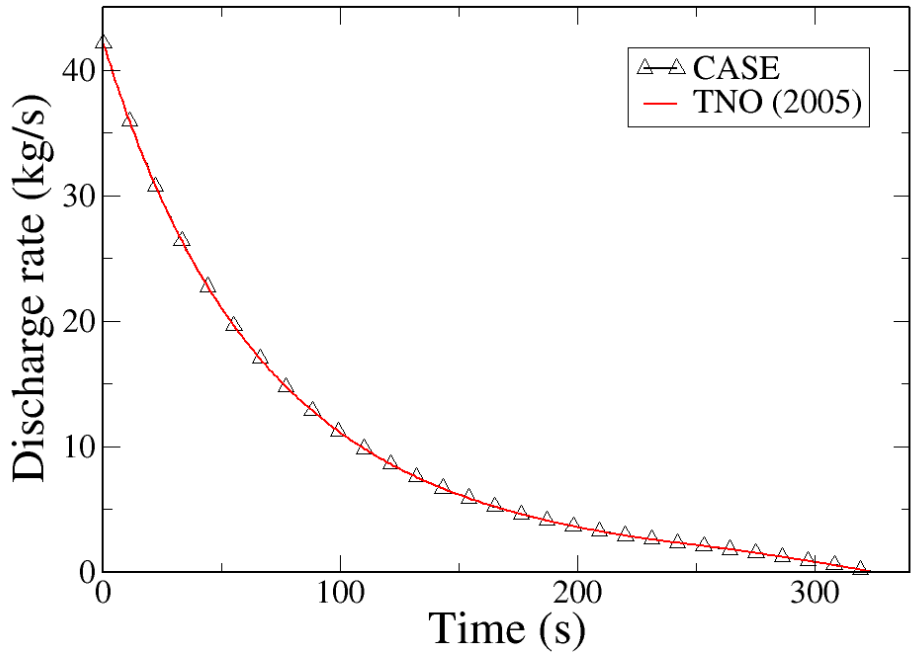

Figure 31. Transient discharge rate of methane after a release through a hole in a vessel (fourth scenario). Comparison between CASE and TNO (2005) results.

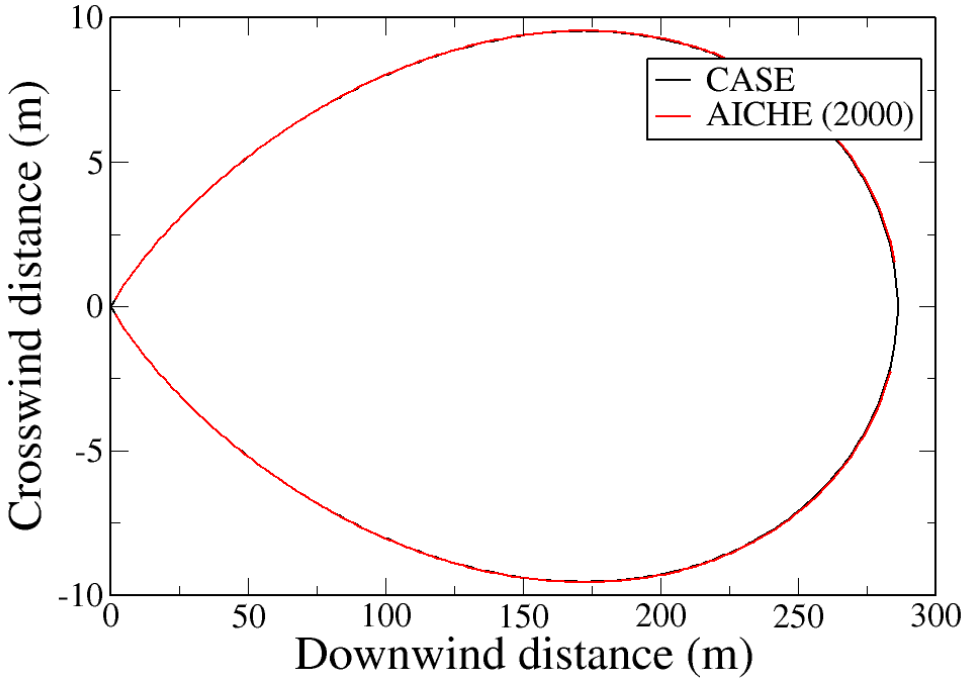

Figure 32. Isopleth for LFL of the plume generated by the methane release of the fourth scenario. Comparison between CASE and calculation using the model presented in AICHE (2000).

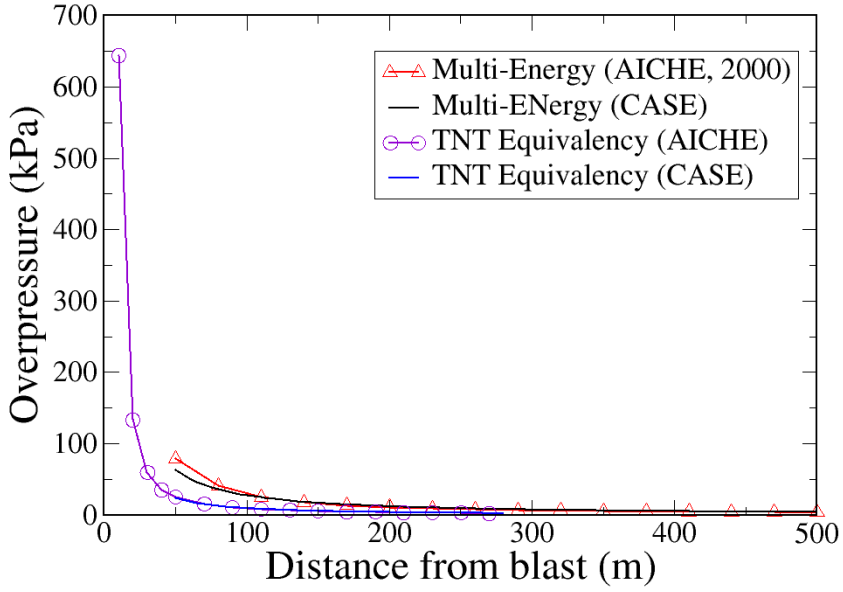

Figure 33. Explosion result for the fourth scenario regarding two models available in CASE (TNT Equivalency and Multi-Energy), according to the distance from the blast centre. Comparison between the results obtained by CASE and by the calculation with the model presented in AICHE (2000).

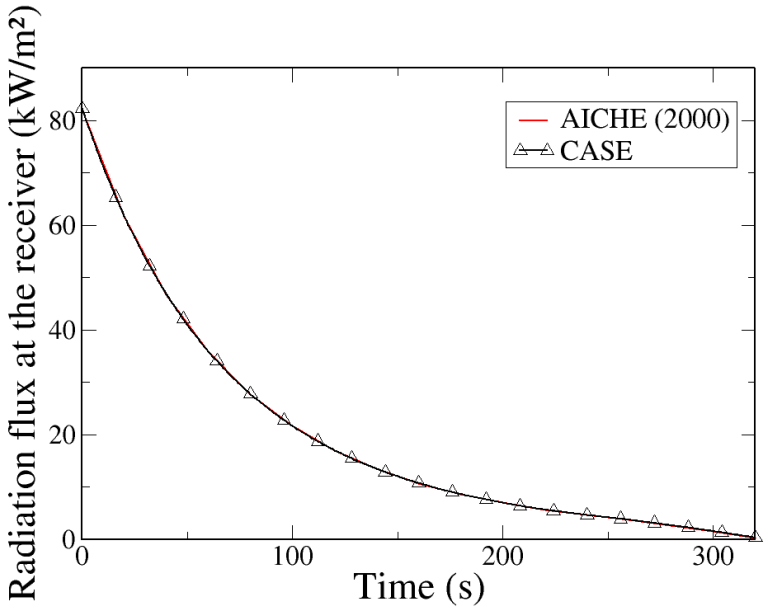

Figure 34. Radiation flux through time of a jet fire caused by methane release (fourth scenario). Receiver at 15 m from the flame. Comparison between results obtained by CASE and the calculation of the model presented AICHE (2000) for this scenario.

The criterion for establishing whether the dispersion is a plume or a puff depends on the puff dispersion coefficient in the downwind direction, which also depends on the time taken after the release. This means that if the time taken after the release is changed, the behaviour of the cloud dispersion may be also modified. Smaller times tend to define the dispersion as a plume, and greater times as a puff, although this is not a rule.

In order to verify the distinction between both plume and puff models, and also to verify the difference in the puff in many distances from the discharge, the fourth scenario has been modified. The modification is the diameter of the hole from 100 mm to 420 mm. Such modification should decrease the total time of the discharge, which also is considered in the criteria of the dispersion. The result is that 1000 seconds after the release, the dispersion behaves as a puff. Figure 35 shows the puff cloud behaviour for different times after the release, hence different downwind distances. Figure 35 can be seen as the size of the cloud that has the concentration of the LFL seen from top. The size of the cloud first starts to grow (from distance 2000 m to 2300 m). This occurs because the cloud is mixing with air and the amount of mass within the flammability limits increases. As time grows, the cloud becomes so diluted that the size of the cloud decreases, and so does the total flammable mass.

The flammable mass behaviour through dispersion time has also been evaluated (Figure 36). As expected, the flammable mass grows with entrainment of air, just like the cloud size. The flammable mass reaches its maximum value at 1400 s after the release.

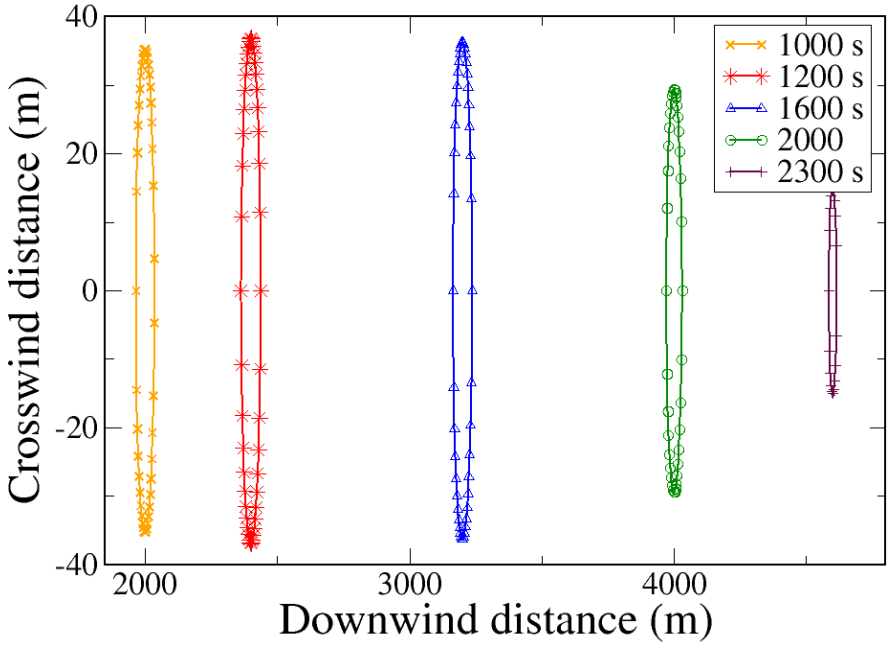

Figure 35. Isopleths for LFL of the puff cloud for different distance and time after the release. Results obtained by CASE for the fourth accident scenario (methane release through hole in a vessel).

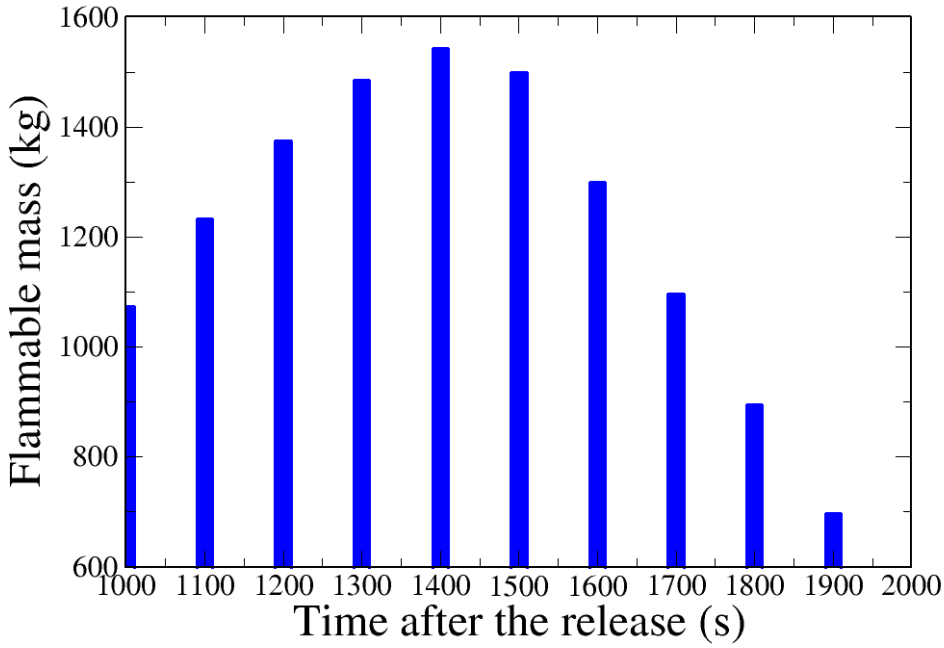

Figure 36. Change in the total flammable mass of the cloud according to the time after the release. Result obtained by CASE. Simulation of the cloud after methane release through hole in a vessel (fourth scenario studied).

4.5 Fifth scenario: two-phase release of propane

The fifth scenario accounts for a liquefied pressurized propane accident, hence a two-phase release. In this scenario, both pool fire and fireball outcome, which is an effect of BLEVE, have been analysed. The data used in such scenario is shown in Table 32.

CASE solves the two-phase discharge model in a constant matter and then the flashing process is obtained. The discharge and flashing results are presented in Table 33.

The radiation effect of both pool fire and fireball are shown in Figure 37, which shows the calculation results of the models after their implementation in CASE. The first comparison that can be made is the great difference between the fireball and the pool fire radiation at near field. It is clear that the BLEVE outcome is more dangerous than the pool fire, as the radiation flux is higher. Actually, the radiation from a fireball in this scenario reaches values higher than the one established by CETESB (2011) as 100% probability of fatality (35 kW/m²). Also, BLEVE outcomes usually are followed by missiles from fragments of the vessel and can cause domino effect, which means that the fatalities and damages can be even greater if these effects are taken into account. The missiles are not accounted in the present work.

Table 32. Input data for the fifth scenario of two phase release of propane. Data for the calculation of discharge, dispersion, pool fire and BLEVE (fireball).

Properties	**Value**	**Properties**	**Value**
Molecular weight of propane (g/mol)	44.10	Kinematic viscosity (m^2/s)	4.0×10^{-6}
Molecular weight of air (g/mol)	28.96	Heat of combustion (J/kg)	4.6×10^{7}
Initial pressure (kPa)	2059.00	Heat of vaporization (J/kg)	4.26×10^{5}
Initial temperature (K)	282.15	Heat capacity (J/kg.K)	2582.0
Volume of the vessel (m^3)	45.0	Saturation pressure (kPa)	1600.0
Length of the vessel (m)	14.0	Volume change in vaporisation (m^3/kg)	0.048
Filling degree	0.8	Discharge coefficient	0.85
Pressure above liquid (kPa)	1600.0	Wind speed (m/s)	2.00
Hole diameter (m)	0.10	Stability class	F
Ambient pressure (kPa)	100.0	Pool thickness (m)	1.0
Relative humidity	0.50	Temperature of the pool (K)	290.0
Temperature of the ground (K)	298.0	Fraction of soot	0.05
Thermal diffusivity of the soil (m^2/s)	4.2×10^{-7}	Surface emissive power of soot (W/m^2)	30.0
Thermal conductivity of the soil (W/m.K)	0.9	Fraction of energy converted to radiation	0.3
Boiling point temperature (K)	230.0	C_T	0.04

Table 33. Discharge results for a two-phase release of propane after an incident in a PLG vessel of propane.

Total discharge (kg/s)	Liquid discharge (kg/s)	Vapour discharge (kg/s)
179.53	105.56	73.97

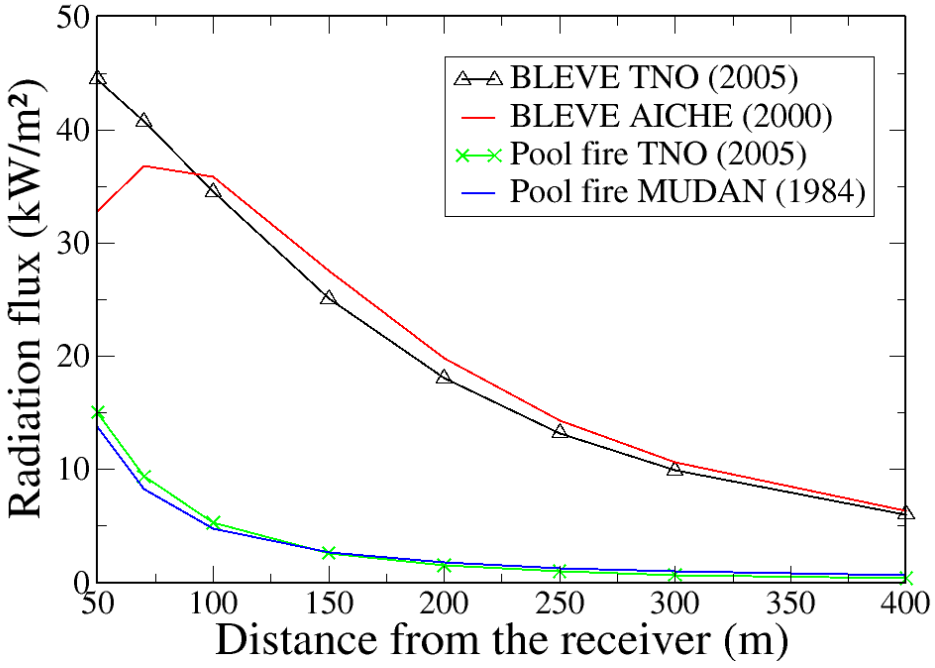

Figure 37. Radiation flux from both BLEVE and pool fire of two-phase propane release. Results calculated by CASE based on two different models for each effect (fireball and pool fire).

4.6 Accidental scenario in an industrial plant

Suppose that an incident occurs in a refinery plant (Figure 38) in the natural gas unit. The accident scenario would be the one presented in Section 4.4, which accounts for a hole in a vessel incident and therefore the discharge of methane presented in it. Both jet fire and explosion effects have been verified as examples of accidents in the refinery, however they do not represent a real accidental scenario in this refinery. Overpressure caused by a vapour cloud explosion is determined, in case the dispersion of the substance in the atmosphere takes place and the cloud meets an ignition source after mixing with air. On the

other hand, if the material is ignited right after its release, a jet fire occurs and its results have also been determined.

Information for the calculation of the physical effect is the one described in Section 4.4. The overpressure has been calculated by the Multi-Energy model with blast strength of 7, according to the rule presented in Table 7 for confined areas. Jet fire has been obtained for different distances from the receiver. The vulnerable areas of the overpressure and the jet fire have been verified for this scenario (Figure 38 and Figure 39, respectively).

Figure 38. Vulnerable area for explosion after an accident in the natural gas unit of the refinery. The supposed accident scenario is the one presented in Section 4.4. (GOOGLE MAPS, 2015)

Figure 38 shows that the vulnerable area of overpressure is larger than the area of radiation flux caused by a jet fire (Figure 39). As already mentioned, this is expected, as the shock wave caused by explosions reach larger areas than fires. According to Table 26, for a radius of 100 meters from the blast centre, the explosion would cause serious structural damages, as the overpressure is 27.7 kPa. The overpressure reduces to 4.01 kPa for a distance of 500 meters from the blast centre, which can cause occasional damage to window frames. Such distance already affects the neighbourhood of the industrial plant, and therefore can cause damages apart from the industrial area.

It is important to bear in mind that besides the damages caused by the shock wave, the explosion can also generate missiles that can affect other parts of the plant. In such cases, the domino-effect of an explosion must be investigated and analysed.

Regarding the radiation flux caused by a jet fire, results show that at 25 meters from the release source the radiation flux is 35.87 kW/m². This represents a probability of fatality of 100%, as the value is larger than 35 kW/m². Although the radiation flux reduces drastically with distance, a fire can also cause domino-effects to occur, like a BLEVE in case the fire reaches another vessel with pressurized liquefied gas.

Figure 39. Jet fire radiation flux after a supposed accident in the natural gas unit of a refinery according to the distance from the receiver. Vulnerable area affected by the jet is represented according to the distance from the receiver. (GOOGLE MAPS, 2015)

4.7 Monte Carlo simulation and CFD add-on

The Monte Carlo simulation is strongly dependent on the random number generated and the probability of each input variable. For this study, the random number generation method presented in Section 3.7 has been implemented with the values presented in Table 34. When not specified otherwise, the number of Monte Carlo simulations performed is 10,000.

Table 34. Values used for the random number generation based on the multiplicative congruential pseudo-random number generator method.

Variable	**Value**
Multiplier, *a*	16807.00
Modulus, *m*	2.15×10^9
Seed	19.00

As already described in Section 3.7, the discharge rate distribution has been divided into 3 categories: small, medium and large discharge rates, according to Table 22, and each of these categories have been studied separately. The probability data for each discharge rate and the leak frequency have been chosen according to the release rate frequency presented in the work of Richardson (2008), which is based on the HCR (Hydrocarbon Releases Database System) data from 1992 to 2008 (Table 35). However, it is important to bear in mind that in real plant studies this data should be taken from the existing plant frequency history. Information about the ignition probability can be seen in the same Table, using the value of the ignition probability of the largest discharge rate of the category, according to the International Association of Oil and Gas Producers (2010b). Ignition probabilities have been selected for gas releases from offshore FPSO process module, as the study of Ferreira and Vianna (2014) used for the calculation of the flammable volume of the cloud has been also performed for an offshore facility. The leakage direction probability has also been chosen based on engineering judgment (Table 36). Finally, the wind direction and speed have been defined according to Table 37 and Table 38,

respectively, and represent the wind rose of the Campos Basin, Brazil (Petrobras Metocean Data, 2005). The ventilation rate is also shown in Table 37, according to the work of Ferreira and Vianna (2014) for the offshore facility with accommodation module (worst case scenario). All of these data should be provided by the user of CASE for the Monte Carlo simulation.

Table 35. Release rate distribution, ignition probability and leak frequency for each category (Richardson, 2008 and International Association of Oil and Gas Producers, 2010b).

Category	Discharge rate (kg/s)	Discharge rate Probability	Ignition Probability	Leak frequency (/year)	Ignition Prob. x Leak Freq.
Small	0.1 0.2 0.5 1.0	0.341 0.227 0.284 0.148	0.0013	0.0478	6.2×10^{-5}
Medium	1.0 2.0 5.0 10.0	0.342 0.289 0.264 0.105	0.0213	0.0206	4.4×10^{-4}
Large	10.0 100.0 500.0 1000.0	0.666 0.167 0.100 0.067	0.15	0.0033	4.9×10^{-4}

Table 36. Probability of each leakage direction.

N	NE	E	SE	S	SW	W	NW
0.09	0.17	0.18	0.07	0.06	0.13	0.14	0.16

Table 37. Wind properties and probabilities: direction (Petrobras Metocean Data, 2005) and ventilation rate (FERREIRA and VIANNA, 2014) of each direction.

Wind direction probability							
N	**NE**	**E**	**SE**	**S**	**SW**	**W**	**NW**
0.09	0.17	0.18	0.07	0.06	0.13	0.14	0.16
Ventilation rate (m^3/s)							
882.80	849.95	563.10	792.30	884.10	932.75	770.80	864.25

Table 38. Wind speed probability of the Campos Basin, Brazil (adapted from Petrobras Metocean Data, 2005).

Wind speed probability							
0-3 m/s	**3-6 m/s**	**6-9 m/s**	**9-12 m/s**	**12-15 m/s**	**15-18 m/s**	**18-21 m/s**	**21-24 m/s**
0.1787	0.2873	0.3148	0.1030	0.0146	0.0243	0.0386	0.0386

Example of the CASE's output for the small category with Monte Carlo simulations is shown in Appendix B, for 40 Monte Carlo simulations. The overpressure probability has almost the same behaviour for each category, considering the probability distribution shown in Figure 40. The most probable overpressure is 0.5 bar for all release categories, which is expected, as usually hazardous scenarios have smaller probabilities. Large release rates and small release rates provided the highest overpressure possible, although with a small probability.

The similar behaviour of the categories can be explained because of the discharge rate distribution for each category. The discharge rate probability of small discharges is very similar to medium discharges, and the discharge rate distribution for large discharge rates is also not very different. Besides that, the normalization of the parameters used in the response surfaces can also influence on this result. Values of the parameter that accounts for the ventilation rate, for example, which is dependent on the discharge rate, are normalised and because of that, even a great discharge rate will not influence the variable so much, as it has a small range from 0 to 1.

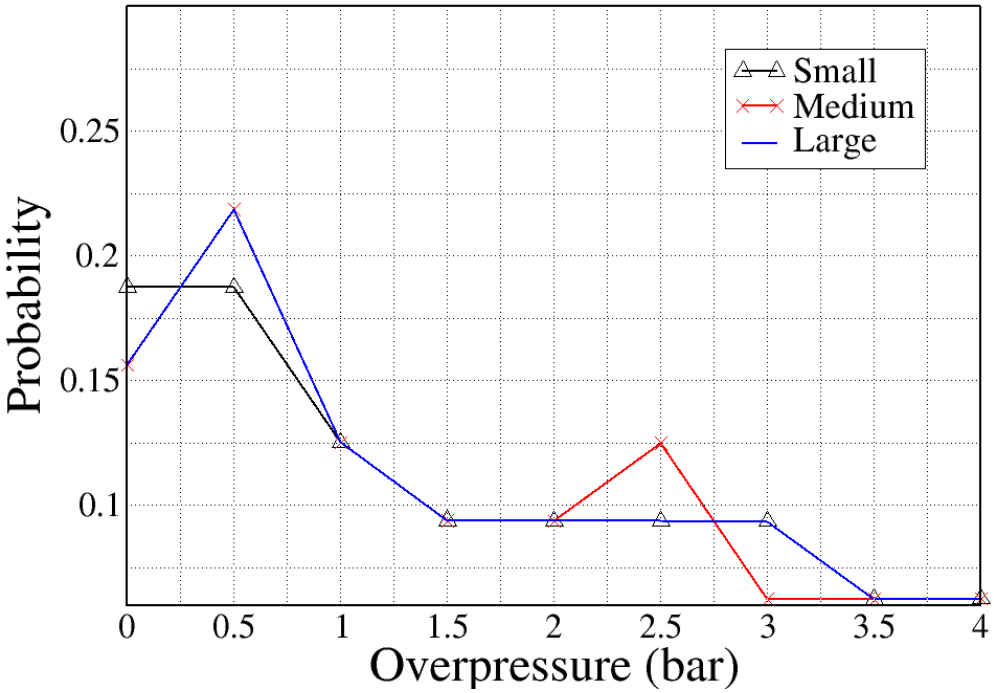

Figure 40. Probability of occurrence of different overpressures values for each discharge rate category.

The same similarity in the behaviour occurs with the accumulated probability of occurrence (Figure 41). Such graph reveals interesting information as it shows the probability of an overpressure equal to or greater than a certain value. For example, an explosion that leads to an overpressure of 2 bars or greater has roughly 40% probability. On the other hand, overpressures greater than 3.5 bars have only approximately 10% chance to take place.

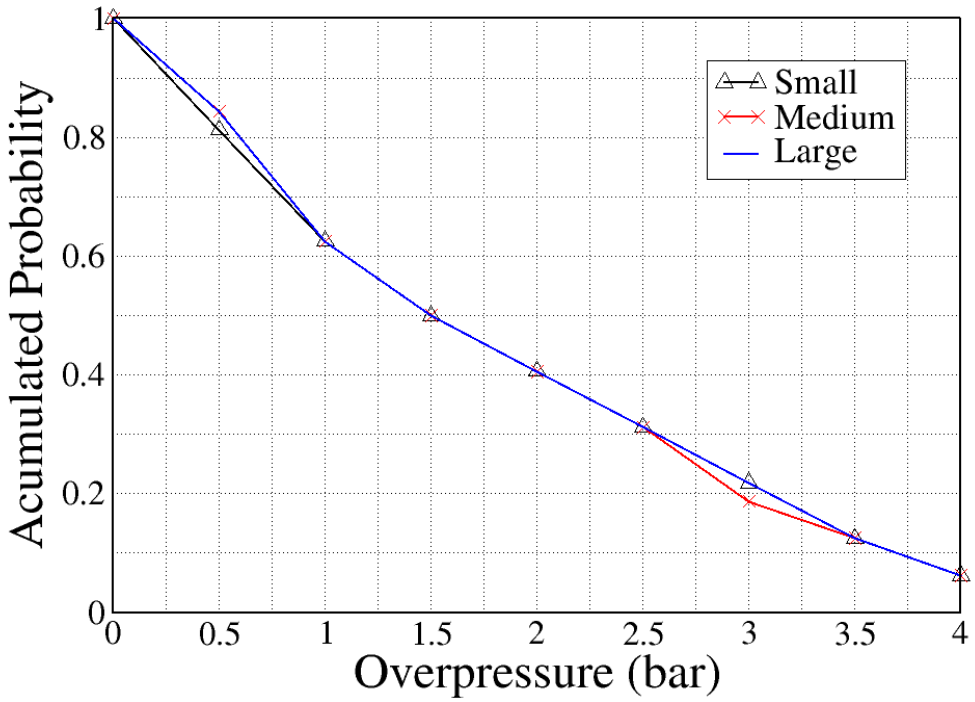

Figure 41. Exceedance probability curve of overpressure occurrence for all release rate categories.

Perhaps the most valuable information of the Monte Carlo methodology presented in this work is, however, the exceedance frequency curve (Figure 42). The frequency of occurrence of overpressure has been determined by multiplying the probability of occurrence of overpressure presented in Figure 41 with the ignition probability and the leak frequency presented in Table 35. Despite the probability results being interesting information, they do not reveal the actual frequency of the outcome, because they do not take into account the leak frequency and ignition probability.

It would be obvious to predict that, as small leaks have greater leak frequency, the small category would provide the most frequent overpressures. This should be expected if the study dealt only with leak frequencies. However, the study also deals with ignition probabilities, and as it is shown in Table 35, because the overpressure would only occur with ignition and explosion of the flammable cloud. The multiplication of the ignition probability and the leak frequency suggests that the greatest frequency is achieved for large release rates, and the medium category has a value near the large one (Table 35). That explains the behaviour of the frequency of overpressures in Figure 42. The total frequency,

considering all categories of discharge rates is also shown in Figure 42. The frequency of all categories is the sum of the frequencies of each category, and represents the risk of explosion of the sector of the plant analysed.

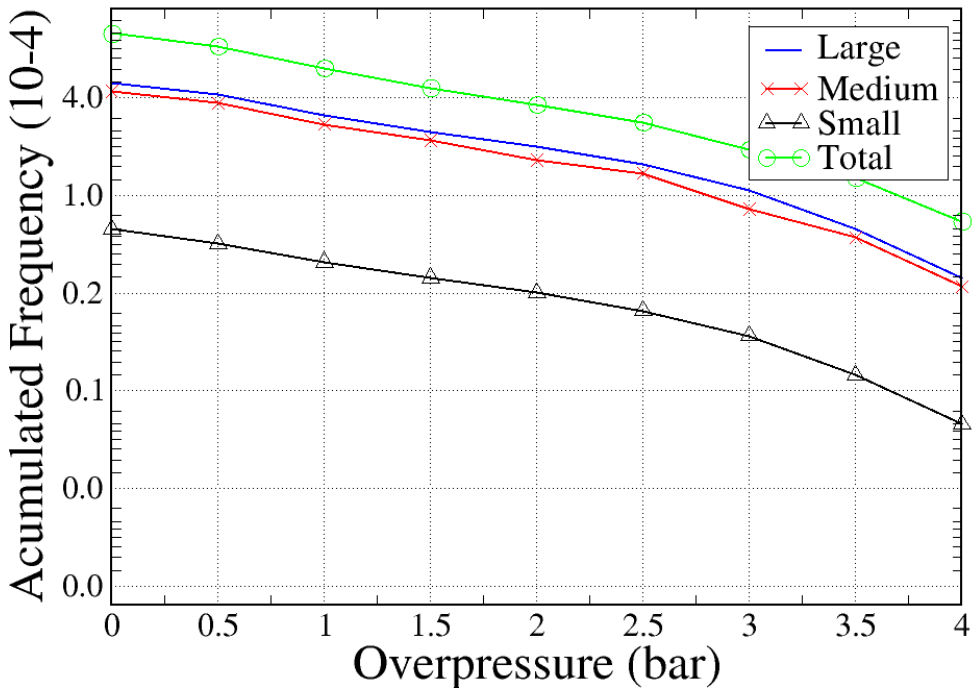

Figure 42. Exceedance frequency curves of overpressure for each category, in logarithmic scale. The total accumulated frequency is also shown here.

The quantitative risk analysis can then be performed with the use of the exceedance curve (Figure 42). According to the tolerable frequency of explosion, the engineer is able to determine the value of overpressure to which the plant must support. For example, considering medium release rates and that the tolerable explosion frequency is 1 x 10^{-4} per year, the plant must therefore support an overpressures of 2.75 bars, according to Figure 42. This analysis is important especially in the plant design because the engineer can save financial efforts by estimating the actual value of overpressure that the plant must support for a risk below the tolerable limit, which is actually the main goal of the risk analysis.

Finally, a verification of the number of Monte Carlo simulations needed to represent the real scenario has been performed for the case of small discharge rates (Figure 43). The

increase in the amount of Monte Carlo simulations changes the behaviour of the overpressure, because it changes the amount of scenarios studied. It occurs because the greater the number of Monte Carlo simulations, the closer to the real probability distribution the result is. The Monte Carlo simulation is used to create samples of the stochastic distribution, therefore the greater, the better the simulation is. Figure 43 shows that 1,000 simulations represent well the phenomenon of overpressure in this scenario, because the behaviour of the probability of occurrence does not change as the number of simulations increase.

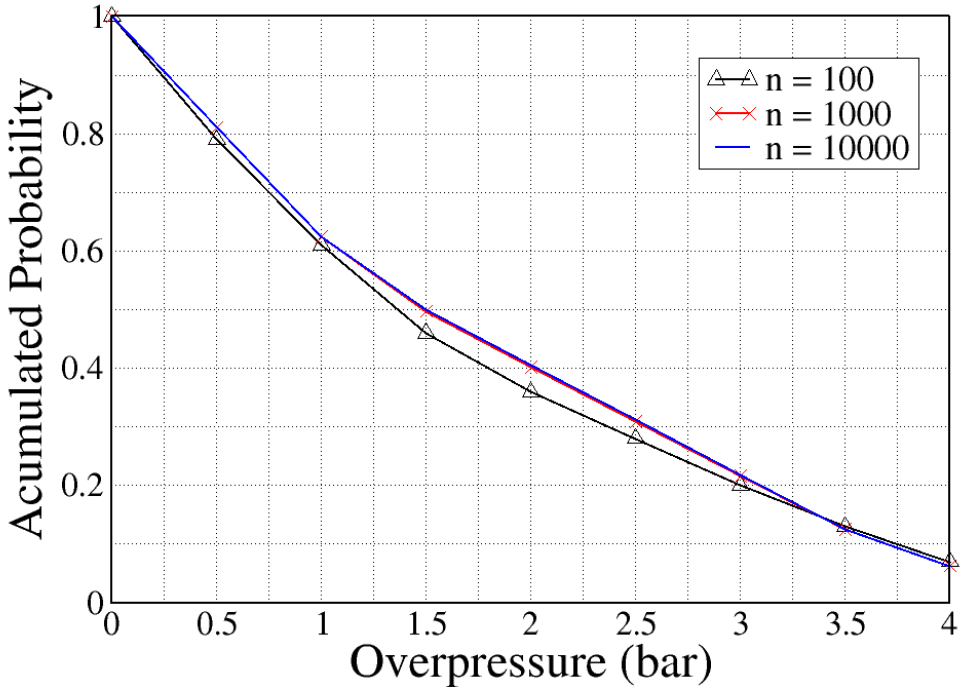

Figure 43. Exceedance probability occurrence curve for small discharge rates, according to the total number of Monte Carlo simulations.

Chapter 5

Conclusion

CASE is in agreement with robust and already known models from the literature. For all scenarios studied, results present good agreement relative to examples from the literature and the behaviour expected for each outcome.

All discharge models implemented in CASE have been validated along with the scenarios studied. First (Section 4.1) and fourth (Section 4.4) scenario presented the same model for the discharge: gas release through a hole in a vessel, but the first is a hydrogen release, and the fourth a methane release. Both scenarios presented the same behaviour, as already expected. Second scenario (Section 4.2) showed a liquid discharge in order to verify the model implemented. The comparison between CASE and the literature showed good agreement, despite the difference between gas and liquid discharge. Such difference is probably because of the great size of the liquid vessel. Finally, two-phase discharge has been evaluated in the third scenario (Section 4.3) in a constant matter, along with the flashing process.

The dispersion modelling has been deeper analysed in the fourth scenario. Both plume and puff have been discussed. The puff model has been shown for different periods, which demonstrated the behaviour of the flammable cloud, which tends to grow until a certain period during the entrainment of air. In addition, the flammable mass has also been verified for each period of time after the release, showing the same behaviour.

A more detailed analysis of explosion effects has been presented in the first scenario (Section 4.1). The difference between TNT Equivalency and Multi-Energy model has been evaluated and is consistent with the behaviour expected for each model. A verification of the influence of the blast strength of the Multi-Energy model has been provided, showing that it is in fact a crucial parameter for the overpressure calculation, and therefore must be carefully chosen considering the density of obstacles and the degree of confinement. The same analysis has been done for the explosion efficiency of the TNT Equivalency model. Although the range of the parameter is usually not wide, small differences provide great differences in the overpressure. Such behaviour shows that this model is strongly dependent on the explosion efficiency, which highlights its simplicity.

Second scenario provided results for the pool fire for both models implemented, and differences in the result have been discussed. Third scenario's outcomes are pool fire and fireball. Both effects have been analysed, and the comparison showed that the fireball tends to provide greater damages than pool fires, as already expected. Finally, jet fire has been studied and results obtained showed good agreement with literature.

An interesting characteristic of CASE is the fact that there is more than one model for almost all accident effects (pool fire, explosion and fireball). This is a good way to increase the reliability of the simulator, as the models must agree with each other, but also have differences according to their degree of simplifications or complexity.

A study of vulnerable areas of an accident in an industrial plant has been performed considering the release scenario of Section 4.4. The study has been done by supposing an incident in a unit of the refinery containing natural gas. Vulnerable areas for overpressures and radiation flux obtained with CASE simulations have been plotted in the industrial plant and the damages caused by such accident have been discussed.

Finally, CASE deals with the most common physical effects that occur in process plants, and therefore could be useful to plant design and also for already existing plants.

Regarding the Monte Carlo simulation based on CFD study for the analysis of stochastic variables, CASE could perform analysis of the main probabilistic parameters of a gas release and vapour cloud explosion. It is able to deal with hundreds of accident scenarios by using Monte Carlo simulation to determine the most probable or frequent

ones. By using the methodology presented in this work, an engineer is able to perform simulation of hundreds of accident scenarios in a fast manner and generate results that are accurate and validated with state of the art technology. The response surfaces used for the analysis are based on CFD studies for flammable volume and overpressure, which enhances the reliability of the methodology, as it is based on state of the art technology. The results of the Monte Carlo simulation methodology are helpful in analysing the plant's risks, as the study provides frequencies of the scenarios.

Another important feature of CASE is that it works both in *Linux* and *Windows* operating systems. The small computational effort and time of CASE should also be highlighted.

Future Work

CASE deals with very familiar empirical and semi-empirical models from the literature, which are used worldwide for consequence analysis. Although the results show good agreement with the expected behaviours of the main parameters, it would be interesting to validate CASE also with existing software for consequence analysis that uses the same models as CASE, like *Phast*^{TM}, for example.

CASE should be live software for consequence analysis, which means that it should always be updated with other recent models from the literature. Adding other models for the outcome effects of accidents could also be considered.

Concerning the Monte Carlo methodology used in this work, it accounts for overpressure and flammable volume calculations based on CFD studies. An interesting future work would be the use of the methodology developed in this work in a real case study. To be executed, such work should perform CFD study for both flammable volume and overpressure for a specific area of a plant and with CFD results, generate the response surfaces as the ones used in the present work. Then, the methodology should be performed and a real exceedance probability or frequency curve could be analysed and used for risk analysis.

References

ABBASI, T.; ABBASI, S. A. The boiling liquid expanding vapour explosion (BLEVE): Mechanism, consequence assessment, management. **Journal of Hazardous Materials**, 2007, p. 489-519.

ABDOLHAMIDZADEH, B.; ABBASI, T.; RASHTCHIAN, D.; ABBASI, S. A. Domino effect in process-industry accidents – An inventory of past events and identification of some patterns. **Journal of Loss Prevention in the Process Industries**, 2011, p. 575-593.

AICHE/CCPS. American Institute of Chemical Engineers. **Guidelines for Evaluating the Characteristics of Vapour Cloud Explosions, Flash Fires and BLEVES**. Center for Chemical Process Safety, 1994 *apud* AICHE/CCPS. Guidelines for Chemical Process Quantitative Risk Analysis. Second edition, 2000.

AICHE/CCPS. American Institute of Chemical Engineers. **Guidelines for Chemical Process Quantitative Risk Analysis**. Second edition, Center for Chemical Process Safety, 2000. Consequence Analysis, p. 57-243.

ALONSO, F. D.; FERRADÁS, E. G.; PÉREZ, J. F. S.; AZNAR, A. M.; GIMENO, J. R.; ALONSO, J. M. Characteristic overpressure-impulse-distance curves for vapour cloud explosions using the TNO Multi-Energy model. **Journal of Hazardous Materials**, 2006, p. 734-741.

ARUNRAJ, N. S.; MANDAL, S.; MAITI, J. Modeling uncertainty in risk assessment: An integrated approach with fuzzy set theory and Monte Carlo simulation. **Accident Analysis and Prevention**, 2013, 242-255.

BADRI, N.; RAD, A.; KARESHKI, H.; ABDOLHAMIDZADEH, B.; PARVIZSEDGHY, R.; RASHTCHIAN, D. A risk-based decision making approach to determine fireproofing

requirements against jet fires. **Journal of Loss Prevention in the Process Industries**, 2013, p. 771-781.

BENEDETTO, A. D. The thermal/thermodynamic theory of flammability: The adiabatic flammability limits. **Chemical Engineering Science**, 2013, p. 265-273.

BJERKETVEDT, D.; BAKKE, J. R.; WINGERDEN, K. **Gas Explosion Handbook**. Journal of Hazardous Materials, 1997, p. 1-150.

BRITTER, R. E.; MCQUAID, J. **Workbook on the Dispersion of Dense Gases**. HSE Contract Research Report No. 17/1988, U.K. Health and Safety Executive, 1988.

CALAY, R. K.; HOLDO, A. E. Modelling the dispersion of flashing jets using CFD. **Journal of Hazardous Materials**, 2008, p. 1198-1209.

CAROL, S.; VILCHEZ, J.; CASAL, J. Updating the economic cost of large-scale industrial accidents Application to the historical analysis of accidents. **Journal of Loss Prevention in Process Industries**, p.49-55, 2000.

COMPANHIA AMBIENTAL DO ESTADO DE SÃO PAULO (CETESB). Norma técnica P4.261: Risco de Acidente de Origem Tecnológica – Método para decisão e termos de referência. Second edition, December, 2011.

CROWL, D. A. Liquid discharge from process and storage vessels. **Journal of Loss Prevention in Process Industries**, 1991, p. 73-80.

CROWL, D. A.; LOUVAR, J. F. **Chemical Process Safety: Fundamentals with Applications**. Third edition. Prentice Hall, 2011.

DITCH, B. D.; RIS, J. L.; BLANCHAT, T. K.; CHAOS, M. JUNIOR, R. G. B.; DOROFEEV, S. B. Pool fires – An empirical correlation**. Combustion and Flame**, 2013, p. 2964-2974.

DNV-GL. **Software Phast™**. Available in: <https://www.dnvgl.com/services/hazard-analysis-phast-1675>. Accessed in: April 9th, 2015.

DOWNHAM, D. Y.; ROBERTS, F. D. K. Multiplicative congruential pseudo-random number generators. **The Computer Journal**, 1967, p. 74-77.

EISENBERG, N. A.; LYNCH, C. J.; BREEDING, R. J. **Vulnerability Model: A Simulation System for Assessing Damage Resulting From Marine Spills**. U.S. Coast Guard, 1975.

FAUSKE, H. K.; EPSTEIN, M. Source term considerations in connection with chemical accidents and vapour cloud modelling. **Journal of Loss Prevention in Process Industries**, 1988, p. 75-83.

FERREIRA, T. D.; VIANNA, S. S. V. A novel coupled response surface for flammable gas cloud volume prediction. **International Journal of Modelling and Simulation for the Petroleum Industry**, submitted, 2014.

GENOVA, B.; SILVESTRINI, M.; TRUJILLO, F. J. L. Evaluation of the blast-wave overpressure and fragments initial velocity for a BLEVE event via empirical 50 correlations derived by a simplified model of released energy. **Journal of Loss Prevention in Process Industries**, 2008, p. 110-117.

GONG, Y. W.; LIN, W. S.; GU, A. Z.; LU, X. S. A simplified model to predict the thermal response of PLG and its influence on BLEVE. **Journal of Hazardous Materials**, 2004, p. 21-26.

GOOGLE MAPS. Imagery ©2015 DigitalGlobe. **Refinaria Duque de Caxias (Petrobras)**. Obtained in: https://www.google.com.br/maps/place/Refinaria+Duque+de+Caxias+Reduc/@-22.7198704,-43.2685017,2914m/data=!3m1!1e3!4m2!3m1!1s0x99731975ffd53d:0xb46f8e0b1a9fbeb4>. Accessed in 2015.

HABIB, A.; SCHALAU, B.; SCHMIDT, D. Comparing Tools of varying Complexity for Calculating the Gas Dispersion. **Process Safety and Environment Protection**, 2014.

HANKINSON, G.; LOWESMITH, B. J. A consideration of methods of determining the radiative characteristics of jet fires. **Combustion and Flame,** 2012, p. 1165-1177.

INTERNATIONAL ASSOCIATION OF OIL AND GAS PRODUCERS. **Consequence Modelling**. OGP – Risk Assesment Data Directory (RADD). Report 434-7, 2010a.

INTERNATIONAL ASSOCIATION OF OIL AND GAS PRODUCERS. **Ignition Probabilities**. OGP – Risk Assesment Data Directory (RADD). Report 434-6.1, 2010b.

JUNG, Y. R.; PARK, W. G.; PARK, O. H. Pollution dispersion analysis using the puff model with numerical flow field data. **Mechanics Research Communications**, 2003, p.277-286.

KAKOSIMOS, K. E.; ASSAEL, M. J. Application of Detached Eddy Simulation to neighbourhood scale gases atmospheric dispersion modelling. **Journal of Hazardous Materials**, 2013, p. 653-668.

KINSELLA, K. **A rapid assessment methodology for the prediction of vapour cloud explosion overpressure**. Proceedings of the International Conference and Exhibition on Safety, Health and Loss Prevention in the Oil, Chemical and Process Industries, Singapore, 1993.

LAUTKASKI, R. Duct venting of gas explosions. Revision of two proposed engineering correlations. **Journal of Loss Prevention in the Process Industries**, 2012, p. 400-413.

LEES, F. P. **Loss Prevention in the Process Industries**. London, third edition, Butterworth-Heinemann, Oxford, UK, 2005.

LENOIR, E. M.; DAVENPORT, J. A. A Survey of Vapor Cloud Explosions – Second Update. **Process Safety Progress**. Industrial Risk Insurers, Hartford, volume 12, number 1, 1993.

LI, J.; ABDEL-JAWAD, M.; MA, GUOWEI. New correlation for vapour cloud explosion overpressure calculation at congested configurations. **Journal of Loss Prevention in the Process Industries**, 2014, p. 16-25.

LISBOA, H. M.; GUILLOT, J. M.; FANLO, J. L. Dispersion of odorous gases in the atmosphere – Part I: Modeling approaches to the phenomenon. **Science of the Total Environment**, 2006, p. 220-228. 51

MATOS, R. P. S.; ARAÚJO, P. J. G.; VIANNA, S. S. V. Development of a model to evaluate the overpressure of a gas explosion in a chamber with vent and obstacles. **International Journal of Modeling and Simulation for the Petroleum Industry**. Submitted for publication. 2014.

MERCX, W. P. M.; VAN DEN BERG, A. C.; HAYHURST, C. J.; ROBERTSON, N. J.; MORAN, K. C. Developments in vapour cloud explosion blast modelling. **Journal of Hazardous Materials**, p.301-3019, 2000.

MUDAN, K. Thermal radiation hazards from hydrocarbon pool fires. **Progress in Energy and Combustion Science**, 1984, p. 59-80.

NIVOLIANITOU, Z.; KOSTANDINIDOU, M.; MICHALIS, C. Statistical analysis of major accidents in petrochemical industry notified to the major accident reporting system (MARS). **Journal of Hazardous Materials**, p.1-7, 2006.

NRG. **Methods for determining and processing probabilities**. Publication Series on Dangerous Substances 4. Red Book, The Hague, Netherlands, 2005.

PETROBRAS METOCEAN DATA. Technical Specification no: I-ET-3000.00-1000-941-PPC-001. Sources: SIMO, collected in Campos Basin from 07.87 to 07.97. 2005.

PGS. Publication Series on Dangerous Substances. **Guidelines for quantitative risk assessment. Purple Book**. Committee for the Prevention of Disasters - CPR18E, 2005.

PIKAAR, J.; BRAITHWAITE, J.; COX, T. Process safety assessment of new existing plants. **Journal of Occupational Accidents**, 1990, p. 103-110.

PITBLADO, R.; ALDERMAN, J.; THOMAS, J. K. Facilitating consistent siting hazard distance predictions using the TNO Multi-Energy Model. **Journal of Loss Prevention in the Process Industries**, 2014, p. 287-295.

RAMAN, R.; GRILLO, P. **Minimizing uncertainty in vapour cloud explosion modelling**. 7th World Congress of Chemical Engineering, 2005, p. 298-306.

RICHARDSON, S. A. **Interpretation of the HCR for QRA – and its application beyond the North Sea**. Symposium Series number 154. Shell Global Solutions UK, 2008.

SANDLER, S. I. **Chemical and engineering thermodynamics**. 3rd edition, 1999, p. 184.

SHARMA, R. K.; GURJAR, B. R.; WATE, S. R.; GHUGE, S. P.; AGRAWAL, R. Assessment of an accidental vapour cloud explosion: Lessons from the Indian Oil Corporation Ldt. accident in Jaipur, India. **Journal of Loss Prevention in Process Industries**, 2012.

SHEPARD, C. M. DIERS bubbly disengagement correlation extended to horizontal cylinders and spheres. **Journal of Loss Prevention in Process Industries**, 1994, p. 3-5.

STREHLOW, R. A.; LUCKRITZ, R. T.; ADAMCZYK, A. A.; SHIMPI, S. A. The Blast Wave Generated by Spherical Flames. **Combustion and Flame**, 1979, p. 297-310.

TAUSEEF, S. M.; RASHTCHIAN, D.; ABBASI, T.; ABBASI, S.A. A method for simulation of vapour cloud explosions based on computational fluid dynamics (CFD). **Journal of Loss Prevention in the Process Industries**, 2011, p. 638,647.

TNO. Netherlands Organization for Applied Scientific Research. **Methods for the calculation of physical effects due to releases of hazardous materials (Liquids and Gases)**. Yellow Book, TNO, The Hague, Netherlands, 3rd ed., Second revised print, 2005.

TNO. Netherlands Organization for Applied Scientific Research. **Methods for the calculation of possible damage to people and objects resulting from the release of hazardous materials**. Green Book, TNO, Netherlands, 1st ed., 1992.

TOROK, Z.; AJTAI, N.; TURCU, A. T.; OZUNU, A. Comparative consequence analysis of the BLEVE phenomena in the context on Land Use Planning; Case study: The Feyzin accident. **Process Safety and Environmental Protection**, 2011, p. 1-7.

VAN DEN BERG, A. C. The Multi-Energy Method: A framework for vapour cloud explosion blast prediction. **Journal of Hazardous Materials**, 1985, p. 1-10.

VAN DEN BERG, A. C.; LANNOY, A. Methods for vapour cloud explosion blast modelling. **Journal of Hazardous Materials**, Amsterdam, 1993, p. 151-171.

VASANTH, S.; TAUSEEF, S. M.; ABBASI, T.; RANGWALA, A. S.; ABBASI, S. A. Assessment of the effect of pool size on burning rates of multiple pool fires using CFD. **Journal of Loss Prevention in the Process Industries**, 2014, p. 86-94.

VIANNA, S. S. V.; CANT, R. S. Explosion pressure prediction via polynomial mathematical correlation based on advanced CFD Modelling. **Journal of Loss Prevention in the Process Industries**, 2012, p. 81-89.

WEN-HE, W.; ZHI-SHENG, X.; BAO-JIANG, S. Numerical Simulation of Fire Thermal Radiation Field for Large Crude Oil Tank Exposed to Pool Fire. **Procedia Engineering**, 2013, p. 395-400.

WITLOX, H. W. M.; HARPER, M. Two-phase jet releases, droplet dispersion and rainout I. Overview and model validation. **Journal of Loss Prevention in the Process Industries**, 2013, p. 453-461.

WOODWARD, J. L. **Estimating the Flammable Mass of a Vapour Cloud**. Center for Chemical Process Safety of the American Institute of Chemical Engineers. 1998.

ZHANG, X.; LI, X.; HADJISOPHOCLEOUS, G. A probabilistic occupant evacuation model for fire emergencies using Monte Carlo methods. **Fire Safety Journal**, 2013, p. 15-24.

Appendix A

CASE Output of the First Scenario (Section 4.1)

```
  CASE - Consequence Analysis Simulation Environment           Version 1.0
Developed by Eng. Isabela Tolentino with supervision of Prof. Dr. Savio Vianna
                 University of Campinas - UNICAMP

User: Isabela Barreto
Project: Hydrogen release


     1. Accident scenario:
     ---------------------

Substance: Hydrogen
Initial temperature:  288.149994 K
Initial pressure:  50. bar
Type of containment: vessel
Volume of the vessel:  100. m3


     2. Gas discharge
     ----------------

     2.1. Input data:

Hole diameter:  100. mm
Discharge coefficient:  0.62
Atmospheric pressure:  1. bar

     2.2. Substance data:

Heat capacity ratio:   1.405
Molecular weight:   2.015894 kg/mol


     2.3. Discharge results
Results of the discharge of the gas through a vessel considering a transient leakage

     Time(s)            Mass released(kg)        Initial pressure(bar)          T(K)                Discharge (kg/s)

       0.0                   0.00000                50.00000               288.14999               15.31177
      10.0                 126.77295                30.22949               249.34270                9.95170
      20.0                 210.21613                18.91862               217.89906                6.66233
      30.0                 266.69940                12.20142               192.06398                4.57670
      40.0                 305.88046                 8.07999               170.57643                3.21600
      50.0                 333.65186                 5.47747               152.51137                2.30565
      60.0                 353.71667                 3.79159               137.17755                1.68285
      70.0                 368.46381                 2.67427               124.05006                1.24816
      80.0                 379.47073                 1.91839               112.72444                0.93928
      90.0                 387.65594                 1.40612               103.06744                0.66393
     100.0                 392.91168                 1.10254                96.08160                0.34910
     109.0                 394.78522                 1.00000                93.39618                0.00000

     3. Jet fire
     -----------

     3.1. Input data:

Temperature of the flame:  2200. K
Distance from the flame:  15. m
Fraction of energy converted to radiation:  0.2

     3.2. Results of the jet fire:

Flame height:    54.808 m

     Time (s)        Discharge (kg/s)      Er (kW/m²)

    0.0                 15.31177           22.88421
   10.0                  9.95170           14.87331
   20.0                  6.66233            9.95719
   30.0                  4.57670            6.84010
   40.0                  3.21600            4.80647
   50.0                  2.30565            3.44591
   60.0                  1.68285            2.51510
   70.0                  1.24816            1.86544
   80.0                  0.93928            1.40380
   90.0                  0.66393            0.99228
  100.0                  0.34910            0.52175
  109.0                  0.00000            0.00000
```

4. Dispersion of the cloud

4.1. Input data:

Discharge height 0. m
Temperature of ambient air: 298. K
Wind speed: 2. m/s
Stability class: F

4.2. Results of the dispersion:

Type of dispersion: plume (continuous)
Discharge rate: 3.589 kg/s
Flammable gas cloud: 907.575 kg

Time(s)	Distance downwind (m)	Concentration (mg/m3)	Isopleth (m)
0.0	0.0	-1.#IND0	0.00000
20.0	40.0	565634.81250	5.12213
40.0	80.0	143370.34375	8.75456
60.0	120.0	64594.68359	11.63871
80.0	160.0	36827.88281	13.94867
100.0	200.0	23886.57617	15.76347
120.0	240.0	16808.53320	17.12210
140.0	280.0	12511.72070	18.03972
160.0	320.0	9704.15039	18.51270
180.0	360.0	7766.43213	18.51795
200.0	400.0	6371.20313	18.00652
220.0	440.0	5332.09668	16.88690
240.0	480.0	4536.60303	14.98043
260.0	520.0	3913.50464	11.86802
280.0	560.0	3415.91138	5.78813
285.6	571.2	3294.45996	0.00000

5. Explosion

5.1. Input data:

Stoichiometric coefficient of combustion: 0.3
Efficiency of explosion (TNT explosion model): 0.05
Distance from the explosion: 50. m
Heat of combustion of the material: 120000000. J/kg
Average heat of combustion (TNO model): 3500000. J/kg
Upper flammability limit: 61829.689 mg/m3
Lower flammability limit: 3297.583 mg/m3

5.2. Results of the explosion:

5.2.1. TNT Equivalency model:

Scaled distance (m)	Distance from blast (m)	Overpressure (kPa)	Impulse (Pa.s)	Duration time (ms)
4.8	50.000	0.471E+02	0.651E+03	0.401E+02
9.5	100.000	0.159E+02	0.342E+03	0.495E+02
19.0	200.000	0.646E+01	0.175E+03	0.619E+02
28.5	300.000	0.381E+01	0.117E+03	0.770E+02
38.1	400.000	0.253E+01	0.876E+02	0.112E+03
40.4	425.000	0.000E+00	0.823E+02	0.125E+03

5.2.2. TNO Multi Energy Model:

Distance (m)	Side-on Overpressure (kPa)	Impulse (Pa.s)
50.000	0.101E+03	0.461E+04
100.000	0.452E+02	0.197E+04
200.000	0.197E+02	0.965E+03
300.000	0.121E+02	0.636E+03
400.000	0.857E+01	0.473E+03
500.000	0.656E+01	0.376E+03
545.000	0.591E+01	0.344E+03

Appendix B

CASE Output of the Monte Carlo Simulation

```
  CASE - Consequence Analysis Simulation Environmen           Version 1.0
Developed by Eng. Isabela Tolentino with supervision of Prof. Dr. Savio Vianna
                 University of Campinas - UNICAMP

User: Isabela T.
Project: Monte Carlo Simulation


     1. Monte Carlo simulation:
     --------------------------

Total amount of rounds: 50


     2. Discharge rate input:
     ------------------------

  Discharge rate (kg/s)     Probability

           0.10             0.34100
  Discharge rate (kg/s)     Probability

           0.20             0.22700
  Discharge rate (kg/s)     Probability

           0.50             0.28400
  Discharge rate (kg/s)     Probability

           1.00             0.14800


     2. Wind rose input:
     ------------------------

  Probability North     Ventilation rate (m3/s)

           0.01            882.80000
  Probability Northeast     Ventilation rate (m3/s)

           0.32            849.95000
  Probability East     Ventilation rate (m3/s)

           0.20            563.10000
  Probability Southeast     Ventilation rate (m3/s)

           0.13            792.30000
  Probability South     Ventilation rate (m3/s)

           0.13            884.10000
  Probability Southwest     Ventilation rate (m3/s)

           0.07            932.75000
  Probability West     Ventilation rate (m3/s)

           0.04            770.80000
  Probability Northwest     Ventilation rate (m3/s)

           0.04            864.25000


     3. Response surface - Flammable Volume:
     ---------------------------------------

     Response Surface formula:

     Flammable Volume = a0 + a1*R + a2*phi + a12*R*hi + a11*R*R + a22*phi*phi


     3.1.1 First quadrant:

     a0 =   -385.92
     a1 =  14659.25
     a2 =  37794.30
     a12 =   6443.20
     a11 =  -5900.00
     a22 =-164004.60

     3.1.2 Second quadrant:
```

a0 = 14927.24
a1 = 45874.62
a2 =-115476.00
a12 = -11566.97
a11 = -28426.26
a22 = 178819.63

3.1.3 Third quadrant:

a0 = 57011.28
a1 = 47897.71
a2 =-181355.90
a12 = -4032.97
a11 = -33580.71
a22 = 136758.40

3.1.4 Fourth quadrant:

a0 = 40427.97
a1 = -29583.64
a2 = -66221.70
a12 = 46709.14
a11 = -3156.67
a22 = 24672.43

4. Response surface - Overpressure:

Response Surface formula:

Overpressure = b0 + b1*Vol + b2*ign + b12*Vol*ign + b11*VOl*Vol + b22*ign*ign

b0 =   -0.1578
b1 =   1.0315
b2 =   1.2690
b12 =   -1.5758
b11 =   -0.9331
b22 =   2.9114

5. Monte Carlo simulation summary:

Overpressure	Probability	Acumulated Probability	Acumulated Frequency
0.0000000	0.2000000	0.9999999	0.0000621
0.5000000	0.1600000	0.8000000	0.0000497
1.0000000	0.1600000	0.6400000	0.0000398
1.5000000	0.1200000	0.4800000	0.0000298
2.0000000	0.0800000	0.3600000	0.0000224
2.5000000	0.0800000	0.2800000	0.0000174
3.0000000	0.0600000	0.2000000	0.0000124
3.5000000	0.0800000	0.1400000	0.0000087
4.0000000	0.0600000	0.0600000	0.0000037
4.5000000	0.0000000	0.0000000	0.0000000

6. Monte Carlo simulation data:

Simulation	Discharge rate (kg/s)	Wind speed (m/s)	Phi	R	Flammable vol (m3)	Overpressure (bar)
1	1.0	15.000	0.5000	0.1276	6546.0063	0.0000
2	0.1	9.000	0.1250	0.0221	2114.4341	1.2121
3	0.1	9.000	0.1250	0.0221	2114.4341	0.6880
4	0.1	9.000	0.1250	0.0221	2114.4341	2.5685
5	0.1	9.000	0.1250	0.0221	2114.4341	0.8470
6	0.1	9.000	0.1250	0.0221	2114.4341	1.6747
7	0.1	9.000	0.1250	0.0221	2114.4341	2.1511
8	0.2	3.000	0.0000	0.2000	34384.9766	0.0670
9	0.2	6.000	0.1250	0.0663	2774.4473	0.3759
10	0.1	9.000	0.1250	0.0221	2114.4341	1.2596
11	1.0	24.000	0.7500	0.0913	5111.1309	0.0176
12	0.1	9.000	0.1250	0.0221	2114.4341	1.6019
13	1.0	12.000	0.3750	0.1509	2391.7092	0.0344
14	0.1	9.000	0.1250	0.0221	2114.4341	0.8958
15	0.1	9.000	0.1250	0.0221	2114.4341	0.7926
16	0.1	9.000	0.1250	0.0221	2114.4341	3.9548
17	0.1	9.000	0.1250	0.0221	2114.4341	3.5367
18	0.1	9.000	0.1250	0.0221	2114.4341	3.3833
19	0.1	9.000	0.1250	0.0221	2114.4341	3.9616
20	0.1	9.000	0.1250	0.0221	2114.4341	0.6596
21	1.0	12.000	0.8750	0.1509	3005.3735	0.0000
22	0.1	9.000	0.1250	0.0221	2114.4341	2.6188
23	1.0	12.000	0.1250	0.1592	4088.6382	0.1192
24	0.2	6.000	0.0000	0.1000	37438.0391	0.0166
25	0.2	3.000	0.0000	0.2000	34384.9766	0.0679
26	0.1	9.000	0.1250	0.0221	2114.4341	1.9453
27	0.2	6.000	0.1250	0.0663	2774.4473	0.3734
28	1.0	12.000	0.5000	0.1592	7557.1250	0.1330
29	0.5	9.000	0.1250	0.1104	3411.4414	0.5530
30	0.1	9.000	0.1250	0.0221	2114.4341	1.3628
31	0.1	9.000	0.1250	0.0221	2114.4341	0.7363
32	0.1	9.000	0.1250	0.0221	2114.4341	3.7996
33	0.1	9.000	0.1250	0.0221	2114.4341	0.9565
34	0.1	9.000	0.1250	0.0221	2114.4341	0.8713
35	0.1	9.000	0.1250	0.0221	2114.4341	1.1994
36	0.1	9.000	0.1250	0.0221	2114.4341	2.9896
37	0.1	9.000	0.1250	0.0221	2114.4341	1.4651
38	0.5	6.000	0.1250	0.1656	4175.3135	0.4941
39	0.1	9.000	0.1250	0.0221	2114.4341	1.7535
40	0.1	9.000	0.1250	0.0221	2114.4341	2.2707